UNIVERSITY OF TURKU

Data-driven decision-making and benchmarking in PBF-LB/M

Master of Science in Technology

Master's Thesis

Mechanical Engineering: Digital Design

Department of Mechanical and Materials Engineering

Author:

Usama Nadeem, B. Sc. (Tech.)

Supervisor:

Adjunct professor Heidi Piili, D.Sc. (Tech.)

Advisors:

Postdoctoral researcher Nikhil Kamboj, D. Sc. (Tech.)

Postdoctoral researcher Chinmayee Nayak, D. Sc. (Tech.)

27.05.2024

Turku

The originality of this thesis has been checked in accordance with the University of Turku quality assurance system using the Turnitin Originality Check service.

Master's thesis

Subject: Mechanical engineering
Author(s): Usama Nadeem
Title: Data-driven decision-making and benchmarking in PBF-LB/M
Supervisor(s): Adjunct professor Heidi Piili, D. Sc. (Tech.)
Advisor(s): Postdoctoral researcher Nikhil Kamboj, D. Sc. (Tech.), Postdoctoral researcher Chinmayee Nayak, D. Sc. (Tech.)
Number of pages: 120 pages
Date: 27.05.2024

Abstract.

This thesis proposes a novel framework for decision-making built on the backend of MATLAB application facilitating the selection of comparable technologies of Laser powder bed fusion for metals (PBF-LB/M). The aim of this research is to enhance the PBF-LB/M benchmarking process by introducing a simplified geometric benchmark artifact that facilitates the proposed framework for precise measurement, result interpretation, and technological comparison. The purpose of the study is to streamline the technology selection process in PBF-LB/M by reducing the reliance on trial-and-error methods.

Main findings include the successful development of a decision-making framework that integrates extensive data collection and analysis from geometrical benchmark artifacts using various metrology tools. The literature review reveals a significant gap in structured decision-making processes within additive manufacturing, which this framework aims to address. The experimental part demonstrates that the framework can save time and material consumption and improve resource management by minimizing the trial-and-error phase typically associated with machine selection.

The use case study included in this thesis highlights the practical benefits of the framework, showing its potential to transform decision-making processes in additive manufacturing. However, further studies and real-world testing are necessary to validate the statistical predictions and future studies could incorporate machine learning algorithms with additional parameters. Overall, this research provides a structured and data-driven approach to technology selection, with the potential to optimize technology usage and decision-making processes.

Keywords: Additive manufacturing (AM), additive manufacturing database, laser powder bed fusion, PBF-LB/M, benchmarking, geometrical benchmark, test artifact, geometric deviation analysis, laser scanning, decision support systems (DSS), Fuzzy AHP, Fuzzy TOPSIS, metrology for additive manufacturing, multiple-criteria decision analysis (MCDM).

Acknowledgments

I would like to express my sincere gratitude to all those who have supported me throughout the course of this thesis.

First and foremost, I would like to thank my supervisor, Professor Heidi Piili, for her invaluable guidance, support, and encouragement. Her expertise and insights have been crucial in shaping the direction and quality of this research.

I am deeply grateful to my advisors, Nikhil Kamboj, and Chinmayee Nayak, who have been crucial in undertaking my work. Their dedication and assistance have been greatly appreciated.

Special thanks to my colleague, Mojtaba Miri Beidokhti, for his help with the experiments. His collaboration and technical support were vital to the successful completion of this research.

I would also like to extend my gratitude to EOS GmbH for their assistance and support in providing the necessary resources and expertise for this study.

I am grateful to my family and friends for their unwavering support and encouragement throughout this process. Their belief in me has been a constant source of motivation.

Table of contents

Appendices

Appendix 1:	Dimensional drawings of the benchmark artifact
Appendix 2:	Data collected in Excel template for benchmark measurements for Aconity3D MIDI+ samples.
Appendix 3:	Data collected in Excel template for benchmark measurements for EOS M290 samples.

Nomenclature

Abbreviation	Explanation
AM	Additive manufacturing
PBF-LB/M	Laser-based powder bed fusion for metals
AMed	Additive manufactured
DA	Dimensional accuracy
Rep	Repeatability
MFS	Minimal feature size
TOPSIS	Technique for order of preference by similarity to ideal solution
AHP	Analytic hierarchy process
MCDA	Multi-Criteria Decision Analysis
TFNs	The triangular fuzzy numbers
FPIS	Fuzzy positive-ideal solution
FNIS	Fuzzy negative-ideal solution
Machine learning	ML
Technology readiness level	TRL

1. Introduction

Additive manufacturing (AM), or industrial 3D printing, is a developing and dynamically advancing technology that has fundamentally transformed product development, manufacturing, and industrialization (Yi et al., 2023). Traditional manufacturing methods have been the industry standard for decades, yet there is a significant expansion in the additive manufacturing industry with trend shown in Figure 1.

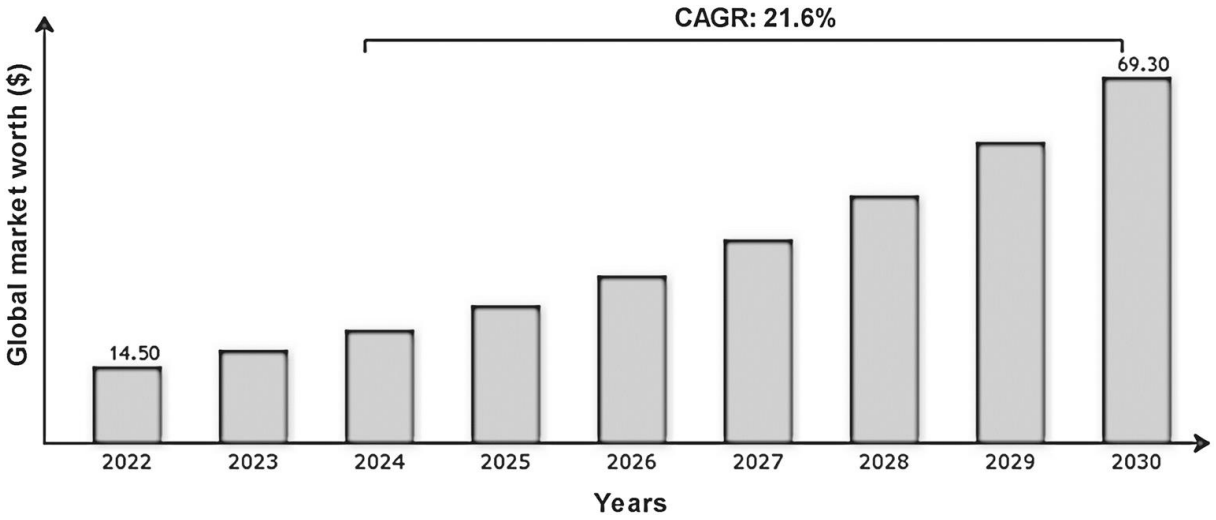

Figure 1: Global AM market projection. Reproduced from (Vantage Market Research, 2023) with permission of Vantage Market Research.

As can be seen from Figure 1, the valuation of the Global AM Market in 2022 was USD 14.5 Billion, and it is expected to grow at a Compound Annual Growth Rate (CAGR) of 21.60% between 2023 and 2030, reaching a value of USD 69.3 Billion by 2030 (Vantage Market Research, 2023). In the past few years, many companies have embraced AM technologies and are beginning to enjoy real business benefits from the investment (Attaran et al., 2017) because AM stands out significantly. Unlike traditional techniques, AM allows for creating a structure in its intended shape through a 'layer-by-layer' approach, resembling a 'bottom-up' manufacturing process (Tofail et al., 2018).

Choosing the most appropriate AM technology for a particular task is challenging because many different procedures and materials are available. Across various technologies in AM, only a handful can create metal parts that satisfy the demands of industrial applications (Herzog et al., 2016). The desirable objectives for a manufacturing process include achieving good dimensional precision, a fine surface finish, a swift build time, and a low building cost.

However, it is essential to note that no single method excels in all these characteristics (Taylor et al., 2021), which leaves a void that needs to be filled through research.

1.1. Research problem

Additive Manufacturing (AM) encompasses various innovative techniques that create objects layer by layer, often using digital 3D-designed models. AM encompasses techniques like Powder Bed Fusion, Material Extrusion, Vat Photopolymerization, Material Jetting, Binder Jetting, Directed Energy Deposition, and Sheet Lamination (Yap et al., 2020), each method offering distinct advantages. Powder bed fusion (PBF) is among the most industrially relevant AM processes (Herzog et al., 2016) due to its extensive advantages, such as high precision, complex geometries, and the ability to produce parts with excellent mechanical properties. It further includes several subcategories, among which PBF-LB holds significance. Powder Bed Fusion with Laser Beam (PBF-LB) is a technique where a laser selectively melts powdered material to create intricate shapes. Within PBF-LB, a further specialization exists known as PBF-LB/M, where the 'M' denotes metals. This subcategory focuses on the laser-based powder bed fusion process for metals, offering distinctive advantages in various industries.

Several technology vendors, with different capabilities and solutions they offer in the PBF-LB/M exist. EOS GmbH, Germany, is a crucial player renowned for its AM industry contributions (Beau Jackson, 2017). Another prominent additive manufacturing vendor is Aconity3D GmbH, which is also making significant advancements (Brian Lord, 2018) and is offering an open, configurable system that blends the highest level of functionality and opens many options for further applications (Aconity3D GmbH, 2024). Both AM technology providers offer a range of PBF-LB/M solutions to cater to the diverse needs of their clientele in the additive manufacturing industry.

This is where benchmarking in AM comes in to play for comparing the performance and characteristics of different AM systems or processes to establish standards and make informed decisions. It is challenging due to the diversity of available technologies from various vendors and materials, or even with one vendor offering several options, complicating the comparison of machine performance.

Choosing the most suitable technology from the vendor for additively manufactured (AMed) products is challenging due to the need for more decision-making data or frameworks from benchmarking, particularly from geometric benchmark artifacts. The discrepancy underscores

the need for research to create robust benchmarking strategies and decision-making tools tailored to meet the diverse needs of users within this rapidly evolving domain.

1.2. Aim of research and research questions

The thesis aims to streamline the complex decision-making process of selecting PBF-LB/M technologies. This effort seeks to introduce a precise benchmark artifact designed to enhance measurement precision, result interpretation, and overall consistency. This artifact is critical to facilitating meaningful comparisons across different technologies, providing stakeholders valuable insights into their capabilities and limitations.

Moreover, the thesis proposes the development of an expandable database coupled with a comprehensive decision-making framework. These resources are intended to assist individuals with varying levels of expertise in the additive manufacturing sector. By establishing a nuanced correlation between manufacturing choices and machine suitability for specific geometries, the thesis aims to empower users with informed decision-making tools. Through this approach, the thesis seeks to demystify the complexities inherent in additive manufacturing and adopt a deeper understanding and appreciation of its potential applications and implications. This thesis answers three research questions.

What is the impact of simplified geometric benchmark artifacts on improving PBF-LB/M technology comparison?

How does a database enhance the process of selecting PBF-LB/M technology for diverse users?

What framework links fabrication choices to machine suitability for specific uses?

This thesis was undertaken within the framework of the "Sustainably Additive!" project, conducted at the Turku Innovation Centre of Additive Manufacturing (TICAM). The project, funded by the European Regional Development Fund through the Helsinki-Uusimaa Regional Council, operated under the project code A80276. From May 1st, 2023, to June 30th, 2026, the initiative aimed to bolster the capabilities of small and medium-sized enterprises (SMEs) in Turku engaged in additive manufacturing, mainly 3D printing.

Collaborating institutions, including the University of Turku, Åbo Akademi University, and Turku University of Applied Sciences, pooled their expertise to advance the proficiency of local SMEs in utilizing additive manufacturing technologies. With a focus on diverse applications

such as machine technology, biomedical and dental technology, and bio- and recycled-based materials, the project sought to empower SMEs to leverage 3D printing effectively.

Central to the objectives of the project was to establish the Turku Innovation Centre of Additive Manufacturing (TICAM), envisioned as a hub for fostering innovation and collaboration within the additive manufacturing ecosystem. By creating synergies across various sectors, including bio- and dental medicine, pharmaceuticals, and machine technology, TICAM aimed to drive advancements in additive manufacturing applications, thereby contributing to regional economic growth and sustainability efforts. The project aims to provide extensive AM training materials for SMEs utilizing virtual reality to enhance company competitiveness.

1.3. Research methods and framing

Research methods include concisely reviewing existing benchmark artifacts and utilizing a database for data gathering throughout the experimental phase. The insights gained from the literature review aided in the design of the benchmark and experimental components, contributing to the development of a database. The process involves designing a benchmark using computer-aided design software and taking precise measurements of the test samples AMed using PBF-LB/M technologies utilizing 316L stainless steel. The results are compared using a 3D laser scanner. Moreover, the framework is developed by correlating the collected data and the expertise of academic professionals and machine operators. A thorough literature review was done, and Google Scholar and Scopus were used as primary resources for pertinent scholarly articles and studies.

The objective of the established framework is to determine the optimal PBF-LB/M technology by assessing several parameters, as illustrated in Figure 2.

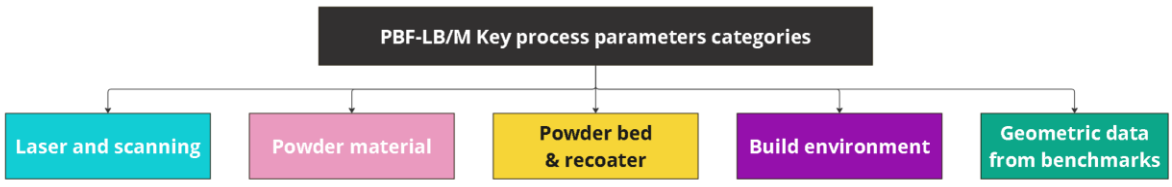

Figure 2: PBF-LB/M key process parameters categories.

As can be seen from Figure 2, the PBF-LB/M process parameters can be classified into four primary domains: laser and scanning, powder material, powder bed, re-coater, and build environment (Spears & Gold, 2016). Furthermore, this thesis introduces a novel classification,

"geometric data from benchmarks," to account for the machine performance. This thesis focuses exclusively on the fifth category and proposes recommendations for future research incorporating other parameters in the context of the PBF-LB/M process.

1.4. Thesis outline

The critical components of the decision-making process for selecting the most suitable PBF-LB/M technology are illustrated in Figure 3.

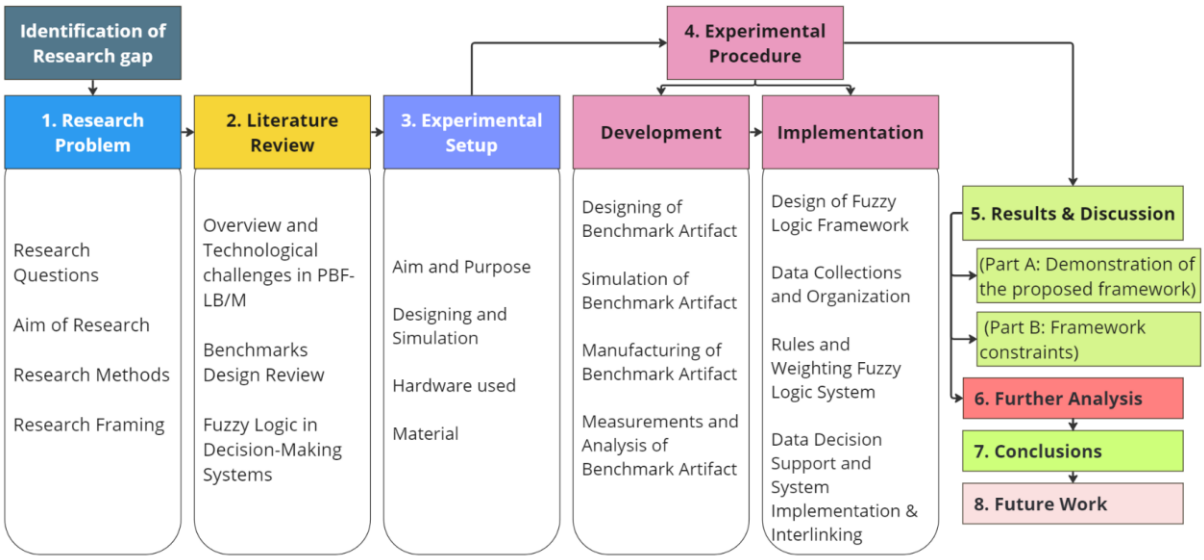

Figure 3: Thesis outline.

As can be seen from Figure 3, each critical phase of the research process provides an organized path for this thesis research. The first step was identifying the research gap and reviewing the literature to support a straightforward design approach to benchmarking. The experimental stage goes further into producing the benchmark and collecting precise data about geometric tolerances.

Following the experimental stage, a framework is created by combining the empirical facts and firsthand knowledge from experienced technology users. The thesis concludes with a case study demonstrating the practical utility of the proposed technique in real-world scenarios. It underscores how this approach can enable informed decision-making regarding selecting PBF-LB/M technology.

2. Literature review

In the discussion of AM, PBF-LB/M is emphasized as a crucial breakthrough that faces both technical difficulties and the interest of effectiveness. Benchmarking is vital for standardization and performance improvement, and data-driven frameworks for equipment selection are emphasized. Several measures have been taken over the years, showing their potential to help navigate this complexity and uncertainty of AM technology.

2.1. Overview of laser-based powder bed fusion for metals (PBF-LB/M)

Since the 1980s, when early research of PBF-LB/M began, the significance of AM in industry has been continuously increasing. This is due to the wide range of geometries achievable through layer-by-layer construction (Jensch et al., 2023). Furthermore, the advantage of being compatible with various types of metals makes it relevant to the industry.

The process begins with the component design using 3D-optimized software, then exports it as an STL file containing the design details of the object. This model is the PBF-LB/M technology blueprint (KDM Fabrication, 2023).

This layer is scanned by a high-powered laser, which melts the powder as per the CAD model to create a solid layer. A powder layer is melted by a laser, covered with another layer of powder once it solidifies, and repeated until the component is formed. The object is built vertically by adding and melting a fresh layer of powder each time, as illustrated in Figure 4,

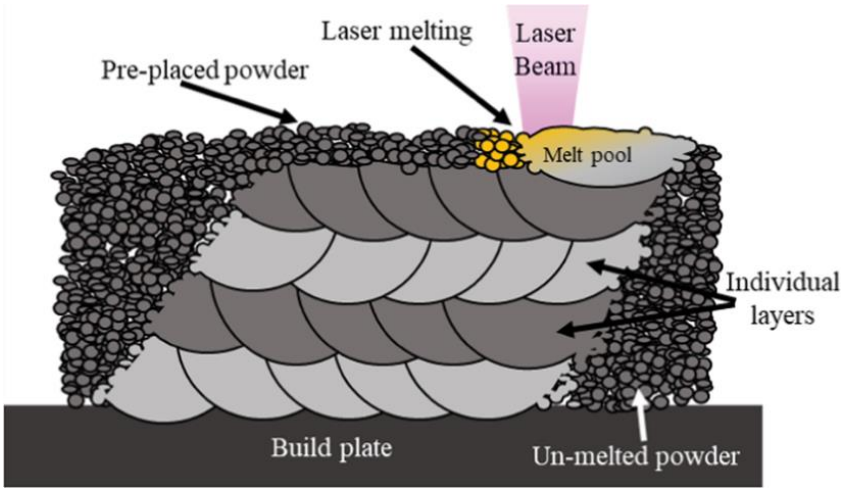

Figure 4: A cross-sectional schematic view of the layer-by-layer PBF-LB/M process. Reproduce from (Melia et al., 2020), which is published under the license of CC BY 4.0 DEED.

As can be seen in Figure 4, the cross-sectional schematic view of the process of laser melting in action with layer-by-layer PBF-LB/M process (Melia et al., 2020). In this technique, a laser beam is precisely focused on pre-placed powder, causing it to melt and solidify. This process is repeated layer by layer, resulting in the creation of complex three-dimensional structures. Figure 4 also highlights the melt pool, individual layers, and the un-melted powder that can be reused. Every layer is typically 20 to 80 µm thick (KDM Fabrication, 2023). Thinner layers offer higher resolution and finer details. However, they may increase printing time and cost, while thicker layers can speed up the process but may result in lower surface quality and resolution. Figure 5 illustrates the PBF-LB/M process (Huber et al., 2018) for constructing components, beginning with design, and concluding with post-processing.

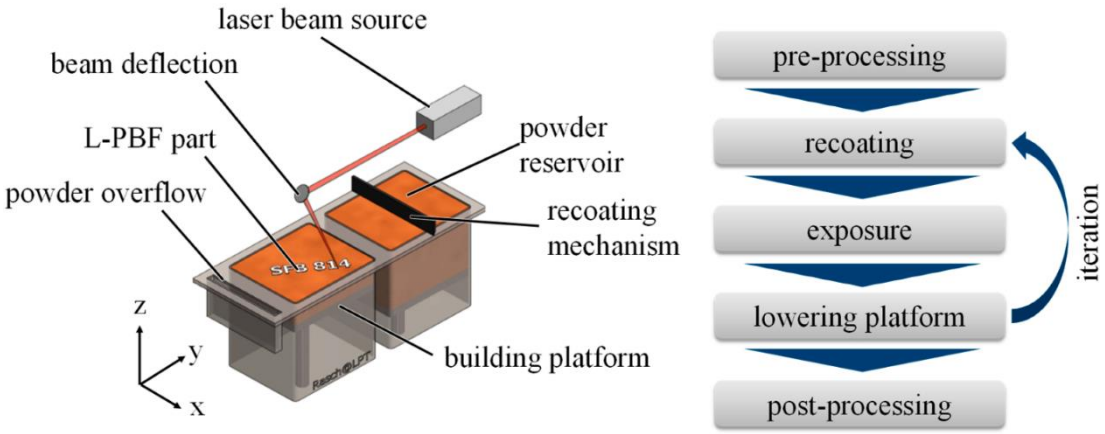

Figure 5: Schematic of the (PBF-LB/M) process. Reproduced from (Huber et al., 2018) under license of CC BY 4.0 DEED.

As Figure 5 shows, the build platform is coated with a thin layer of powder by the recoating mechanism before the process begins. Next, following the layer design, a laser melts this powder selectively to produce the solid AMed part. Layer by layer, until the component is finished, the build platform is gradually lowered to create a place for the subsequent powder layer after each fuse. The overflow reservoir is used to gather extra powder for later usage. The procedure is a meticulous iteration of spreading powder, fusing it with a laser, and lowering the platform until the object is fully formed.

The AMed parts may undergo various post-processing procedures to enhance their mechanical qualities and reduce internal tensions. It may include removing excess powder, treating heat to relieve internal tensions, and completing the surface to achieve the desired quality. These

measures are crucial to ensuring that the finished product satisfies the standards and requirements relevant to its intended usage.

2.2. Technological challenges in PBF-LB/M

Despite the advancements in PBF-LB/M technology, several challenges, as compiled in Figure 6, hinder its more comprehensive implementation and improved performance.

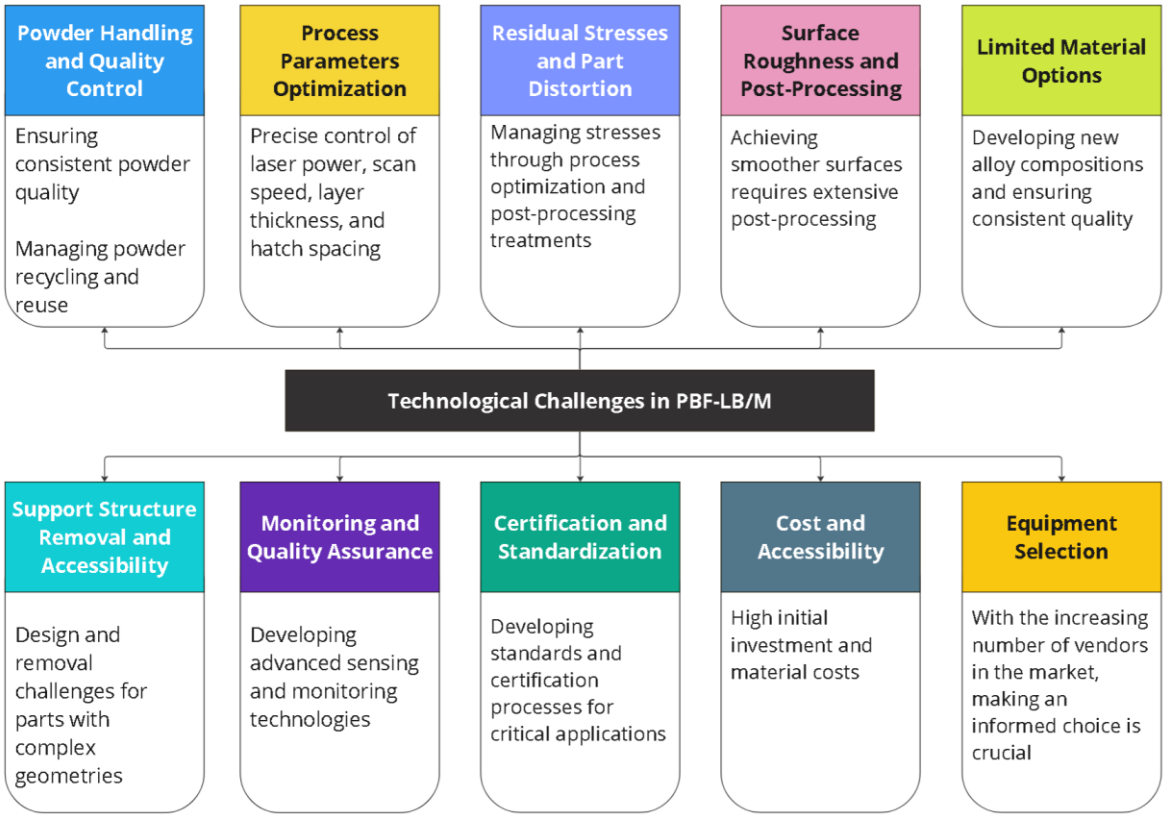

Figure 6: Summary of technological challenges in PBF-LB/M

As seen from Figure 6, several challenges include maintaining the quality and uniformity of the metal powder (Vock et al., 2019), accounting process parameters to attain the required mechanical properties and precision (Martucci et al., 2022), controlling residual stresses and part distortion (Bartlett & Li, 2019) resulting from fast thermal cycles, and addressing surface roughness (Ertürk et al., 2023) through post-processing and developing in-situ monitoring and quality assurance techniques (Spurek et al., 2022), designing and removing support structures (Piili, 2023), broadening the range of appropriate materials (Metal AM magazine, 2023) while maintaining quality, navigating the challenges of certification and standardization (ISO, 2023)

for crucial applications, and overcoming the high costs associated with materials and equipment (Bernsmann et al., 2023).

In addition to the challenges faced in PBF-LB/M, including design complexity, process stability, material characteristics, and scalability of production processes (W. Zhang et al., 2020), the abundance of new technologies from various manufacturers introduces several complexities. These demand ongoing research and development efforts for resolution, especially as PBF-LB/M applications diversify to cater to users with varying levels of expertise.

The decision regarding PBF-LB/M equipment or services is critical and can significantly impact how well AMed parts turn out. With a growing number of suppliers on the market, choosing necessitates carefully weighing various aspects to ensure vendors' capabilities match the unique requirements of projects. When selecting a PBF-LB/M machine, a shop floor with multiple technologies will need to provide the geometrical evaluation of the AMed part more attention.

2.3. Benchmarking in additive manufacturing

Minimizing fluctuations in quality metrics, such as dimensional tolerances, surface roughness, material consistency, and others, is a crucial requirement for the progress of AM technologies. Although several process measuring methods have been created and showcased for PBF/L-M, the main difficulty is still in analyzing and interpreting these measurements (Spears & Gold, 2016). Two main approaches are employed in manufacturing metrology to assess a machine and a process performance: (1) measuring various aspects of the machine and process directly and (2) measuring made test artifacts (Moylan et al., 2012).

This is where benchmarking in AM is significant. Test artifacts have been utilized to assess specific procedures (Chua et al., 2017) or to compare the same processes on different machines (Byun & Lee, 2005) to ascertain which methods are best suited for a given set of applications. The number of machine platforms manufacturers offer for the same process has increased with growing AM acceptance and capacity. This makes a comparison of their respective processes' capacities necessary. Typically, the test artifact has specific characteristics that enable the measurement of various process attributes (Chua et al., 2017). While benchmarking has been gaining relevance for over a decade, there is still a lack of standardized generic benchmark parts (Moshiri et al., 2019).

2.4. Types of benchmarks

A classification system for benchmark artifacts in AM processes was proposed two decades ago. The system categorizes the artifacts into three main groups based on their primary purpose (MANI MAHESH, 2004; Rebaioli & Fassi, 2017), as illustrated in Figure 7.

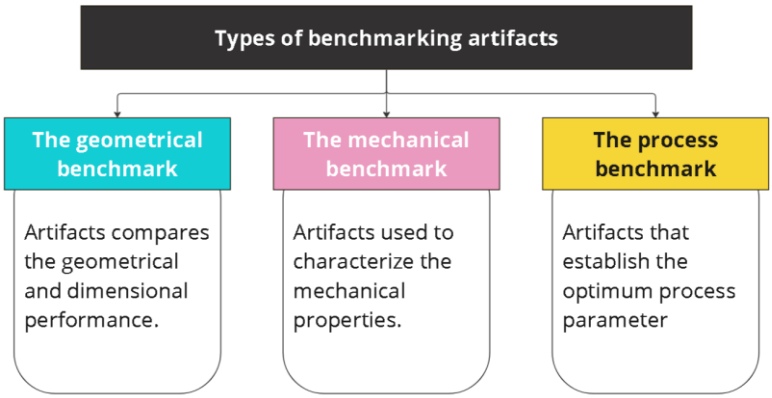

Figure 7: Types of benchmarking artifacts.

As can be seen in Figure 7, the first group is the geometrical benchmark, which compares only geometrical and dimensional performance. The subsequent group is the mechanical benchmark, which characterizes the mechanical properties. The last group is the process benchmark, which consists of artifacts that establish the optimum process parameters.

While test artifacts have been employed for assessing AM systems since the early 1990s, over 65 artifacts have been utilized until 2021 (Taylor et al., 2021). Ongoing research and development efforts in additive powder bed fusion with laser (PBF-LB/M) focus on improving the understanding of the process, guaranteeing quality, and producing standardized test objects. The resulting data is disseminated through AM Bench Data Management Systems, developed by NIST AM (NIST, 2023).

It is well known that in most AM processes, AMed part geometry has the most impact on building time, surface quality, and final part accuracy (Xu et al., 2001). Since this thesis mainly focuses on the first benchmark group related to geometrical benchmarking, three primary characteristics of AM technology can be precisely evaluated by the benchmark artifacts for geometrical performance determination: dimensions or geometrical accuracy, repeatability, and minimum achievable feature size. (Rebaioli & Fassi, 2017).

2.5. Design of PBF-LB/M benchmark artifacts

In 1992, Kruth introduced the first benchmark artifact for evaluating AM accuracy to evaluate the overall effectiveness of various AM approaches (Kruth, 1991; Rebaioli & Fassi, 2017), and several attempts to create a standard artifact for diverse uses have been made since then. This NIST AM project aims to advance measurement science, standards, and technology to support the widespread adoption of metal-based additive processes in the United States. It has been working on this project and developing various standards, but the test artifact is still not an ASTM standard (Moylan et al., 2012). The test artifact is under consideration by the F42 committee and is being further developed (NIST, 2023).

Despite different benchmark designs, every AM test artifact documented in the literature has standard ground rules. Commonalities are expected since many researchers were influenced by the "rules" proposed by Richter and Jacobs, and most studies build on the findings of earlier work (Richter, 1991).

A standard benchmark should be able to highlight defects and limits in a machine or process and tie those limits and restrictions to the system features (Chua et al., 2017). The test artifact may include feature duplicates to enable repeatability and assess the processing capacity to produce the same characteristics at several locations.

The following guidelines apply for creating any benchmark, per the literature (de Pastre et al., 2020; Moylan et al., 2012):

1. *Sufficiently large to assess machine performance at both the periphery and center of the building volume.*
2. *Features a diverse array of small, medium, and large geometry.*
3. *Includes various holes and bosses for beam width compensation verification.*
4. *Designed for a reasonable build time with minimal material usage.*
5. *Straightforward to measure.*
6. *Encompasses a broad spectrum of actual part features, such as thin walls, flat surfaces, and holes.*

Furthermore, recommendations have been made regarding the geometric forms to be incorporated into the benchmark on all axes (Byun & Lee, 2003; de Pastre et al., 2020). These shapes should incorporate features utilized to ascertain the minimum possible feature size, as illustrated in Figure 8.

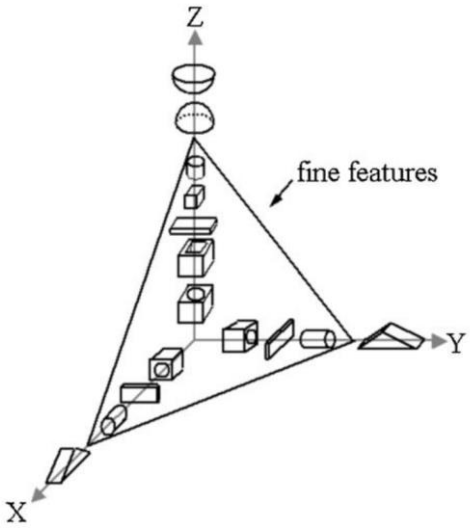

Figure 8: Definition of axis-aligned features. Reproduced from (Byun & Lee, 2003; de Pastre et al., 2020) with permission from Springer Berlin Heidelberg

Figure 8 shows the features that can be included in the test phase of the artifact design process for the geometrical approach for benchmark artifact design (Byun & Lee, 2003).

Though PBF-LB/M offers flexibility in manufacturing parts, it is essential to note that this does not provide unrestricted freedom to create any shape imaginable. As covered in the following chapters, there are some limitations to design that are exclusive to this thesis and some that are conventional and created through various research projects as discussed in (Kranz et al., 2015; Protolabs Network, 2024.; Renishaw plc, 2014). These limitations encompass a range of design considerations crucial to utilizing the full potential of PBF-LB/M, highlighting the need for a deep understanding of the capabilities and limitations of technology.

Many recommended features can be designed to evaluate the main geometrical tolerances (de Pastre et al., 2020; Moylan et al., 2012; Rebaioli & Fassi, 2017) with some of them listed in Table 1.

Table 1: Measure of geometrical tolerance in the benchmark. Geometric features are to be included in benchmark artifacts (de Pastre et al., 2020; Moylan et al., 2012; Rebaioli & Fassi, 2017).

Geometrical tolerance	Features considerations
Flatness	Cubes, slots, rectangular bosses, thin walls, base surface
Straightness	Cubes, slots, rectangular bosses, thin walls, base surface
Circularity	Circular holes, cylinders, round holes, bosses, and tubes (in multiple directions)
Parallelism	Cubes, rectangular bosses and holes, thin walls, square holes
Perpendicularity	Cubes, circular bosses and holes, square holes
Cylindricity	Circular holes, solid and hollow cylinders
Angularity	Inclined surfaces, tilted surfaces, angles
Position	Holes, cylinders, side notches (such as those seen in Figure 8)
Profile	Spheres, hemispheres, cones
Concentricity	Circular holes and bosses
Minimum feasible size	Fine features, holes, pins, thin walls, freeform structures, towers (higher aspect ratio than vertical bosses)
Additional Features	Rectangular holes, bosses, and tubes (in multiple directions), conical bosses, L-shaped bosses, ramps, overhangs

Table 1 outlines geometric tolerances crucial for benchmarking in additive manufacturing and combines the geometric shapes recommended in various literature studies (de Pastre et al., 2020; Moylan et al., 2012; Rebaioli & Fassi, 2017). It shows geometrical features like flat surfaces, straight edges, circular holes, and angles, which can be assessed for geometric qualities such as flatness, straightness, and circularity.

These geometric shapes ensure that the PBF-LB/M process can meet the required tolerances for different types of geometric features. This is critical when selecting a machine for specific manufacturing tasks. Comparing the capabilities of other machines against these geometric benchmark artifacts helps make informed decisions.

2.6. Review of PBF-LB/M benchmark artifacts

There are several designed artifacts in the literature in the last two decades, and some of the PBF-LB/M benchmark artifacts are compiled in Table 2.

Table 2: Summary of PBF-LB/M benchmarks. Evaluation type, design, material, dimension, and designer reproduced from (Rebaioli & Fassi, 2017) under permission of Springer-Verlag London

Reference	Test	Dimensions	Material Tested	Design
(J. Kruth et al., 2005)	DA, MFS	Overall dimensions 50 mm 50 mm 9 mm	Polymer-coated stainless steel Tool steel, stainless steel 316 L, bronze	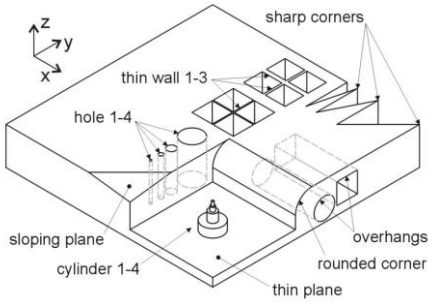
(Laura Castillo, 2005)	DA, MFS	Overall Dimensions 60 mm 100 mm 81 mm	AISI 420 steel AISI 316 L steel, TiAl6V4	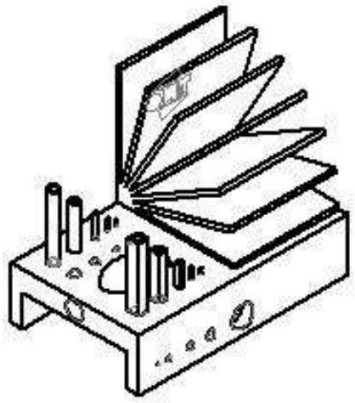
(Luisa et al., 2010)	MFS	Overall dimensions 70 mm 70 mm 25 mm	18 Ni Marage 300 steel	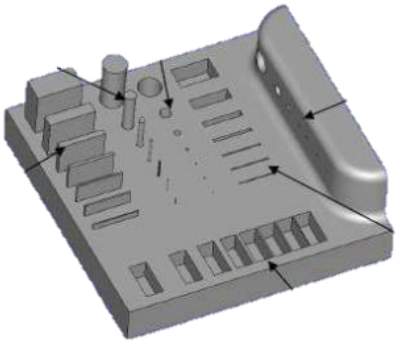
(Kniepkamp et al., 2016)	DA	Overall 5mm max 0.1mm min	316 L steel	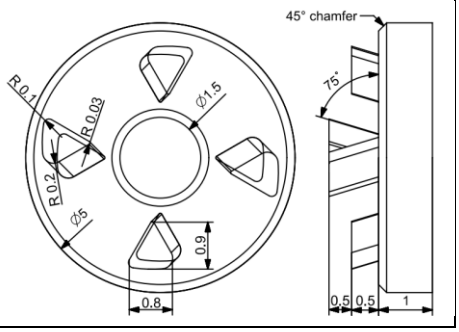

Reference	Test	Dimensions	Material Tested	Design
(Sercombe & Hopkinson, 2006)	DA	Overall dimensions 90 mm 90 mm 105 mm	Aluminum powder with nylon	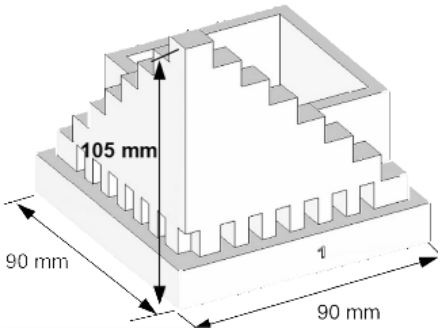
(Delgado et al., 2010)	Rep	Overall dimensions 20 m 20 mm 20 mm	Direct Metal 20 (bronze-based powder with nickel)	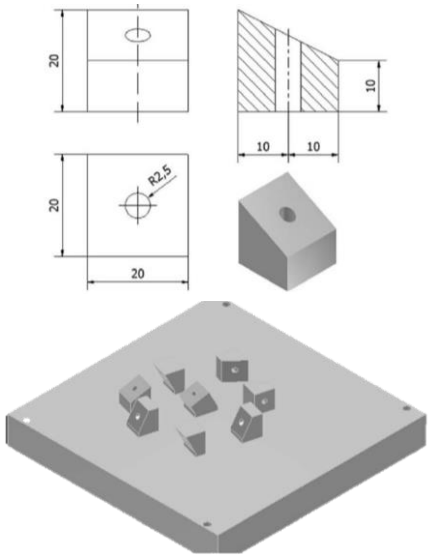

Each of the benchmarks illustrated in Table 2 is marked with type of geometrical performance tested for in terms of dimensional accuracy (DA), repeatability (Rep), and minimal feature size (MFS), which eventually paved the way for the design of the benchmark for this thesis.

To evaluate the dimensional accuracy along the X, Y, or Z directions, the features are created with alignment along all machine cartesian axes in mind. In addition, considering the chosen measuring system, the features were arranged to allow and facilitate the measurement process. Based on these criteria, a suitable benchmark artifact can be created to assess the relevant performance metrics (Rebaioli & Fassi, 2017).

2.7. Data-driven decision-making in manufacturing

The selection of appropriate AM technology stands as a critical decision, exerting a reflective influence on the operational efficacy and performance outcomes of AMed products. This decision-making process is notably complex, further compounded by the expansion of diverse AM technology companies and third-party material providers offering various technologies,

materials, and machine specifications (Ransikarbum & Khamhong, 2021). As such, data-driven decision-making is essential to making well-informed decisions about AMed products before fabrication.

Over the past two decades, numerous methodologies have been employed to navigate the selection of AM technologies tailored to specific objectives. Apart from the Table 2 summary of artifacts, the literature has extensively covered the selection of the optimal AM technology to date. A comprehensive overview of some of these methodologies to evaluate the AM technology is provided in Table 3 (Pouti, 2022);

Table 3: AM technology selection frameworks. Summary of the methodology used to select suitable AM technology using several criteria (Pouti, 2022; Zheng et al., 2017)

Reference	Method	Criteria used for decision-making
(Mahesh et al., 2005)	Fuzzy logic rules	Surface finish, resolution, and clarity, feature dimensional accuracy, mechanical properties
(Ransikarbum & Khamhong, 2021)	Fuzzy analytic hierarchy process and TOPSIS	Product, material, machine characteristic
(Y. Zhang et al., 2014)	Measuring the amount of knowledge	Surface finish, time, cost, overall dimensional Accuracy, mechanical properties
(Mahapatra & Panda, 2013)	Grey relationship analysis	Overall dimensional accuracy, mechanical Property, cost, and time
(Anand & Vinodh, 2018)	Multi-criteria decision-making, TOPSIS, and fuzzy hierarchical analysis	Strength, aspect ratio, speed, roughness and Inequality, minimum size feature, separability, layer, geometric complexity, cost, layer thickness, and material adaptability.
(Lan et al., 2005)	Expert system integrated with fuzzy hybrid evaluation	Surface finish, resolution, overall dimensional accuracy, build envelope, complexity, mechanical property, cost, time, and post-processing.

Table 3 illustrates that several methodologies have predominantly aimed at discerning the optimal AM process or identifying the most suitable technology for achieving the desired results. All the methods studied were merely implemented to choose between suitable AM processes. Still, no frameworks are intended to make it clear to choose between several machines offering identical AM processes (in this thesis case, PBF-LB/M). This shortcoming highlights the necessity for a decision-making framework that combines user input regarding necessary geometrical specifications with data generated from geometric assessments of benchmark artifacts.

2.8. Integration of Fuzzy AHP and TOPSIS for decision making

Various methods can be used to choose between the PBF-LB/M machines based on user input and geometric evaluation of a benchmark artifact. As summarized in Table 3, specific approaches from the literature are better suited to this problem, whereas other methods complicate the decision-making process. The techniques used in Table 3 of the literature can be used for the research problem in this thesis for appropriate decision-making.

The problem of this thesis requires complex decision-making scenarios where multiple criteria must be considered. These criteria have different levels of importance based on user inputs, which may need to be precisely defined. Therefore, Table 4 outlines further explanation to continue analyzing why the literature utilized the specific methodology for decision-making.

Table 4: Comparison of decision-making methodology. The best-suited method is based on the problem to be solved.

Method	When to use	Suitability for this research problem
Fuzzy logic rules	Simple reasoning for decisions with clear if-then statements (Bai & Wang, 2006).	The research problem of multi-criteria complexity might only be fully captured with an extensive rule development process.
Grey relationship analysis	Situations where information is incomplete or ambiguous and to comprehend how variables relate to one another (Nayakappa et al., 2019).	It is only appropriate if it analyzes patterns or relationships in uncertain data to make decisions.
Expert system integrated with fuzzy hybrid evaluation	Complex problems require fuzzy evaluation for uncertainty and expert knowledge encoded into a system (Douligeris, 2001).	It can be appropriate if there is a capacity to encode specialist knowledge necessary for machine evaluation.
Multi-criteria decision-making, TOPSIS, and Fuzzy hierarchical analysis	Scenarios for multifaceted evaluations in which hierarchical criteria analysis informs decisions (Ishak & Wanli, 2020).	It is highly suitable because it integrates ranking (TOPSIS) and hierarchical breakdown (Fuzzy AHP), effectively handling the multi-criteria component of the issue at hand.
Fuzzy AHP and fuzzy TOPSIS	Making complex decisions based on various criteria requires methodical analysis and ranking (Kusumawardani & Agintiara, 2015).	It is highly suitable since it enables complex comparisons and rankings according to performance and weighted criteria.

Table 4 summarizes the literature methodology, the reasoning behind when to use it, and whether it was suitable for this thesis research problem, eventually leading to the selection of the best methodology.

As indicated in Table 4, two approaches multi-criteria decision-making: (i) TOPSIS, and fuzzy hierarchical analysis and (ii) fuzzy AHP and fuzzy TOPSIS) fit perfectly for evaluating multiple criteria and complex trade-offs in the decision-making process. Several variables, user preferences, and an organized method of weighing, evaluating, and classifying the machines according to their geometric performance of various PBF-LB/M technologies can all be included with these two methods.

The first one is the multi-criteria decision-making with TOPSIS (technique for order of preference by similarity to ideal solution) and Fuzzy AHP (Fuzzy hierarchical analysis), which can be one of the methodologies suited for this thesis problem.

However, considering this level of complexity and vagueness of benchmark data, a combination of Fuzzy TOPSIS and Fuzzy AHP (Madanchian & Taherdoost, 2023; Saaty, 2001) seems to be the best alternative. This combination method works well when decisions must be made under vagueness, like choosing the best AM system, where it is necessary to weigh the users' subtle preferences against the capabilities of the machine to determine the best option.

Combining Fuzzy AHP and Fuzzy TOPSIS is also more meaningful since they use Fuzzy pairwise comparisons to establish the criteria weights. The subsequent section of this thesis explains how choosing fuzzy methods (Fuzzy TOPSIS methodology and Fuzzy AHP) enhances their respective classical versions to handle data uncertainty. The ultimate objective of this strategy is to utilize the data gathered on the geometrical benchmark artifact for geometrical accuracy from various PBF-LB/M machines on hand to decide.

3. Aim and purpose of the experimental part

PBF-LB/M is a rapidly advancing technology in the AM field. However, users need data-driven decision-making to choose the appropriate technology available before probing into the complexities of the fabrication of the desired product. This experimental study aims to develop and assess the effectiveness of the benchmarking artifact designed to improve the decision-making process for selecting the most appropriate PBF-LB/M machine. The study focuses specifically on evaluating the geometric tolerances to ensure optimal machine performance. Figure 9 illustrates the visualization of the background summary, the experimental objectives, purpose of the study, and potential future implications.

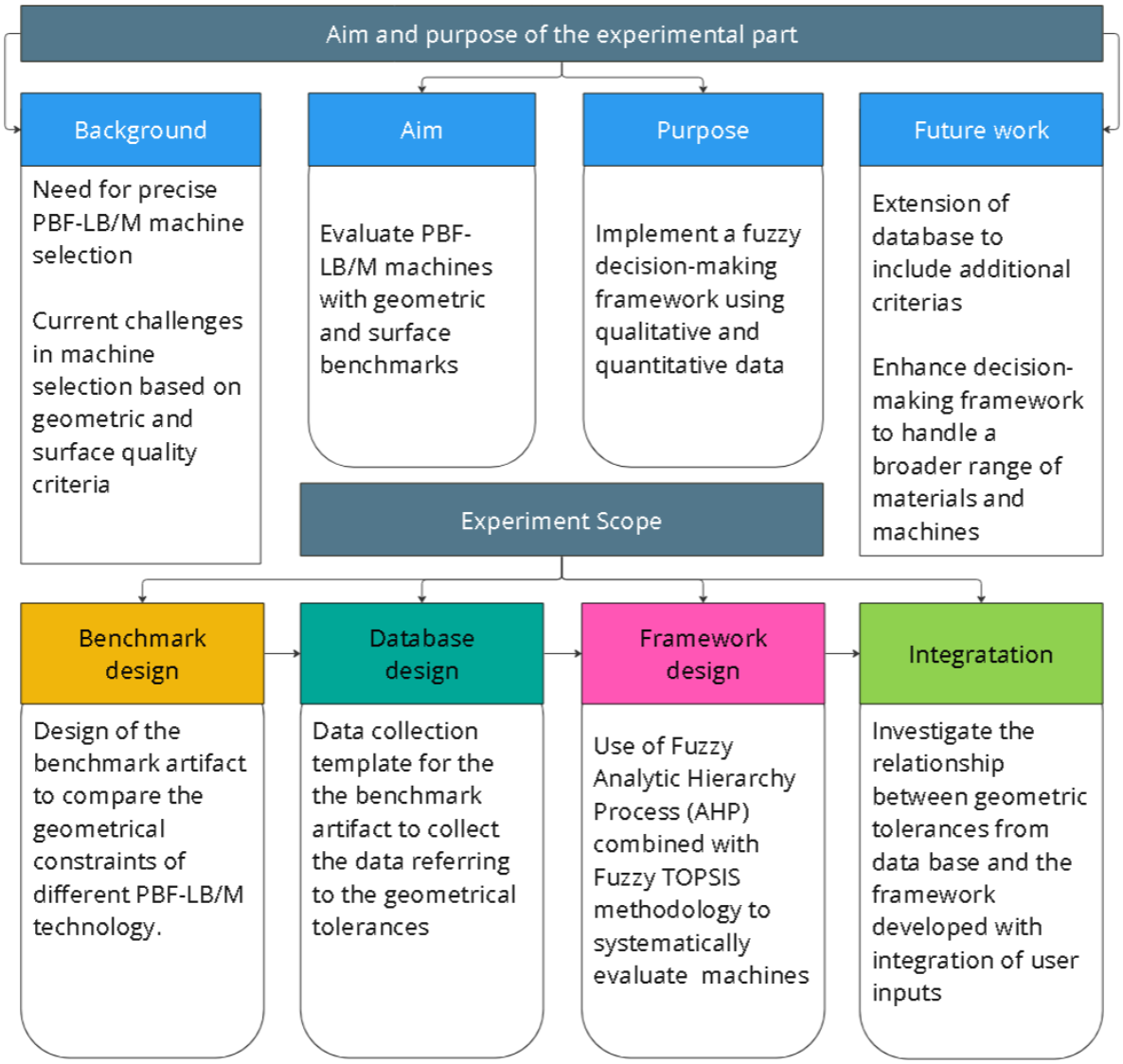

Figure 9: Representation of thesis foundations, dimensions, and prospective utilization of findings.

As shown in Figure 9, the aim and purpose are carried out within the scope of the thesis experiment phase, which covers the four essential components from the benchmark design to the decision-making process. Figure 9 also details the procedures undertaken in the experimental phase for creating a framework. This framework integrates the geometric benchmark database with the design for user input in weighted decision-making using the multi-criteria decision-making technique.

It includes data gathering and framework development to attain valued information for making educated decisions. The integration and data gathering are vital for determining how the framework will provide outcomes favoring a specific PBF-LB/M technology. This is where Fuzzy AHP and the Fuzzy TOPSIS methodology are used to evaluate machines analytically.

The experiment part aims to address the background research gap. However, with the current limitation of experimental scope only to geometrical benchmarks, future work requires expanding this framework to address increasingly complicated scenarios and to accommodate additional criteria based on the parameters of PBF-LB/M and user inputs. The database must be expanded to include more information from the benchmark to improve the quality of curated results.

4. Experimental setup

From the first stages of design concept generation to the final analysis, each stage is crucial and should be built upon to improve the validity and reliability of the findings. Therefore, the experimental setup of this thesis research is divided into multiple discrete phases; each thoughtfully planned to maximize the efficacy of the experimental results.

4.1. Designing and slicing

The designing and slicing of the benchmark artifact involved a multi-software approach to ensure precision in design and AMed compatibility with different additive manufacturing machines.

4.1.1. SolidWorks

SolidWorks from Dassault Systèmes was utilized to design a detailed 3D CAD model of the benchmark artifact. SolidWorks is widely recognized for its user-friendly interface and powerful engineering capabilities, making it ideal for creating detailed, complex 3D models required in additive manufacturing (Dassault Systèmes, 2024). It allowed intricate design specifications to be met with high accuracy, ensuring that the initial benchmark design was robust and fully detailed for AMed.

4.1.2. Autodesk Netfabb and EOSPRINT

Slicing and preparation of the models for additive manufacturing were carried out using Autodesk Netfabb alongside EOSPRINT. These tools optimized the models for additive manufacturing, handling tasks such as orientation, support generation, and slicing, thereby ensuring the models were machine-ready and optimized for the specific capabilities of the additive manufacturing machines.

EOS uses its native-built software, EOSPRINT, which is crucial for optimizing job and parameter settings in additive manufacturing, especially when using EOS systems. It integrates seamlessly with pre-configured EOS Material Sets, significantly reducing setup time and ensuring consistent, high-quality outputs (EOS GmbH, 2024).

As part of this thesis, it is essential to note that specific parameters used in the EOSPRINT software for slicing the benchmark artifacts were not disclosed and remained confidential

following the company policy. On the other hand, Aconity3D MIDI+ uses Autodesk Netfabb (Autodesk Inc., 2024), a comprehensive additive manufacturing software that streamlines the preparation, optimization, and validation of 3D models before additive manufacturing (Autodesk Inc., 2024).

4.2. Hardware for additive manufacturing

The additive manufacturing machines for this thesis are critical to the success of the experiments and directly impact the quality and effectiveness of the results.

4.2.1. EOS M 290

The EOS M290 is a cornerstone in the PBF-LB/M industry because of its reputation for dependability and adaptability (EOS GmbH, 2024b). Manufacturing superior metal parts with fine detail and flawless surface polish is a good fit for this thesis. Its accuracy and dependability are advantageous for research requiring reliable results across several runs.

4.2.2. Aconity3D MIDI+

The Aconity3D MIDI+ stands out for its modular design, allowing for a high degree of customization to suit specific research needs (Aconity3D, 2024). This machine is perfect for cutting-edge additive manufacturing applications since it can handle a variety of metal powders and intricate geometric shapes. Its versatility is beneficial in areas related to academia and research where experiment flexibility is essential.

4.3. Hardware/software for measurements

Complementing the additive manufacturing machines, a laser 3D scanner was used, a critical step for capturing accurate geometrical data from the AMed artifacts. This tool is essential for validating manufacturing accuracy and providing detailed feedback on the dimensional integrity of each AMed component.

4.3.1. Zeiss T-Scan 20 scanner

The ZEISS T-SCAN 20 is a versatile 3D scanner that delivers precise measurements for various applications, collecting *1312* points per line at a data rate of *210,000* points per second with a measuring volume of up to *20m³*. Its modular design combines a tracking camera and hand-

held scanner, making it ideal for quality control, reverse engineering, and rapid prototyping (Carl Zeiss AG, 2024).

The T-Scan technology has a nominal uncertainty of ± *0.04 mm* and offers a precise means for measuring distances. It comes with Colin3D software, which creates a triangular mesh from the measurement points. This mesh is used for further measurements, such as distances, diameters, and flatness.

4.3.2. Bruker Alicona Infinite Focus G6

The Bruker Alicona Infinite Focus G6 is an optical surface roughness and shape measuring instrument known for its high-resolution, reproducible, and traceable readings by sophisticated optical 3D surface measurement system (Alicona Imaging GmbH, 2024a). In this thesis, the Infinite Focus G6 is primarily used to measure the surface finish produced by additive manufacturing precisely. Its ability to provide detailed surface texture and form measurements makes it invaluable for assessing the quality and accuracy of AMed components.

4.3.3. Geomagic Control X

Geomagic Control X is a leading software platform for 3D inspection and metrology (Oqton, 2024). It is beneficial for processing large datasets efficiently, performing complex alignments, conducting detailed inspections, and producing insightful reports from the mesh obtained from 3D laser scanning. These features enable a thorough and detailed inspection process, allowing for the insights required for this thesis.

4.4. Material for AMed benchmark

316L stainless steel is widely appreciated for its superior mechanical qualities, broad industry applicability, and corrosion resistance (EOS GmbH, 2024). This thesis contains two different 316L stainless steel formulations tailored to the specific technologies employed. EOS stainless steel 316L was used for the EOS M290 machine, a material optimized for the EOS technology, ensuring high-quality AMed parts with fine detail and consistency.

Conversely, the Aconity system 316L, a variant provided by SLM Solutions, was utilized for additive manufacturing benchmark samples.

5. Experimental procedure (Part A: Development)

The development phase is a keystone of the present thesis, with the benchmark design serving as a critical enabler for data generation. This step is crucial as it supports the data-driven decision-making processes that influence the selection of PBF-LB/M technologies. It establishes the foundation for future studies, ensuring that decisions are based on robust logical, quantitative, and qualitative data.

5.1. Initial design of benchmark artifact

The benchmark design requires considering many constraints, including the technology by which it will be fabricated and the general designing guide for AM (Renishaw plc, 2014). These constraints align with the criteria as this benchmark will differentiate between available technologies. The approach used in this benchmark design is to test the limits of the PBF-LB/M technology without fail with the characteristics mentioned in Table 5.

Table 5: PBF-LB/M technology consideration. General specifications of the two machines on which the benchmark artifact will be tested for evaluation(EOS GmbH).

Features	Aconity MIDI+	EOS M 290
Building volume	*Ø 250 mm x H 250 mm*	*250 mm x 250 mm x 325 mm*
Beam focus diameter	*80 µm*	*100 µm*
Thin walls	*160 - 240 µm*	*200 - 300 µm*
Circular holes (diameter)	*120 - 160 µm*	*150 - 200 µm*
Circular pins (diameter)	*120 - 160 µm*	*150 - 200 µm*

Table 5 illustrates the overall build base size, a critical factor to contemplate while determining the overall dimensions of the benchmark. The minimal feature size that these machines can produce depends on many factors. However, the beam focus diameter provides a general starting point for understanding the minimum feature sizes that can be created.

So, the smallest size of a feature or detail that the machine can reliably produce is related to focus diameter. The assumption is that the laser beam focus diameter is usually bigger than the smallest size due to limits from process dynamics and material properties. If a machine has a spot size of 100 µm, the smallest diameter of a circle it could generate would typically need to be at least *1.5x to 2x* the spot size to guarantee a completely formed feature. The minimal diameter would range from around *150-200 µm*; however, this is a preliminary estimate and may vary based on other factors.

Similarly, the minimum achievable wall thickness is significantly larger than the spot size. The melting and solidification dynamics influence the wall thickness, which may lead to the material spreading slightly beyond the focal point of the laser. Manufacturers target wall thicknesses *2* to *3* times the spot size for high-precision applications to guarantee structural integrity and reliability. Hence, using a spot size of *100 μm,* a suitable minimum wall thickness could range from *200-300 μm* or slightly more, following the material and machine settings.

Keeping the constraints of the minimum features in focus, the next crucial thing was to fix the limitations on the design of the benchmark artifact. Table 6 summarizes the additional features of the constraints kept in mind, along with their reason for the specific feature in the artifact design.

Table 6: Benchmark artifact constraints. Constraints kept into consideration while designing the benchmark artifacts with some relevance taken from (Taylor et al., 2021)

Feature	Constraint	Reason
Artifact dimension	Consistent with under-observation PBF-LB/M machine build plates	Ensures artifacts can be AMed for repeatability tests across different equipment.
Placement consistency	AMed artifacts at multiple locations on the build plate per test	Aids in assessing the repeatability of artifact production within a single machine.
Artifact design	Flat surfaces on each side for secure handling	Facilitates consistent gripping and precise cross-sectional analysis.
No fail test	Varying complexity in design features	Tests the capability of machines to render complex geometries without failure accurately.
Central feature	Markers to define the center for measurement	Enables exact determination of the artifact center for investigative comparison.

Table 6 combines the constraint with the reasoning used for the geometrical benchmark designed for this thesis. The design is carefully customized to achieve a high success rate in testing, with a minimum dimensional accuracy for features set at 0.4 mm, as recommended in the general design guide of AM (Protolabs, 2024.; Renishaw plc, 2014). Avoiding the failure test was preferred since assessing such geometrical tolerance only provides limited information based on pass/fail criteria.

The benchmark design consists of many features, and each feature in the benchmark is strategically positioned to avoid the impact of thermal distortion that may arise from neighboring features, a precaution based on a review of the existing literature compiled in Table 2. This careful positioning ensures that the heat transfer from one feature does not affect the

integrity of another, which is especially important for features on the lateral sides, which are designed without any superimposed elements to prevent heat-induced distortion from upper layers. Table 7 combines all these features and the identification scheme for benchmark design.

Table 7: Benchmarking artifact feature descriptions

Dimensions of every feature design on the benchmark, with a description and labels with some relevance taken from (Cruz Sanchez et al., 2014).

ID	Category	Feature reference	ID	Description	Accuracy
A	Long thin wall	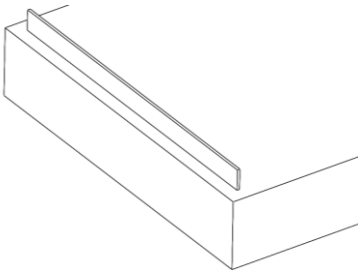	A1	Thickness 0.4 mm, Height 3 mm, Length 46 mm	Residual stress
B	Through holes	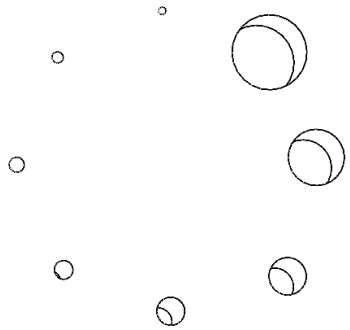	B1–B9	Diameters: B1 = 6 mm, B2 = 4 mm, B3 = 3 mm, B4 = 2 mm, B5 = 1.5 mm, B6 = 1 mm, B7 = 0.8 mm, B8 = 0.5 mm, B9 = 0.4 mm	Diameters
C	Notches		C1–C6	Sizes: C1 = 0.5 mm, C2 = 1 mm, C3 = 1.5 mm, C4 = 2 mm, C5 = 3 mm, C6 = 4 mm	Normal and thin notches
D	Concentric cylindrical boss	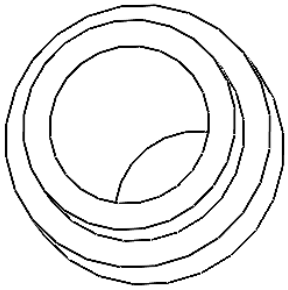	D1–D2	D1 = Ø 10 mm, D2 = Ø 8 mm	Diameters

ID	Category	Feature reference	ID	Description	Accuracy
E	Square boss extrudes	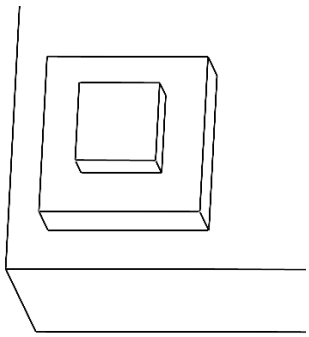	E1–E2	E1 = 8x8x2 mm, E2 = 4x4x2 mm on top	Dimensional accuracy XYZ plane
F	Positive staircases	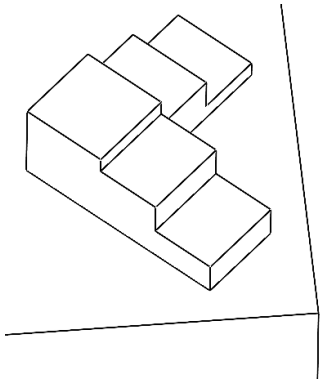	F1–F5	Heights: F1 = 5 mm, F2 = 4 mm, F3 = 3 mm, F4 = 2 mm, F5 = 1 mm, Width: 5 mm	Dimensional accuracy XYZ plane
G	Negative staircases	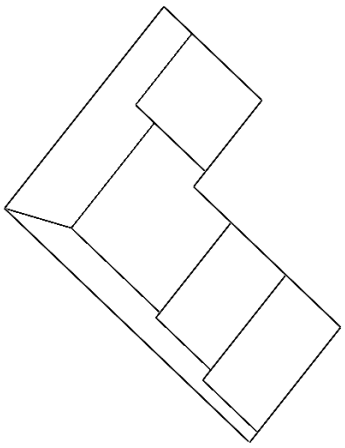	G1–G5	Heights: G1 = 5 mm, G2 = 4 mm, G3 = 3 mm, G4 = 2 mm, G5 = 1 mm, Width: 5 mm	Dimensional accuracy XYZ plane
H	Hemisphere	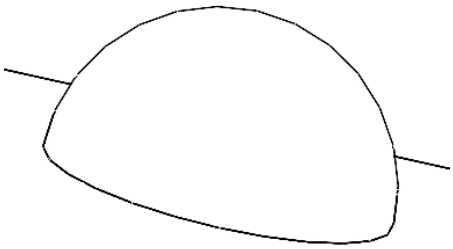	H1	Ø = 7 mm	Blends
I	Lateral features		I1–I9	Circles: I1 = Ø 0.4 mm, I2 = Ø 0.5 mm, I3 = Ø 1mm,	Diameters

ID	Category	Feature reference	ID	Description	Accuracy
				I4 = Ø 2 mm; Squares: I5 = 1x1, I6 = 4x4 Diamonds: I7 = 45° 3 mm z-axis, I8 = 60° 3 mm z-axis, I9 = 30° 0.8 mm z-axis Depth: 5 mm	
J	Slots	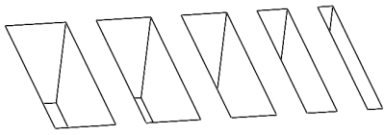	J1–J5	J1 = 2 mm, J2 = 1.5 mm, J3 = 1 mm, J4 = 0.5 mm, J5 = 0.4 mm Depth: 5 mm	Normal and thin slots
K	Thin walls	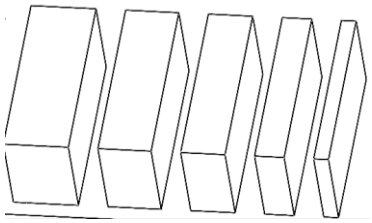	K1–K5	K1 = 2 mm, K2 = 1.5 mm, K3 = 1 mm, K4 = 0.5 mm, K5 = 0.4 mm	Dimensional accuracy XYZ plane
L	Crosses	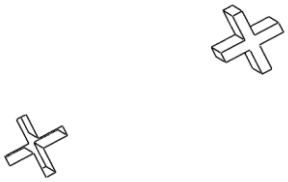	L1–L4	Outward: L1 = 0.4 mm, L2 = 0.5 mm; Inward: L3 = 0.4 mm, L4 = 0.5 mm Depth: 3 mm	Structural crosses
M	Inclinations	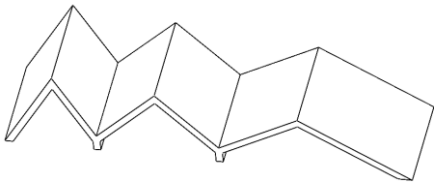	M1–M3	M1 = 45°, M2 = 60°, M3 = 30°	Overhangs
N	Pins and circular boss	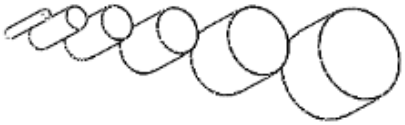	N1–N6	N1 = Ø 3 mm, N2 = Ø 2.5 mm N3 = Ø 1.5 mm N4 = Ø 1 mm N5 = Ø 0.5 mm N6 = Ø 0.4 mm	Diameters

ID	Category	Feature reference	ID	Description	Accuracy
				Depth: 5 mm	
O	Outer dimensions	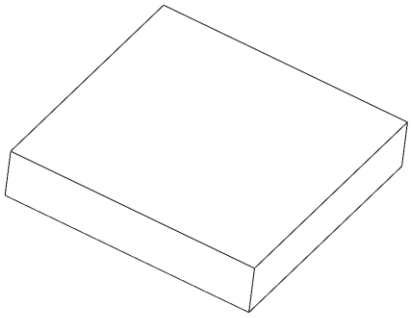	O	50 × 50 × 10 mm	Dimensional accuracy XYZ plane

The benchmark analogy consists of features with a dimensional range of 0.4mm to 50mm, allowing for a thorough examination of the geometric capabilities of the selected PBF-LB/M technology. For a detailed overview of the benchmark features, Table 7 offers insights, complemented by the visual aids of Figure 10 and Figure 11.

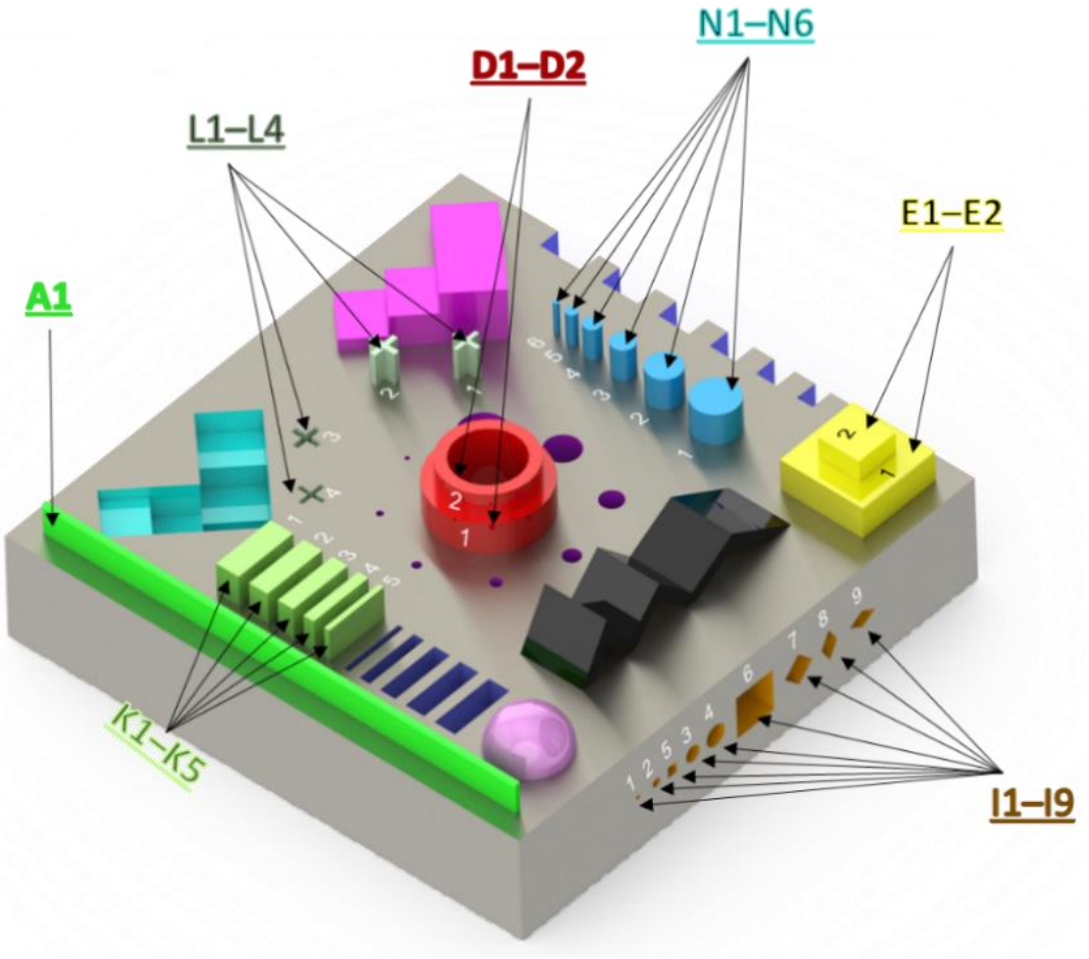

Figure 10: Benchmark artifact feature identification part A.

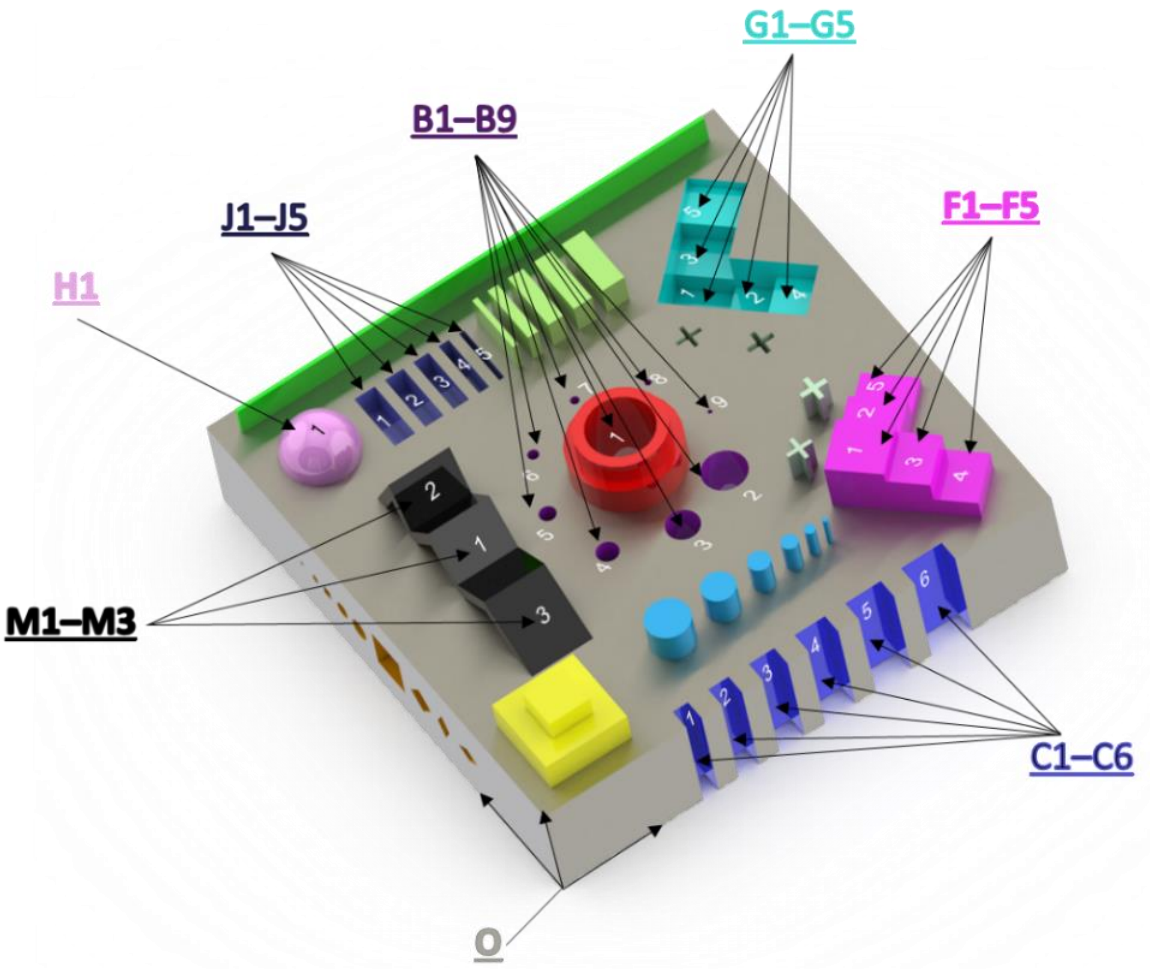

Figure 11: Benchmark artifact feature identification part B.

Figure 10 and Figure 11 illustrate a color-coded scheme to enhance comprehension and ease the identification of specific features relevant to the geometric tolerance data gathering. Table 7, along with Figures 10 and 11, provides a comprehensive overview of the features incorporated into the benchmark design. The features are assigned IDs from A to O, corresponding to their respective categories, with shapes in the third column of Table 7. Each feature within a category is sequentially numbered, starting from 1 to the total number of features in that category.

For insistence, ID "K" pertains to rectangular bosses, encompassing five features K1–K5, each distinguished by size and thickness as detailed in the description. These features are primarily employed to assess dimensional accuracy along the XY plane or the Z axis, providing insightful data to consider the precision capabilities of the PBF-LB/M technology.

For another illustration, ID "N" relates to the category of pins and circular boss, encompassing six features N1–N6, each distinguished by a change in the diameter as detailed in the

description. These features are used to distinguish between the ability of PBF-LB/M machines to make the dimensions of various dimensions accurately.

The process of measuring these features and obtaining valuable data from the benchmark artifact is crucial, and a template for gathering the data is to be made to have a uniform depiction of the measurements to be taken, as further explained in the following parts.

Figure 12 illustrates the complete design of a geometrical benchmark, which boasts straightforward, simplified geometries that avoid the complexity of overlapping features on top of each other, except for those created through multistage extrusion processes.

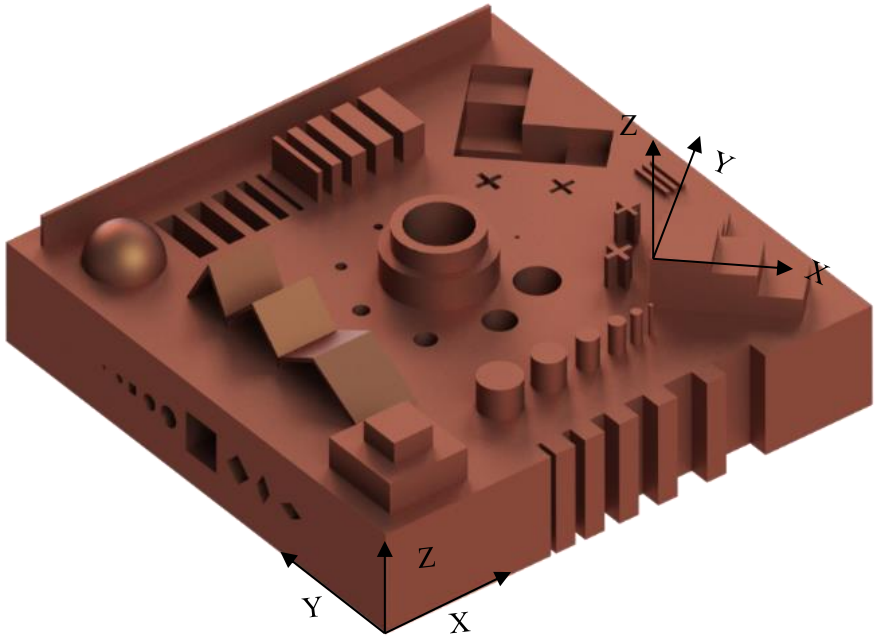

Figure 12: Proposed benchmark artifact CAD design with some relevance taken from (Cruz Sanchez et al., 2014; Moshiri et al., 2019; Moylan et al., 2012).s

The design shown in Figure 12 also includes several lateral features to test the accuracy in different dimensions, as explained in Table 7. Additionally, it is designed to be AMed independently without supporting structures, facilitating a streamlined manufacturing process. The benchmark design in Figure 12 also aligns with the established criteria detailed in Table 1, which outlines various feature considerations for assessing different geometric tolerances. For an in-depth examination of the dimensional features of the benchmark, refer to Appendix 1, which contains the dimensional drawing of the benchmark artifact.

5.2. Evaluation strategy of benchmark artifact

The measurements from the benchmark are the most critical for the database and will pave the way for deciding the preference of one PBF-LB/M technology over the other. The data that needs to be collected from the benchmark is divided into four general aspects in Table 8 to clarify how it will contribute to the decision-making process.

Table 8: Evaluation criteria of benchmark artifact. General aspects will benchmark the artifact through different measurement methods (Moshiri et al., 2019).

General Aspect	Specification	Measurement Method	Desired Outcome
Accuracy	Dimensional accuracy	Precision measuring tools (e.g., 3D laser scanner, CMM) are used to compare against CAD dimensions.	Within ±0.05 mm
	Surface roughness	Focus-variation principle through optical 3D surface measurements.	High similarity
	Feature reproducibility	Production of various samples of artifacts in the middle of the build plate in different directions to measure variance, aiming to minimize the influence of re-coater variability.	Consistent reproduction
Thin features	Complexity handling	Evaluation of the fine details of the artifact and its complex geometries.	No defects in complex areas
Residual stresses distortion	Distortion measurement	Analysis of part curl up at the edges	Homogenous distribution of residual stresses
Built speed	Time required	Time required to produce the artifact	Less the better

The aspects shown in Table 8 portray the true characteristics of the benchmark usefulness in measuring the capabilities of the machine. As this benchmark is used only for geometrical tolerances, the four aspects of accuracy, fine features, residual stresses, and built speed indicate how the machine performs in this category.

Accuracy encompasses three key aspects: dimensional accuracy, surface roughness, and feature reproducibility, each defined by specific criteria. Dimensional accuracy involves comparing the measurements of various features to their nominal values as specified in CAD designs, ensuring the AMed part matches the intended geometry. On the other hand, surface roughness evaluates surface texture by detecting flaws or deviances from an utterly smooth plane. Finally, to assess feature repeatability, multiple samples can be generated concurrently. This ensures that the machine consistently replicates complex features throughout. This three-way method of

assessing accuracy is essential for verifying the accuracy and dependability of the PBF-LB/M process.

The capacity of the machine to articulate features, mainly when the re-coater direction significantly impacts PBF-LB/M and ensures a uniform layer thickness for every laser pass, is known as the repeatability element. The direction in which this recoating takes place might affect the AMed part in several ways. The accuracy of the dimensions may be impacted by how precisely the re-coater applies the powder. Variations in direction may result in uneven recoating, producing layers with different thicknesses and compromising the overall geometric accuracy. This is where measurements from various features across several samples AMed in different directions on the same build plate provide valuable information for making decisions.

The fine features group in Table 8 evaluates the complex details and intricate geometries of the artifact. This group measures a variety of geometries to document deviations from nominal values.

The residual stress group is not the actual measure of residual stress, but it results from the distortion from the fine long features on the benchmark. Residual stress in PBF-LB/M can be harmful since it can cause the parts to deform and curl up at the edges because layers are added on top of one another. Larger cross-section features tend to have longer weld tracks and more room over which the shear stresses can act. Hence, these effects are more noticeable in these elements. A layer of metal layered on top of it cools and hardens, and because the solid structure underneath confines the new metal, shear forces are created between the layers when they contract (Renishaw plc, 2014). Residual stresses in thin sections can cause warping or distortion. To quantify the impact of this distortion, the evaluation of the longest thin feature gives a meaningful result. The assigned ID mark "A1" is shown in Table 7. The degree of deviation caused by residual stresses can be determined by comparing the parallelism of this thin feature to the opposing parallel wall.

The duration of time needed to AMed the artifact is represented by the final group-built speed in Table 8. Before beginning the process of producing the part, the time when the artifact is being produced can assist in making informed decisions.

The challenging portion was developing a consistent method for recording the measurements once it was determined which set of measurements would be obtained from the benchmark under which conditions. This is the point at which the identification of features in Table 9 was

created to provide accurate data for feature geometrical tolerances measurements in the benchmark.

Table 9: Benchmarking artifact dimensional accuracy. Features ID corresponding to the accuracy it will measure with relevance taken from (Cruz Sanchez et al., 2014).

Dimensional Accuracy	Feature ID	Description
X-Y plane	A1, E1, E2, F1, F2, F3, F4, F5, G1, G2, G3, G4, G5, K1, K2, K3, K4, K5, O	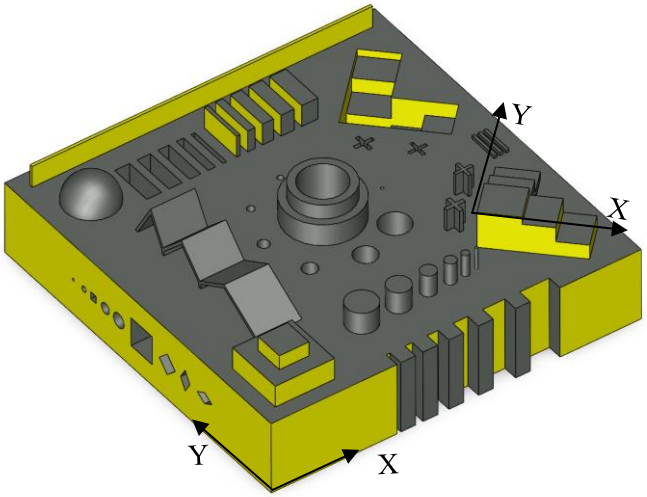
Z plane	D1, D2, E1, E2, F1, F2, F3, F4, F5, G1, G2, G3, G4, G5, H1, I5, I6, I7, I8, I9, K1, K2, K3, K4, K5, M1, M2, M3, O	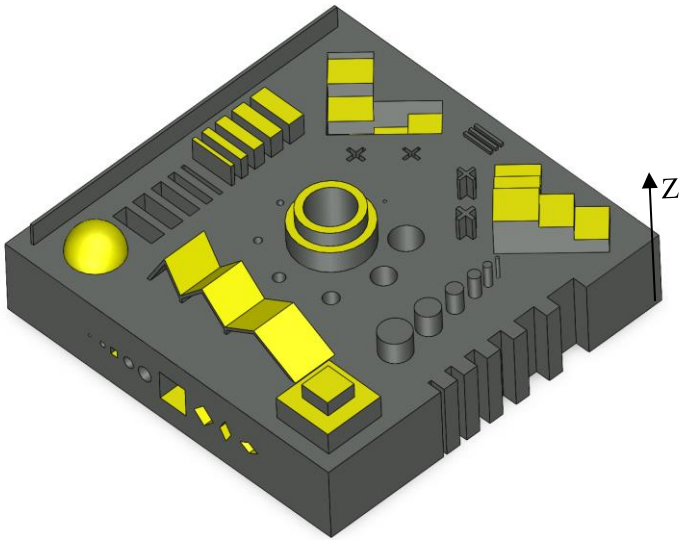

Dimensional Accuracy	Feature ID	Description
Diameters	B1, B2, B3, B4, B5, B6, B7, D1, D2, I3, I4, N1, N2, N3, N4, N5	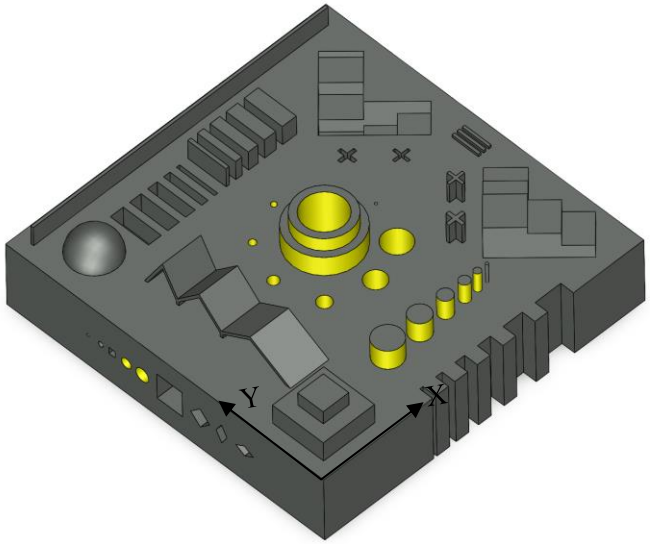
Thin features	B8, B9, C1, C2, C3, C4, C5, C6, I1, I2, J1, J2, J3, J4, J5, L1, L2, L3, L4, N6	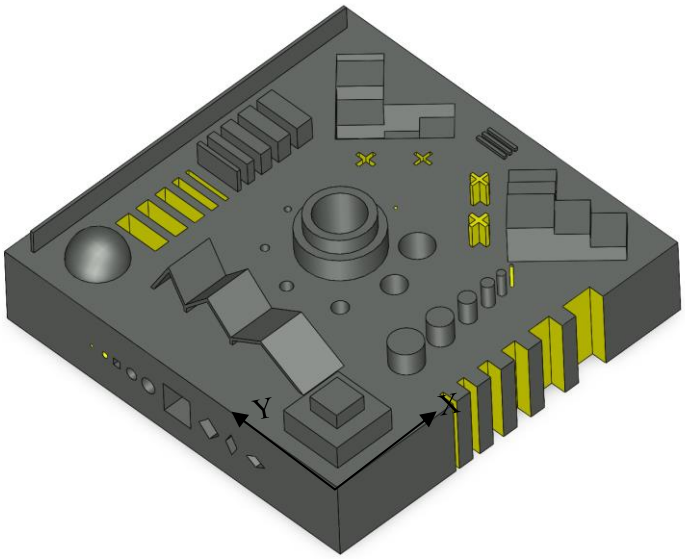

The feature ID column in Table 9 directly links to the specific feature accuracy being reviewed to establish a standardized methodology for measuring feature accuracy. Highlighted in yellow on the benchmark design are the specific features for measurement indicated to ensure an accurate dimensional accuracy assessment. Furthermore, the table provides the XYZ axis to guide the plane where measurements should be recorded.

This methodical approach makes it easier to analyze the data that has been gathered. It ensures that every measurement adds to a thorough grasp of the dimensional accuracy of the part. The creation of a data collection template, outlined in the following section, focuses on all measurements, facilitating the process for efficient and organized data analysis.

5.3. Criteria-specific benchmarking

Each benchmark measurement can be assessed based on criteria further classified under the four general aspects of the benchmark artifact evaluation discussed in the previous section in Table 8. Table 10 further categorizes those four general aspects.

Table 10: Criteria to be accessed for geometrical benchmark under each aspect.

Main Criteria	Sub Criteria	Measurement Method
Accuracy (C1)	Holes (C11)	Geometrical accuracy measured in mm (minimum value is better) relating to AMed component when compared to the CAD model.
	Notches (C12)	
	Slots (C13)	
	Squares (C14)	
	Cylinders (C15)	
	Inclinations (C16)	
	Hemisphere (C17)	
	Crosses (C18)	
Thin features (C2)	Walls < 0.5mm wall thickness (C21)	
	Cylinders < 0.5 mm diameter (C22)	
	Holes < 0.5 mm diameter (C23)	
Residual stress (C3)	Distortion angle	
Built speed (C4)	No sub-category	Comparison of simulation time to the time taken to build the actual AMed component when compared to the CAD model

From Table 10, the Accuracy (C1), the main criterion, evaluates the AMed components' geometrical precision compared to their original computer-aided design (CAD) models. The minimum deviation is the primary objective here, while the sub-criteria cover other geometric aspects under accuracy and are given below.

Holes (C11): Evaluate the AMed component hole dimensional correctness by measuring how closely the holes match the intended diameters.

Notches (C12): Evaluate the accuracy of the notches, paying particular attention to the depth and width that the design specifies.

Slots (C13): Analyze slot features' length and width in relation to the benchmark design parameters to determine how accurate they are.

Squares (C14): Verifies that square geometries are accurate by comparing their angles and side lengths to the CAD model.

Cylinders (C15): Measures the dimensional reliability of cylindrical features, focusing on diameter and axis alignment.

Inclinations (C16): Examines the accuracy of inclined or overhanging surfaces, where the incline angle is critical.

Hemisphere (C17): Assesses the curvature and diameter of hemispherical features against the design intent.

Crosses (C18): Checks the dimensional accuracy of cross-shaped features, including arm lengths and intersection angles.

From Table 10, Thin Features (C2), this second main category evaluates the accuracy and manufacturability of features that are particularly difficult because of their small thickness or diameter.

Walls < 0.5mm wall thickness (C21): Analyze the AM process' accuracy in producing walls thinner than 0.5 mm without any flaws.

Cylinders < 0.5 mm diameter (C22): Measures the precision of producing fine cylindrical features with diameters less than 0.5mm.

Holes < 0.5 mm diameter (C23): Assesses the AM process ability to accurately create small holes with diameters under 0.5mm.

Residual Stress (C3): This section investigates the presence of distortion angle with the horizontal plane due to residual stresses within the longest thin wall feature, which can affect structural integrity and dimensional accuracy.

Build Speed (C4): Contrasts the time needed to create the AMed component with the estimated simulation build time. Faster build times indicate higher process efficiency in this criterion.

5.4. Measurement approach

As mentioned in Table 10, those categories are based on the characteristics and geometric forms that correlate to a particular degree of dimensional accuracy. An approach is needed to extract meaningful information from the raw data from each category; Figure 13 shows the three steps of the data measurement strategy necessary to extract meaningful information from measurements made from benchmark artifacts criteria.

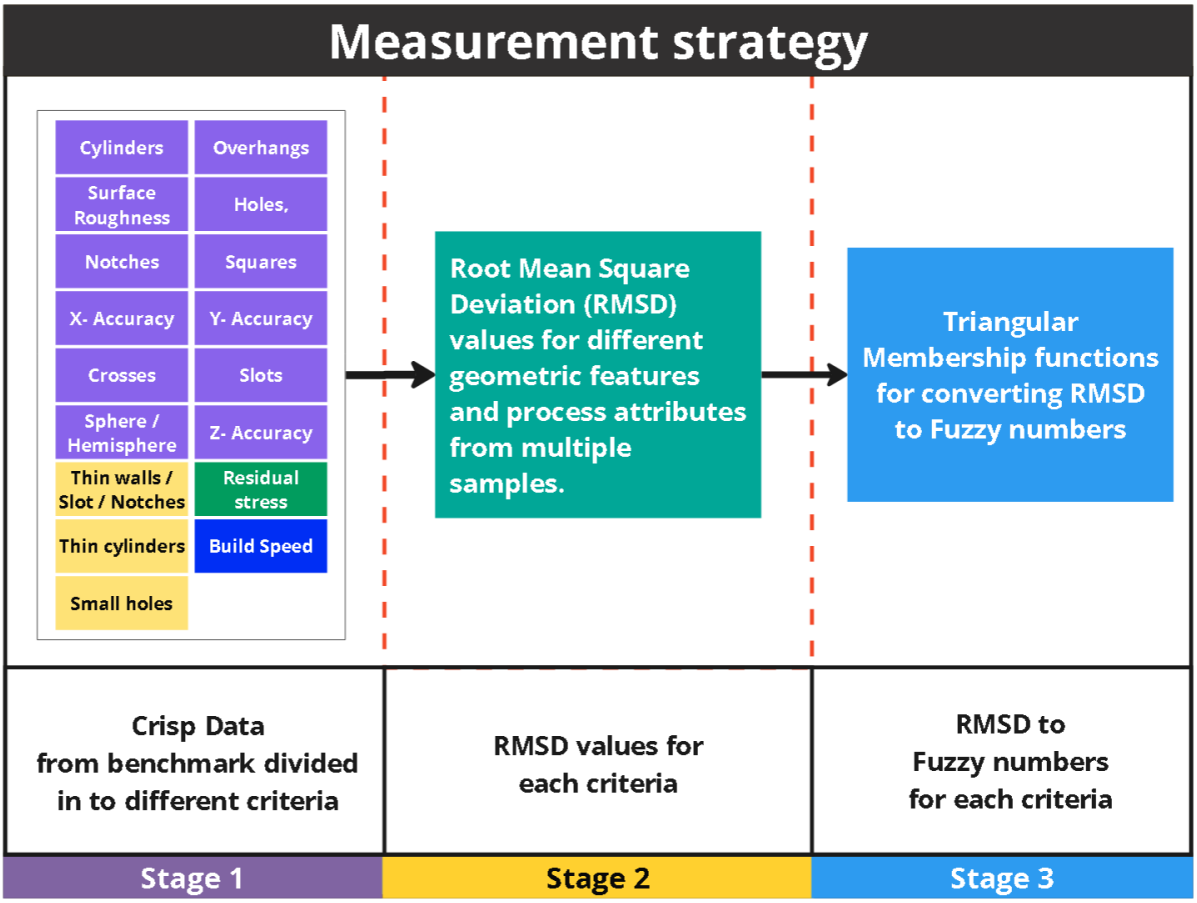

Figure 13: Benchmark criteria and measurement strategy before the decision-making process.

In Figure 13, the measurement strategy for assessing a benchmark artifact is divided into three stages, each crucial for generating raw data into actionable insights. The initial stage involves obtaining "crisp data" from the benchmark, where precise measurements of various features and geometric shapes are taken for each sample. These measurements include a range of criteria, from dimensional accuracy to surface features, outlined as cylinders, holes, notches, and more, as discussed in Table 10.

However, more than this, crisp data needs to be immediately informative. It needs to be contextualized, leading us to the second stage. Here, measurements from multiple samples are analyzed to calculate the Root Mean Square Deviation (RMSD) for different geometric features and process attributes. RMSD is a quantitative tool for comparing the samples against nominal values, providing a clear, numerical representation of each criterion accuracy. Additionally, the build time criteria of the AMed process are evaluated by comparing the estimated times to the actual, with deviations captured by corresponding RMSD values. This stage transforms individual measurements into a uniform metric of quality. RMSD is calculated by Eq. (1) (S. Hussain Ather, 2020).

$$RMSD = \sqrt{\frac{\sum(x_e - x_o)^2}{n}} \qquad (1)$$

RMSD calculation indicating summing the squared differences and dividing by the number of observations, $(x_e - x_o)^2$ represents the squared difference between the nominal x_e and the observed value x_o in the samples during evaluation. While n is the number of observations or the number of samples, in this case, under observation.

The last stage is to integrate these accurate RMSD computations into a decision-making framework by transforming them into fuzzy numbers. The crisp RMSD measurements are converted into fuzzy values that can be used to assess the benchmark artifact comprehensively through triangular membership functions that can be adjusted and created by skilled machine operators. This stage makes it possible to have a decision-making system that can manage the inherent fluctuation and uncertainty in the data while also facilitating a more relevant understanding.

This three-stage approach ensures that each aspect of the benchmark artifact is measured accurately and evaluated within a comprehensive decision-making framework, and conversion is discussed further in the following sections.

5.5. Organization of collected data in Excel template

Building on the detailed explanations in the preceding section, structuring the data collection process is essential for ensuring an efficient and structured approach to analyzing and selecting

PBF-LB/M machines. Figure 14 illustrates the tabs of an Excel workbook, designed as a template to support the backend decision-making process.

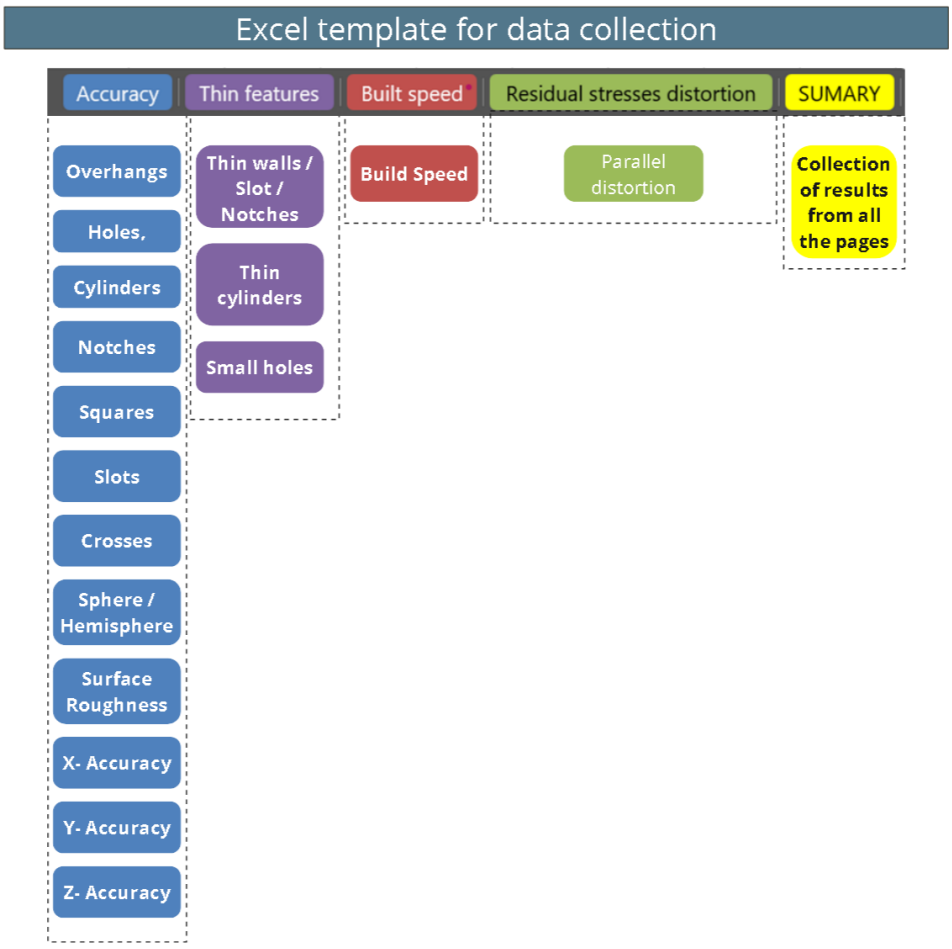

Figure 14: Tree of benchmark artifact data collection template designed in Excel.

The sheet names of the Excel template are shown in Figure 14; this template is crucial for organizing data systematically before employing the Fuzzy AHP and Fuzzy TOPSIS methodologies, which align with the classifications shown in Table 8. Figure 14 provides a clear flowchart for the recording procedure to further enhance this structure by indicating how many measurement tables for each criterion are assigned to each group. This organizing scheme makes a streamlined method of data gathering possible, and data collection in this scheme is explained in Appendix 2: Data collected in Excel template for benchmark measurements for Aconity3D MIDI+ samples.

Furthermore, the Excel template recommends a balanced quantity of measurements necessary to derive meaningful outcomes under each table in red color notes. It operates on the grounds that increased evaluations tend to elevate the quality of results. On the other hand, the

integration of gathered data with the framework for making decisions is purposefully emphasized within the scope of this thesis. This approach puts the usefulness of the limited measurements recorded to be used ahead of the sheer number of measurements that are gathered.

This approach ensures that the data utility is maximized, nurturing informed decisions without overwhelming the process with unnecessary complexity. The aim of the thesis is embodied in this balance between practical applicability and depth of research, which prepares the ground for an extensive yet targeted investigation of the variables influencing machine selection.

5.6. Four stages of MCDA using Fuzzy AHP and Fuzzy TOPSIS

The core proposition of this thesis is an MCDA design that leverages RMSD data from benchmarking to inform a decision-making framework. As discussed in the literature, the combination of Fuzzy AHP with Fuzzy TOPSIS was selected as it constitutes an appropriate methodology for this thesis problem, offering a complete decision-making framework.

This initial part of MCDA is the Fuzzy AHP that utilizes the authority of user judgment combined with subjectivity and uncertainty (Emrouznejad & St, 2022, p. 29). It allows experts to put their intuitive judgments into numerical form instead of precise values, directly integrating complex judgments into consideration. Here, the goal is to find the weights of several criteria, creating a hierarchy that reflects their relative importance in decision-making.

The second part of MCDA is the Fuzzy TOPSIS, which complements the preliminary stage by quantifying the proximity of each potential solution to the ideal and the solution that has the worst level for all criteria to rank the alternatives (Nădăban et al., 2016). It accurately identifies the inherent ambiguity and ambiguity in expert judgments, making it a crucial tool for complex decision-making processes.

Fuzzy AHP alone does not automatically evaluate alternatives to the ideal solution; it is an excellent tool for evaluating the relative importance of many criteria. In contrast, TOPSIS needs pre-established weights for its parameters to assess alternatives and reliable techniques like AHP to calculate these weights. Although AHP and TOPSIS are strong separately, their combination overcomes their shortcomings. Furthermore, the combination of these MCDA approaches used in this thesis is tailored to incorporate direct user inputs into the system, deviating from the conventional methodologies typically seen in the literature. Figure 15

presents the entire procedural construction established to construct the framework to tackle the thesis research problem.

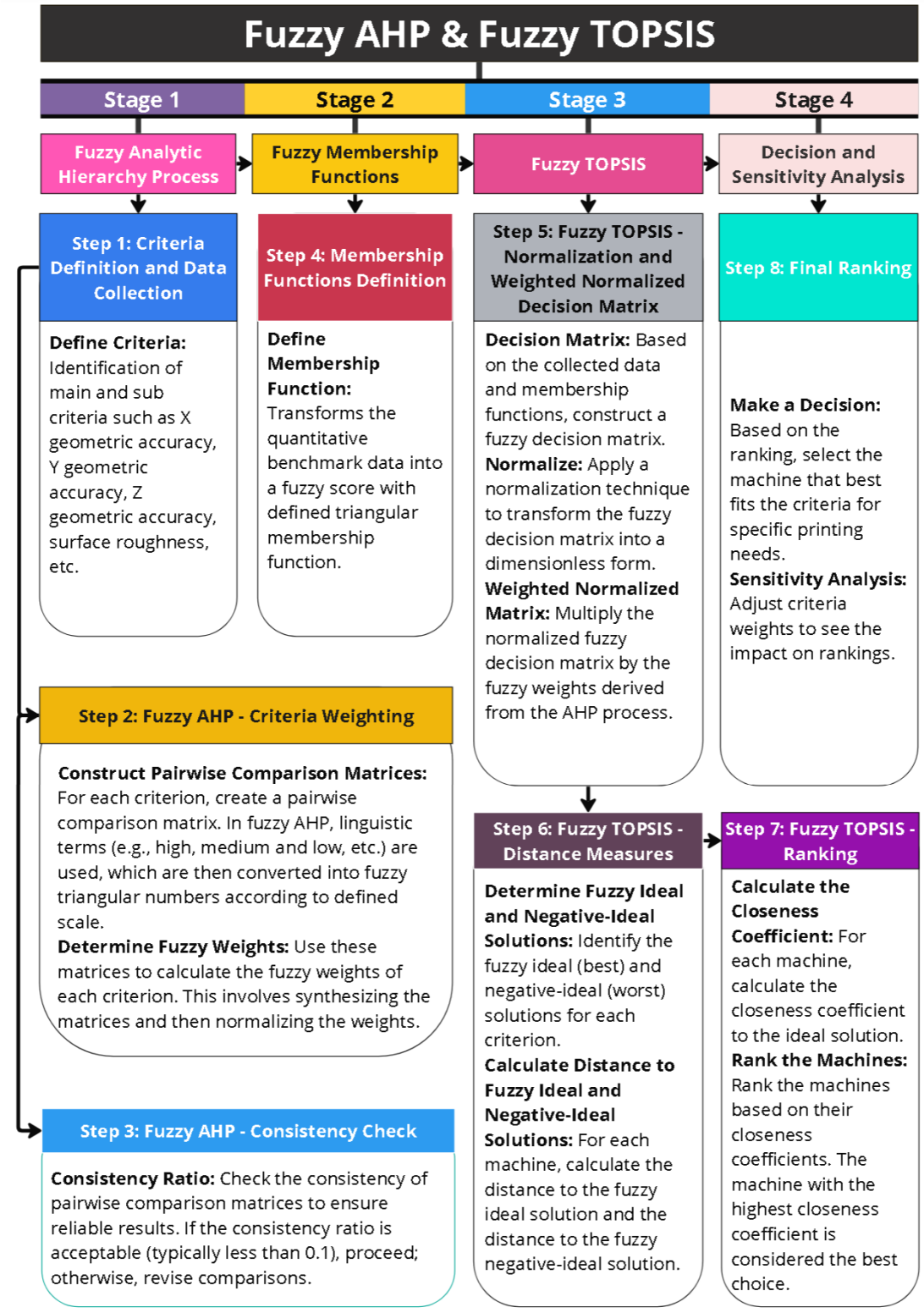

Figure 15: Eight steps divided into four stages is a comprehensive approach for using Fuzzy AHP and Fuzzy TOPSIS to choose the best PBF-LB/M technology using a geometrical benchmark artifact.

As can be seen in Figure 15, for the entire framework to rank the alternatives according to user inputs and RMSD data obtained from the geometrical benchmark, eight essential steps must be completed under four main stages.

A detailed explanation of each stage, including all the steps required to complete the arithmetic of the suggested framework, is provided below.

5.6.1. Stage 1: Fuzzy analytic hierarchy process

Stage one, as shown in Figure 16, uses the Fuzzy AHP with the consistent objective of incorporating user input weights for every criterion listed in Table 10 to get the weighted criteria for the Fuzzy TOPSIS in the second stage.

Step 1: Criteria definition and data collection

Using the same analogy, Figure 16 presents the hierarchy for Fuzzy AHP, for which user inputs will be gathered to maintain the applicability of the geometrical benchmark criterion.

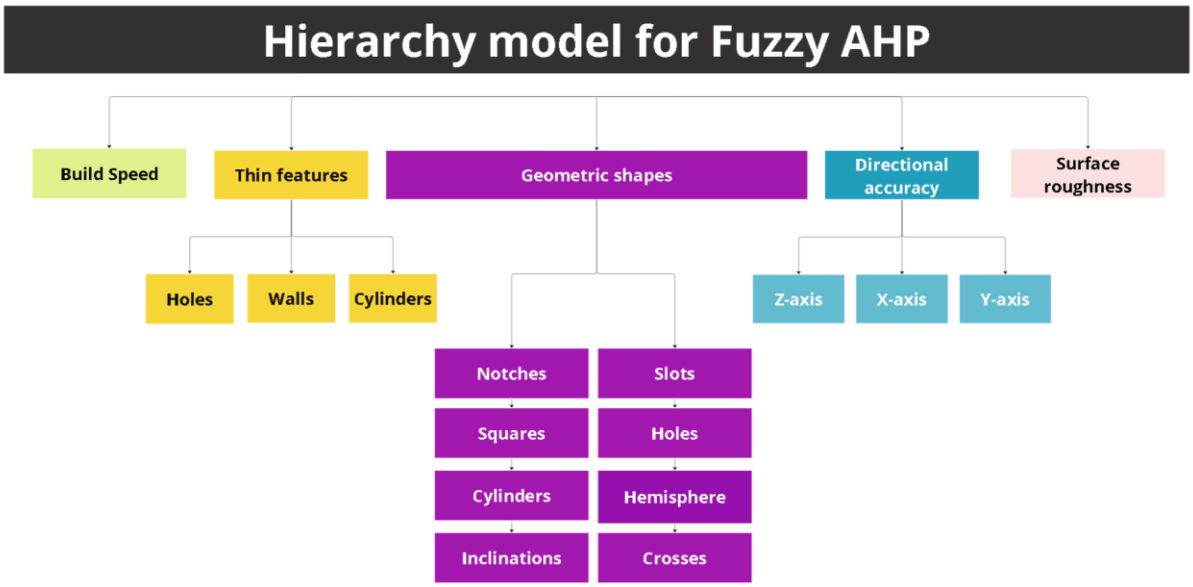

Figure 16: Fuzzy AHP criteria hierarchy.

As seen in Figure 16, the criteria in the hierarchy are the same as those established earlier for benchmark evaluation in Table 10, and these same criteria will be used to consider the user input weights.

Step 2: Fuzzy AHP - criteria weighting

The user inputs will be collected based on a pre-established scale, where the precise inputs from the user, such as "high," "medium," and "low," related to the occurrence of similar geometries in the part to be AMed, will be converted into fuzzy numbers using a membership function. In Fuzzy set theory, membership functions quantify the degree of truth or the grade of membership of an element to a Fuzzy set (Dr. Seema Mishra, 2023). The Triangular Membership Function (TMF) is defined: a curve that determines how each point in the input space is mapped to a membership value between 0 and 1. The function is demonstrated by three parameters representing the lower, middle (peak), and upper points, respectively (Debasis Samanta, 2024). Based on three points, membership function μ(x) is defined using Eq. (2):

$$\mu(x; a, b, c) = \begin{cases} 0 & \text{if } x \leq a \\ \dfrac{x-a}{b-a} & \text{if } a < x \leq b \\ \dfrac{c-x}{c-b} & \text{if } b < x \leq c \\ 0 & \text{if } x > c \end{cases} \qquad (2)$$

Where, generic membership function (x) can be used to determine a (lower boundary) and c (upper boundary) where membership degree is zero, and b (the center) where membership degree is "1" (Debasis Samanta, 2024). From Eq. (2), analogous values for TFNs of "high," "medium," and "low" can be generated. This conversion will introduce fuzziness into the importance given by the user to each criterion. The scale for user input is illustrated in Figure 17.

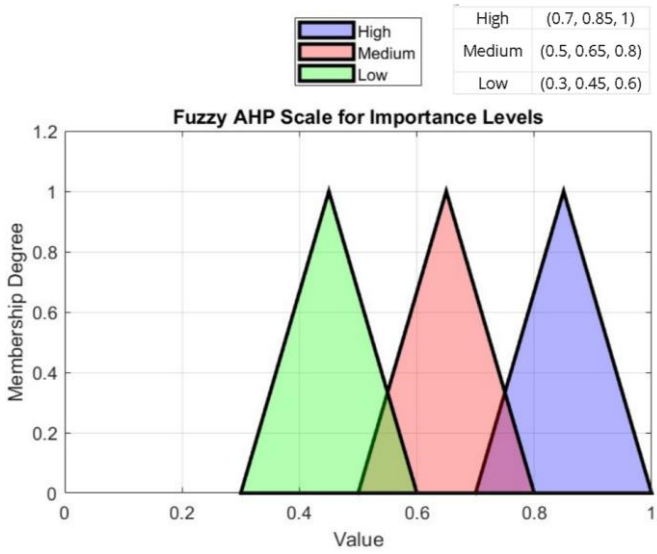

Figure 17: Scale of converting user inputs to fuzzy score.

In Figure 17, the scale of TFNs for "high," "medium," and "low" is established for user inputs that were only crisp values. However, now we can introduce fuzziness in the framework for better decision-making with the help of this scale. The same analogy of Eq. (2) was used for the Figure 17 scale, and a set of Eq. (3), Eq. (4), and Eq. (5) for TFNs for "high," "medium," and "low" used for generating this scale is provided below.

$$\mu_{\text{High}}(x) = \begin{cases} 0 & \text{if } x \leq 0.7 \\ \dfrac{x - 0.7}{0.85 - 0.7} & \text{if } 0.7 < x \leq 0.85 \\ \dfrac{1 - x}{1 - 0.85} & \text{if } 0.85 < x \leq 1 \\ 0 & \text{if } x > 1 \end{cases} \tag{3}$$

$$\mu_{\text{Medium}}(x) = \begin{cases} 0 & \text{if } x \leq 0.5 \\ \dfrac{x - 0.5}{0.65 - 0.5} & \text{if } 0.5 < x \leq 0.65 \\ \dfrac{0.8 - x}{0.85 - 0.65} & \text{if } 0.65 < x \leq 0.8 \\ 0 & \text{if } x > 0.8 \end{cases} \tag{4}$$

$$\mu_{\text{Low}}(x) = \begin{cases} 0 & \text{if } x \leq 0.3 \\ \dfrac{x - 0.3}{0.45 - 0.3} & \text{if } 0.3 < x \leq 0.45 \\ \dfrac{0.6 - x}{0.6 - 0.45} & \text{if } 0.45 < x \leq 0.6 \\ 0 & \text{if } x > 0.6 \end{cases} \tag{5}$$

Where the μ_{High}, μ_{Medium} and $\mu_{\text{Low}}(x)$ represents the TFNs for "high," "medium," and "low" values of "x" at any given point on the membership function. A process of iteration is used to select the above scale range for user-provided Fuzzy inputs. The main goal is to match numerical representations to the qualitative aspects of human judgment and the consistency of fuzzy AHP. To ensure a smooth transition from verbal to quantitative analysis, the TFNs for "high," "medium," and "low" are further created to capture the ambiguity inherent in linguistic judgments. The ambiguity in human evaluations is reflected in the overlap between various TFNs, which allows for varying interpretations of the same phrase. The distance between the TFNs represents the intensity of the difference in importance of each criterion.

Next, based on the membership function described above, each criterion will undergo pairwise comparisons based on the user inputs in the hierarchy system dimensions, as in step 1 for Figure

15. For each pair, the user will be asked to assign linguistic terms to express the importance of that criteria. The pair-wise comparison is illustrated by Eq. (6) (Sun, 2010):

$$\tilde{A} = \begin{bmatrix} 1 & \tilde{a}_{12} & \cdots & \tilde{a}_{1n} \\ \tilde{a}_{21} & 1 & \cdots & \tilde{a}_{2n} \\ \vdots & \vdots & \ddots & \vdots \\ \tilde{a}_{n1} & \tilde{a}_{n2} & \cdots & 1 \end{bmatrix} = \begin{bmatrix} 1 & \tilde{a}_{12} & \cdots & \tilde{a}_{1n} \\ \frac{1}{\tilde{a}_{12}} & 1 & \cdots & \tilde{a}_{2n} \\ \vdots & \vdots & \ddots & \vdots \\ \frac{1}{\tilde{a}_{1n}} & \frac{1}{\tilde{a}_{2n}} & \cdots & 1 \end{bmatrix} \quad (6)$$

Syntax of pair-wise comparison, the criteria $\tilde{a}_{ij}$ are above the diagonal, while below the diagonal, the values are taken reciprocal and reversed. The Eq. (6) pair-wise comparison will be computed for each criteria group in the main or sub-criteria. For the problem of this thesis, in Figure 15, there are three pair-wise comparison matrices for the groups of sub-criteria and one pair-wise comparison for the main criteria.

So, through four pairwise comparisons, we establish a set of all judgments in the comparison matrix (Hanine et al., 2016). The set of elements is compared to itself by using the fundamental scale of pair-wise comparison, as in Figure 18.

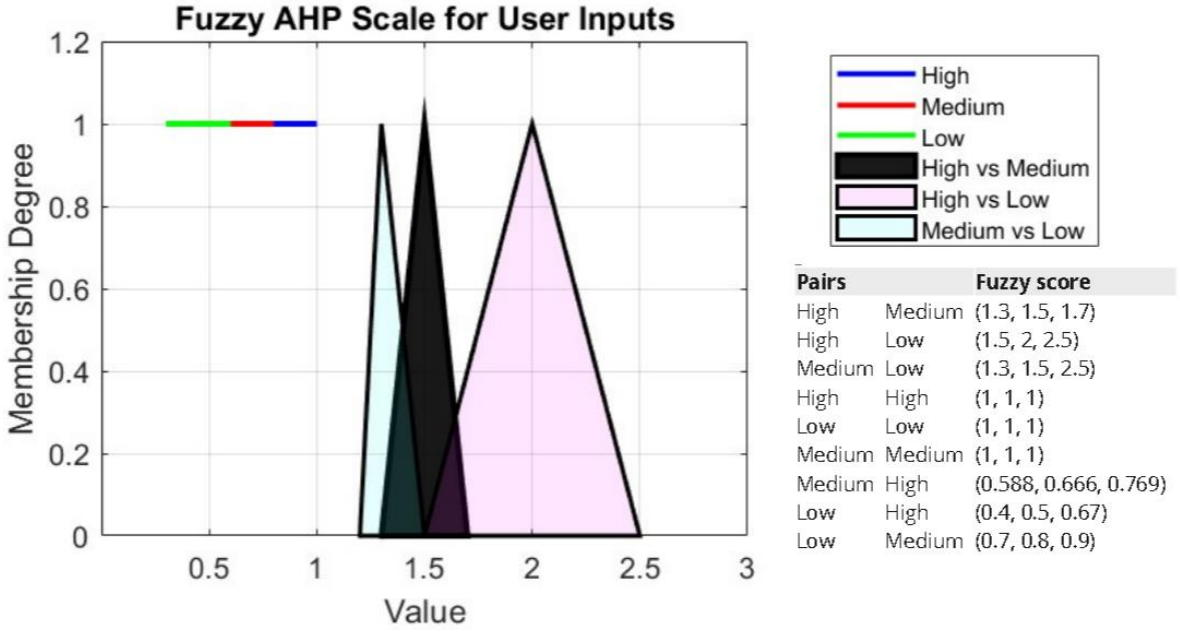

Pairs		Fuzzy score
High	Medium	(1.3, 1.5, 1.7)
High	Low	(1.5, 2, 2.5)
Medium	Low	(1.3, 1.5, 2.5)
High	High	(1, 1, 1)
Low	Low	(1, 1, 1)
Medium	Medium	(1, 1, 1)
Medium	High	(0.588, 0.666, 0.769)
Low	High	(0.4, 0.5, 0.67)
Low	Medium	(0.7, 0.8, 0.9)

Figure 18: Scale of pair-wise comparison, including the "high," "medium," and "low" for user inputs.

As seen from Figure 18, whatever pairwise comparison comes in the matrix, a corresponding pair value is assigned to that matrix entry. Once we have the pairwise matrix for each sub-criteria and the main criteria, the next step is to use these matrices to calculate the fuzzy weights of each criterion.

This involves synthesizing the matrices and normalizing the weights (Sun, 2010). To calculate the weights of each criterion, the geometric mean of the fuzzy comparison value of the criterion is used (Sun, 2010) and given by Eq. (7), while the calculated weights are given by Eq. (8):

$$\tilde{r}_i = \left(\tilde{a}_{i1} \otimes \cdots \otimes \tilde{a}_{ij} \otimes \cdots \otimes \tilde{a}_{in}\right)^{\frac{1}{n}} \tag{7}$$

$$\tilde{w}_i = \tilde{r}_i \otimes \left[\tilde{r}_1^{-1} \oplus \cdots \oplus \tilde{r}_i^{-1} \oplus \cdots \oplus \tilde{r}_n^{-1}\right]^{-1} \tag{8}$$

Where in geometric mean calculation, where $\tilde{a}_{ij}$ is the fuzzy comparison value of the dimension i to criterion j, thus, $\tilde{r}_i$ is a geometric mean of the fuzzy comparison value of the criterion i to each criterion. While $\tilde{W}_i$ is the fuzzy weight of the ith criterion, can be indicated by a TFN, $\tilde{W}_i = (l\tilde{w}_i, m\tilde{w}_i, u\tilde{w}_i)$. The $l\tilde{w}_i$, $m\tilde{w}_i$ and $u\tilde{w}_i$ stand for the lower, middle, and upper values of the fuzzy weight of the ith dimension.

To integrate the sub-criteria evaluations into the overall decision-making framework, the derived weights from each pairwise comparison are combined with the principal criteria weights by simple multiplication, resulting in a comprehensive set of weighted criteria for subsequent application in the Fuzzy TOPSIS methodology.

Step 3: Fuzzy AHP - consistency check

The last step for Fuzzy AHP is to check the consistency of pairwise comparison matrices to ensure reliable results. The consistency ratio is acceptable when, typically, less than 0.1; otherwise, the inputs from the user need to be revised to make the pair-wise comparisons again. The consistency checks for the fuzzy pairwise comparison matrices were introduced by (Gogus and Boucher, 1998) and given in Eq. (9), Eq. (10), and Eq. (11):

$$A_i = (l_i, m_i, u_i), A_m = [a_{ijm}], A_g = \left[\sqrt{l_{ij}u_{ij}}\right], \quad (9)$$

$$CI_m = \frac{\lambda_{max}^m - n}{n-1}, CI_g = \frac{\lambda_{max}^g - n}{n-1}, \quad (10)$$

$$CR_m = \frac{CI_m}{RI_m}, CR_g = \frac{CI_g}{RI_g} \quad (11)$$

For FAHP consistency check, the CR_m and CR_g is calculated with the help of λ_{max}^m and λ_{max}^g, which are the principal eigenvalues of A_m and A_g. Here n is the size of the matrix, and the main matrix is A_i while A_m is a matrix with mean values, while the A_g matrix with a geometric mean. The value of RI_g and RI_m was also calculated by (Gogus & Boucher, 1998), as illustrated in Table 11.

Table 11: Random indices. Reproduced from (Gogus & Boucher, 1998) under license of CC BY 4.0 DEED.

n	RI_m	RI_g
1	0	1
2	0	2
3	0.4890	0.1796
4	0.7937	0.2627
5	1.0720	0.3597
6	1.1996	0.3818
7	1.2874	0.4090
8	1.3410	0.4164
9	1.3793	0.4348
10	1.4095	0.4455
11	1.4181	0.4536
12	1.4462	0.4776
13	1.4555	0.4691
14	1.4913	0.4804
15	1.4986	0.4880

From Table 11, for fuzzy pairwise comparison matrices, depending on the order of the matrix n, the values for RI_g *and* RI_m were used, which is fixed in this thesis problem dependent on the criteria.

5.6.2. Stage 2: Fuzzy membership functions

Completing the three steps of Fuzzy AHP will give us weights for each criterion that we can directly incorporate into Fuzzy TOPSIS. However, to construct the decision matrix for Fuzzy TOPSIS, we need to integrate the benchmark data into the framework. The methodology for incorporating the measurement data into the framework is already discussed in Figure 14.

Step 4: Membership functions definition for RMSD

As discussed previously, the RMSD values from the geometrical benchmark artifact measurements need to be converted into a Fuzzy score to be used in the Fuzzy TOPSIS framework, and Figure 19 illustrates the scale for RMSD, which will account for the fuzziness of the crisp data.

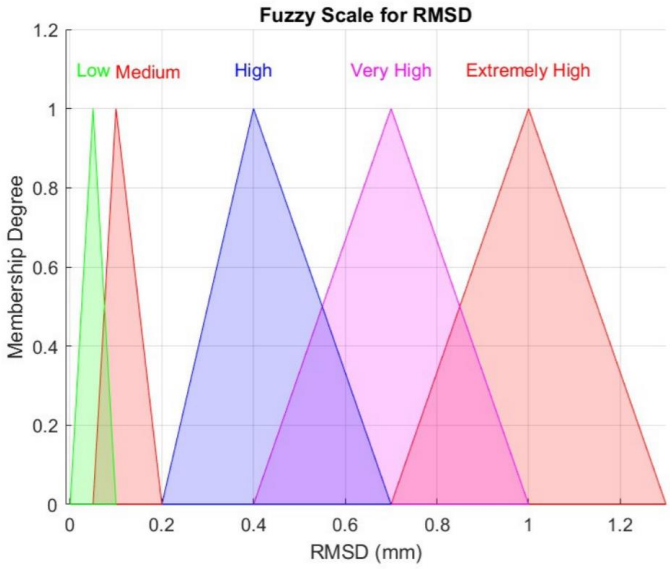

RMSD Rating	RMSD Range	Triangular Fuzzy Number
Low (L)	RMSD ≤ 0.05 mm	(0, 0.05, 0.1)
Medium (M)	0.05 mm < RMSD ≤ 0.1 mm	(0.05, 0.1, 0.2)
High (H)	0.1 mm < RMSD ≤ 0.2 mm	(0.1, 0.2, 0.4)
Very High (VH)	0.2 mm < RMSD ≤ 0.4 mm	(0.2, 0.4, 0.7)
Extremely High (EH)	RMSD > 0.4 mm	(0.4, 0.7, 1.3

Figure 19: RMSD Scale to convert and relate the geometrical benchmark data by transforming the quantitative data into a fuzzy score.

In Figure 19, triangular fuzzy numbers are used for each scale because they are simple and capable of interpreting the imprecision inherent in the measurement of geometrical accuracies. RMSD measures the deviation of manufactured part dimensions from their CAD designs; thus, smaller RMSD values indicate greater accuracy than the intended geometry, indicating greater accuracy.

The chosen scale for categorizing Root Mean Square Deviation (RMSD) values into "Extremely high" to "Low" and others with corresponding triangular fuzzy numbers is designed to mirror the precision levels attainable in metal additive manufacturing. This range

segmentation can be further tuned to be anchored along practical industry benchmarks and expert knowledge, ensuring that each category distinctly represents a level of geometric accuracy given by the below set of Eq. (12), to Eq. (16), of membership functions:

$$\mathrm{L}\,(r) = \begin{cases} (0, r, r + 0.05) & \text{if } r \leq 0.05 \\ (0, 0.05, 0.1) & \text{otherwise} \end{cases} \tag{12}$$

$$M(r) = \begin{cases} (r - 0.05, r, r + 0.05) & \text{if } 0.05 < r \leq 0.1 \\ (0.05, 0.1, 0.2) & \text{otherwise} \end{cases} \tag{13}$$

$$\mathrm{H}\,(r) = \begin{cases} (r - 0.1, r, r + 0.2) & \text{if } 0.1 < r \leq 0.2 \\ (0.1, 0.2, 0.4) & \text{otherwise} \end{cases} \tag{14}$$

$$\mathrm{VH}\,(r) = \begin{cases} (r - 0.2, r, r + 0.3) & \text{if } 0.2 < r \leq 0.4 \\ (0.2, 0.4, 0.7) & \text{otherwise} \end{cases} \tag{15}$$

$$\mathrm{EH}\,(r) = \begin{cases} (r - 0.4, r, r + 0.3) & \text{if } r > 0.4 \\ (0.4, 0.7, 1) & \text{otherwise} \end{cases} \tag{16}$$

Membership functions for each RMSD category can be seen from the Eq. (12) to Eq. (16) and Figure 19, the scale of RMSD will correspond to the fuzzy score in the decision matrix that was used in the analysis of Fuzzy TOPSIS in stage 3, explained in the next section.

5.6.3. Stage 3: Fuzzy TOPSIS

Stage three employs the Fuzzy TOPSIS with the aim of combining fuzzy values of the RMSD scale to be used from benchmark data and weighted criteria obtained from the stage two Fuzzy AHP to rank the alternatives according to the order preference by similarity to the ideal solution.

Step 5: Fuzzy TOPSIS - Normalization and weighted normalized decision matrix

For employing the Fuzzy TOPSIS, Eq. (17) and Eq. (18) illustrate the syntax of a fuzzy decision matrix.

$$\tilde{D} = \begin{bmatrix} \tilde{x}_{11} & \tilde{x}_{12} & \cdots & \tilde{x}_{1n} \\ \tilde{x}_{21} & \tilde{x}_{22} & \cdots & \tilde{x}_{2n} \\ \vdots & \vdots & \ddots & \vdots \\ \tilde{x}_{m1} & \tilde{x}_{m2} & \cdots & \tilde{x}_{mn} \end{bmatrix} \begin{matrix} i = 1,2,\ldots,m; \\ j = 1,2,\ldots,n \end{matrix} \tag{17}$$

$$\tilde{x}_{ij} = \frac{1}{K}\left(\tilde{x}_{ij}^{1} \oplus \cdots \oplus \tilde{x}_{ij}^{k} \oplus \cdots \oplus \tilde{x}_{ij}^{K}\right) \tag{18}$$

For fuzzy performance/decision matrix as seen in Eq. (18), $\tilde{D}$ is the decision matrix of criterion performance $\tilde{x}_{ij}$ which is obtained by comparing the performance of the criteria C_i against the alternative A_i evaluated by an expert in order, as shown in Eq. (19) (Sun, 2010):

$$\begin{array}{cccccc} & C_1 & C_2 & \cdots & C_n \\ A_1 & \tilde{x}_{11} & \tilde{x}_{12} & \cdots & \tilde{x}_{1n} \\ A_2 & \tilde{x}_{21} & \tilde{x}_{22} & \cdots & \tilde{x}_{2n} \\ \vdots & \vdots & \vdots & \ddots & \vdots \\ A_m & \tilde{x}_{m1} & \tilde{x}_{m2} & \cdots & \tilde{x}_{mn} \end{array} \tag{19}$$

Syntax of criteria C_i against the alternative A_i is given by Eq. (19), and for the context of this thesis, RMSD scale was developed, as given in Figure 19, which will act as an expert scale to convert the benchmark data, acting as the performance of a specific machine against that criterion. Once the decision matrix has been established, the next step is to normalize this decision matrix with the following Eq. (20), and Eq. (21) (Sun, 2010):

$$\tilde{R} = [\tilde{r}_{ij}]_{m\times n}, i = 1,2,\dots,m; j = 1,2,\dots,n \tag{20}$$

$$\tilde{r}_{ij} = \left(\frac{l_{ij}}{u_j^+}, \frac{m_{ij}}{u_j^+}, \frac{u_{ij}}{u_j^+}\right), u_j^+ = \max \tilde{u}_{ij} | i = 1,2,\dots,n \tag{21}$$

Where, $\tilde{R}$ is the normalized fuzzy-decision matrix and the normalization is achieved by each fuzzy number in the decision matrix gets normalized by dividing its components by the highest upper bound u_{ij} of the respective criterion across all alternatives (Sun, 2010). Normalization ensures that different criteria, measured in different scales and units, are brought onto a standard scale to be aggregated and compared. Once the normalized matrix has been established, the weighted fuzzy normalized decision matrix is established by Eq. (20) (Sun, 2010):

$$\tilde{V} = [\tilde{v}_{ij}]_{n\times n}, i = 1,2,\dots,m; j = 1,2,\dots,n, \quad where\ \tilde{v}_{ij} = \tilde{r}_{ij} \otimes \tilde{w}_j. \tag{20}$$

The normalized decision matrix $\tilde{v}_{ij}$ is obtained by multiplying the criteria weights $\tilde{w}_j$ obtained through the Fuzzy AHP framework.

Step 6: Fuzzy TOPSIS - Distance measures

Next step is to calculate the fuzzy positive-ideal solution (FPIS) and fuzzy negative-ideal solution (FNIS) (Sun, 2010). Here, we know the RMSD TFN, and their ranges belong to the closed interval [0, 1]. Therefore, the FPIS and FNIS are calculated by Eq. (21).

$$A^+ = \left(\tilde{v}_1^*, \dots, \tilde{v}_j^*, \dots, \tilde{v}_n^*\right), \qquad A^- = \left(\tilde{v}_1^-, \dots, \tilde{v}_j^-, \dots, \tilde{v}_n^-\right) \tag{21}$$

$$where\ \tilde{v}_j^* = (1,1,1) \otimes \tilde{w}_j = \left(l_{w_j}, m_{w_j}, u_{w_j}\right)$$
$$\text{and } \tilde{v}_j^- = (0,0,0), i = 1,2,\dots,n.$$

FPIS A^+ and FNIS A^- within the closed interval range of the RMSD membership function [0, 1] allows us to use the $\tilde{v}_j^*$ values as directly the weights calculated in Fuzzy AHP, while the $\tilde{v}_j^-$ becomes zero.

After establishing the FPIS and FNIS, we can calculate the distance. d_i^+ and $\tilde{d}_i^-$ of each alternative from FPIS and FNIS through the area compensation method (Sun, 2010) and then use d_i^+ and $\tilde{d}_i^-$ of each alternative to find the similarities CC_i to an ideal solution as given in the set of Eq. (22) to Eq. (24):

$$d_i^+ = \sum_{j=1}^{n} d\left(\tilde{v}_{ij}, \tilde{v}_j^*\right) \quad i = 1,2,\dots,m; \quad j = 1,2,\dots,n \tag{22}$$

$$\tilde{d}_i^- = \sum_{j=1}^{n} d\left(\tilde{v}_{ij}, \tilde{v}_j^-\right) \quad i = 1,2,\dots,m; \quad j = 1,2,\dots,n \tag{23}$$

$$CC_i = \frac{\tilde{d}_i^-}{d_i^+ + \tilde{d}_i^-} = 1 - \frac{d_i^+}{d_i^+ + \tilde{d}_i^-}, i = 1,2,\dots,m \quad (24)$$

Calculation of the distances d_i^+ and $\tilde{d}_i^-$ for each alternative and similarities CC_i to an ideal solution (Sun, 2010) is given by Eq. (22) to Eq. (24), which is a comprehensive way of knowing how fuzzy gaps should be improved to achieve aspiration levels among a fuzzy set of feasible alternatives.

Based on the CC_i, now, alternatives can be ranked, which, in this case, is the best technology for AMed for the given component incorporating user inputs.

5.6.4. Stage 4: Decision and sensitivity analysis

Based on the existing rankings, the selection of the machine is performed that meets the requirements for AM requirements. To further understand how variations in user inputs might influence the rankings of the best PBF-LB/M selection, user can conduct a sensitivity analysis which is computed in the backend of MATLAB script.

This technique will help us determine how different values of independent variables influence a particular dependent variable under a set of assumptions. By altering the user-defined importance levels of "high," "medium," and "low" and revisiting Stages 1 and 3 of Figure 15, we can modify the criteria weights to observe their effects on the rankings.

5.7. Summarized hierarchy model for PBF-LB/M selection

The hierarchical model for selecting a PBF-LB/M machine involves multiple steps and stages that ensure a comprehensive and structured decision-making process. The mathematical calculations for the framework are vital and each step is crucial in achieving the final decision, ensuring that all relevant factors are considered.

The hierarchy model for PBF-LB/M selection depicted in Figure 20 summarizes the previously explained stages and illustrates a structured approach to decision-making in AM using the multiple criteria and different scales.

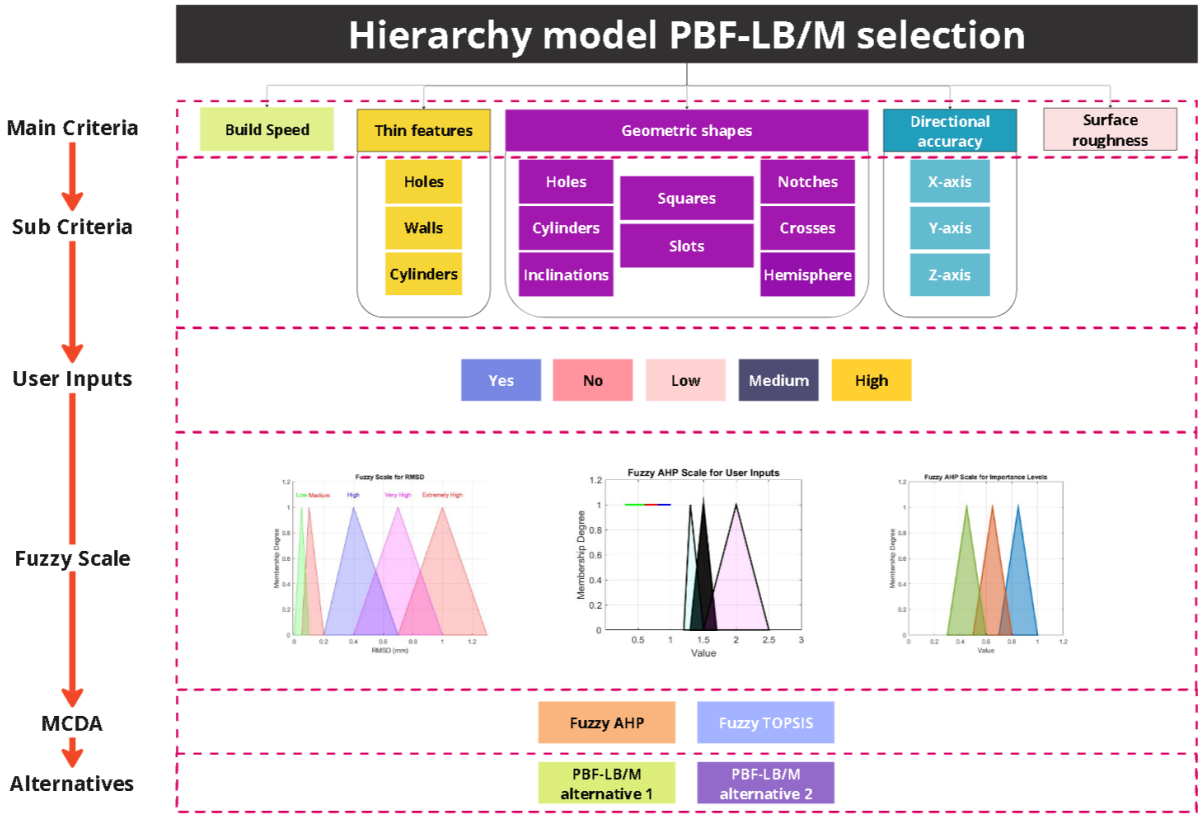

Figure 20: Hierarchy model of criteria for decision-making with user inputs.

As seen in Figure 20, the process begins with defining the main criteria and breaking them down into specific sub-criteria. User inputs: indicating preferences such as 'Yes,' 'No,' 'Low,' 'Medium,' or 'High' that are then applied to the sub-criteria, which are evaluated using a fuzzy scale to handle the imprecision inherent in individual judgment. Here, the additional inputs of 'Yes' and 'No' in the interface were assigned the fuzzy score, as illustrated in Figure 17. For 'Yes, Yes,' the values were 0.50, 0.70, and 0.90. For 'No, No,' the values were 0, 0, and 0. For 'Yes, No,' the values were 0.50, 0.70, and 0.90, and similarly, for 'No, Yes,' the values were 0.50, 0.70, and 0.90.

This feeds into a Multi-Criteria Decision Analysis (MCDA) framework, employing techniques like Fuzzy AHP to weigh the importance levels and Fuzzy TOPSIS to rank the alternatives. The output of this process is a selection of PBF-LB/M machines, prioritized by the specified criteria and user inputs, enabling an informed and tailored decision for specific AM technology requirements.

5.8. Setbacks of benchmark artifact initial design

The benchmark artifact was created using an Aconity3D MIDI+. However, issues occurred during the real-life evaluation and design realization due to a flaw associated with the inclinations labeled "M" in Table 7. The first failed AMed artifact is shown in Figure 21.

Figure 21: The first AMed artifact on Aconity3D MIDI+ appears to be a failed attempt to make the inclination surface used to assess the overhangs.

As shown in Figure 21, when using the Aconity3D MIDI+ with the default optimized parameters provided by the vendor, the machine struggled to produce the features related to inclinations accurately. Before investigating the machine capabilities for manufacturing this artifact, the benchmark design underwent a thorough reanalysis to identify potential improvements.

This process involved examining the design feasibility and exploring possible modifications that could enhance the manufacturability of these complex features and the issue identified was related to the design of the inclination. Figure 22 illustrates the initial flaw in the benchmark inclinations and the subsequent design modifications to address these issues.

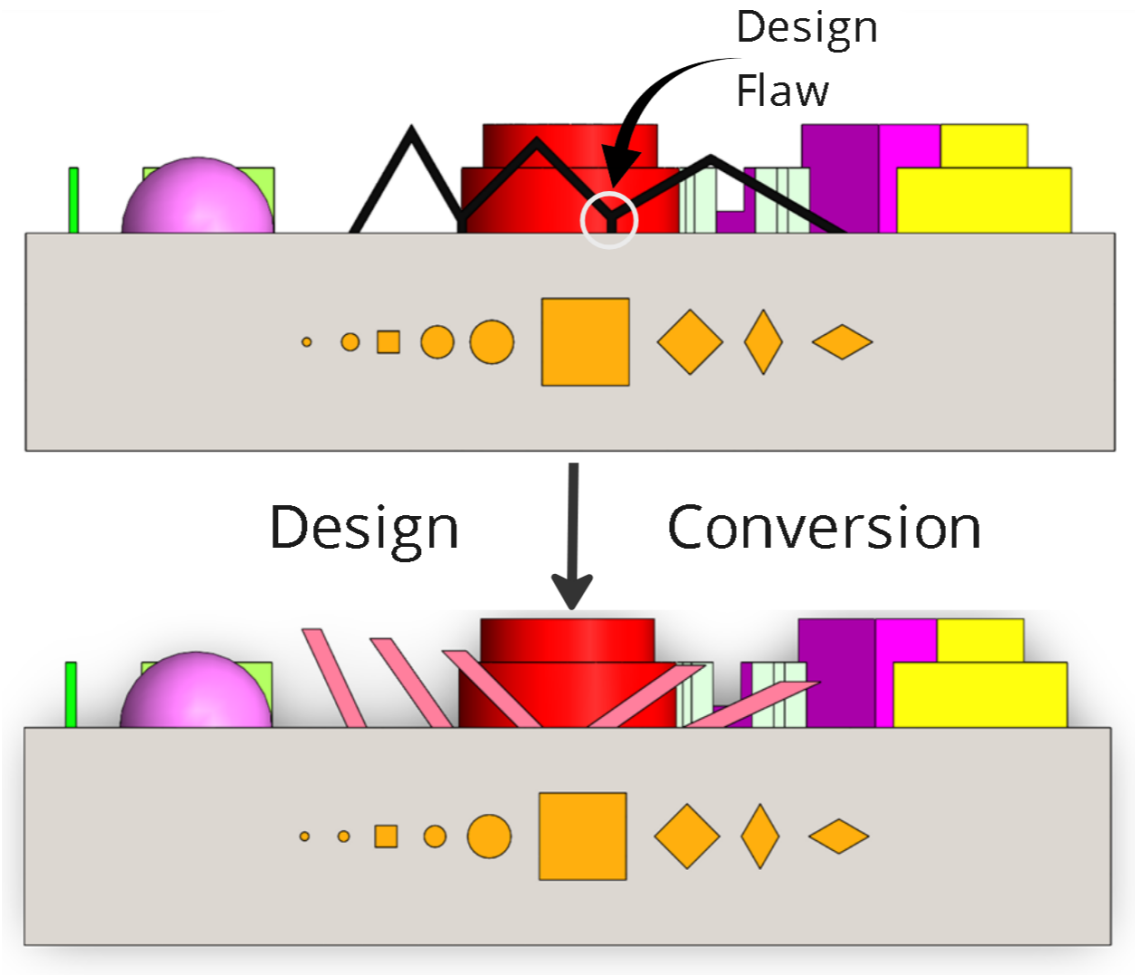

Figure 22: The inclination features "M" for angles M1 = 45°, M2 = 60°, M3 = 30° changed to M1–M5 with angles ranging from 65° to 25° from left to right with 10° increment for each feature.

As depicted in Figure 22, the inclination features labeled "M" were modified because the original design included a base support structure at the bottom of the inclination before the angled feature began. This resulted in failures, as the inclination features should ideally start from the bottom surface.

After redesigning, further angles were incorporated to explore a broader range of overhang distortions. Now, the entry in Table 7 has changed to multiangle.

M	Inclinations	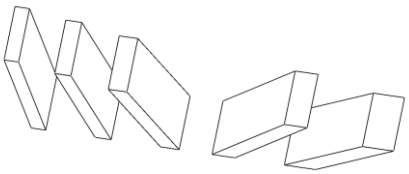	M1–M3	M1 = 65°, M2 = 55°, M3 = 45° M4 = 35° M5 = 25°	Overhangs

The dimensional drawing of the initial and modified benchmark artifact can be seen in Appendix 1.

5.9. Development and analysis of geometric benchmark artifacts

To ensure a comprehensive machine evaluation, multiple samples were AMed on each machine: two samples featuring a modified benchmark design to test specific machine capabilities and one utilizing an old benchmark design to establish a baseline for comparison. This methodical approach gives a clear view of the performance differences across the machines by directly comparing how each machine handles various designs.

The measurement and analysis of these artifacts are critical components of this research phase. Each sample is meticulously scanned and measured using high-precision equipment to quantify deviations from the digital model. This data is crucial as it provides empirical evidence of the ability of each machine to reproduce complex shapes and fine details accurately. Measurements are considered by comparing the dimensional accuracy, surface finish, and time taken to complete the job from each machine, and here, the complete methodology is explained for a single job taken from the Aconity3D MIDI+ and is then repeated for all the samples to record the data.

5.9.1. AMed benchmark artifacts

The critical component of the thesis focused on the additive manufacturing (AM) of benchmark artifacts using the Aconity3D MIDI+ and EOS M290 machines, employing the optimized parameters recommended by the manufacturers rather than custom settings. This approach was intended to facilitate a fundamental comparison between the two machines. However, the initial benchmark artifact produced on the Aconity3D MIDI+, as depicted in Figure 21, prompted a redesign of the benchmark. The Aconity3D MIDI+ could not construct features measuring 0.40 mm using the manufacturer-optimized parameters. This minimum feature limitation of Aconity3D MIDI+, failed the overhang features due to their reliance on a support structure of 0.4 mm at the base. Consequently, adjustments to the optimized parameters for the Aconity3D MIDI+ were necessary to achieve the desired results for 0.40 mm features. In contrast, the EOS M290, while capable of producing 0.40 mm features, exhibited visible heat distortions, particularly noticeable in the N6 cylindrical feature, as documented in Table 7.

These observations underscored that the Aconity3D MIDI+ could not produce 0.4 mm features using merely the optimized parameters suggested by the vendor. Meanwhile, the EOS M290, despite its capability to handle 0.40 mm features, suffered from significant heat-related distortions. These findings will be highlighted to inform decision-makers before incorporating the data into the MATLAB application.

Due to restricted access to the EOS M290, all three benchmark samples were fabricated on a single build plate. Conversely, each of the three benchmark samples on the Aconity3D MIDI+ was manufactured separately on individual build plates. The parameters applied for manufacturing all benchmark samples were derived from Table 12. Each machine produced one sample with the original design and two with the revised design.

Table 12: Optimized parameters suggested by vendors for AMed benchmark artifacts on EOS M 290 and Aconity3D MIDI+.

Criteria	Explanation	EOS M 290	Aconity3D MIDI+	Units
Laser power	Power used during the hatch pattern	214.20	150	W
	Power used during the contouring process	136.10	130	W
Scan speed	Speed of scanning during hatch pattern	928.10	900	mm/s
	Speed of scanning during contouring	446.90	600	mm/s
Layer thickness	Thickness of each layer	0.04	0.03	mm
Hatch spacing	Distance between hatch lines	0.10	0.08	mm
Spot size	The diameter of the laser spot	0.08	0.08	mm
Rotation angles	Angular rotation between layers	47	67	degrees
Hatch pattern	Patterns like stripe, quad, island, zigzag	Stripe	Stripe	geometry
Stripe	Width of the stripe in the hatch pattern	12	5	mm

As detailed in Table 12, the parameters employed were those optimized and recommended by the vendors. For the EOS M 290, the optimized parameters remained unchanged. However, for the Aconity3D MIDI+, a modification was necessary: the manual inclusion of the contour parameters for 0.40 mm features, which had not been automatically selected in the initial

additive manufacturing of the benchmark artifact designated as sample 3. This oversight resulted in the absence of the 0.40 mm features, as depicted in Figure 23. This adjustment was critical to addressing the deficiencies observed in the initial AMed part, ensuring the accurate reproduction of thin features in subsequent manufacturing processes.

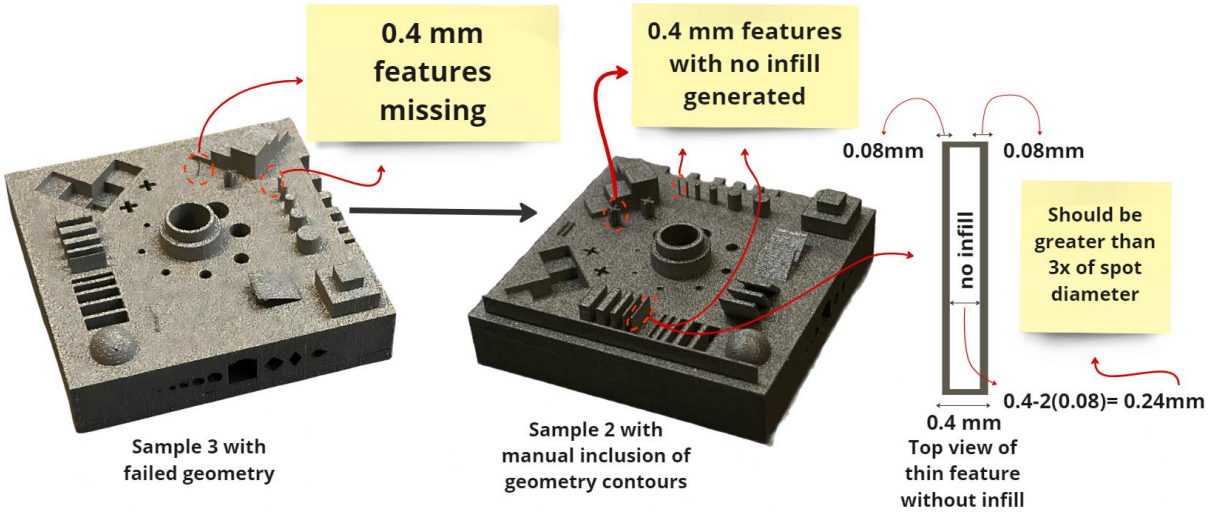

Figure 23: Missing features in sample 3 and successfully constructed features in sample 2 with Aconity3D MIDI+ with missing infill.

In Figure 23, a notable discrepancy is observed between sample 3 and sample 2 concerning the presence of 0.40 mm features. This difference stemmed from the inability of the machine to generate hatch infill for features of this dimension. Consequently, all 0.40 mm features were absent from the AMed sample corresponding to sample 3. In contrast, sample 2 successfully retained these features due to the manual inclusion of contour parameters related to Volumen hatching (V_s) and Volumen shape (V_k). Despite this inclusion, sample 2 faced challenges in infill generation, where only hollow contours were produced instead of filled structures.

The underlying cause of this issue is linked to the recommendations provided by Aconity3D (Aconity3D GmbH, 2024). According to the official guidance of the vendor, the optimal thickness for wall structures should be three times the spot diameter. This specification implies that for successful infill and proper feature representation, adjustments to the machine parameters must ensure that wall thickness aligns with this criterion. This insight highlights the critical need for precise parameter settings to achieve the intended structural integrity and detail in additive manufacturing processes.

In the case depicted on the right end in Figure 24, the spot diameter is 0.08 mm, resulting in sidewall contours of the 0.40 mm wall features. Due to this, the space for infill becomes only

0.24 mm, which falls short of the recommended by more than three times the spot size. Although the contours were manually included in the slicer software of the Aconity3D MIDI+, with the contours of the wall thickness of 0.40 mm achievable, the infill occupied only 0.24 mm, rendering it suboptimal for construction by machine. So, all the thin features with 0.40 mm dimensions only appeared as hollow contours without infill. Moreover, it was observed that infill in space greater than 0.25 was achievable only. While the discrepancies observed in the results obtained by the Aconity3D MIDI+ may necessitate further research to fine-tune the slicer software parameters and achieve complete infilling, it is essential to note that, for this thesis, the decision-making process relied on using the AMed part without parameter optimization.

In total, three samples were produced, one with the initial design and two of the samples AMed on Aconity3D MIDI+ with a modified design based on the optimized parameters as stated in Table 12, as well as the inclusion of the contours for the thin features resulted in the successful building of benchmark modified design.

Figure 24 shows the parameters chosen in Autodesk Netfabb for this specific job in this thesis for setting up the STL file.

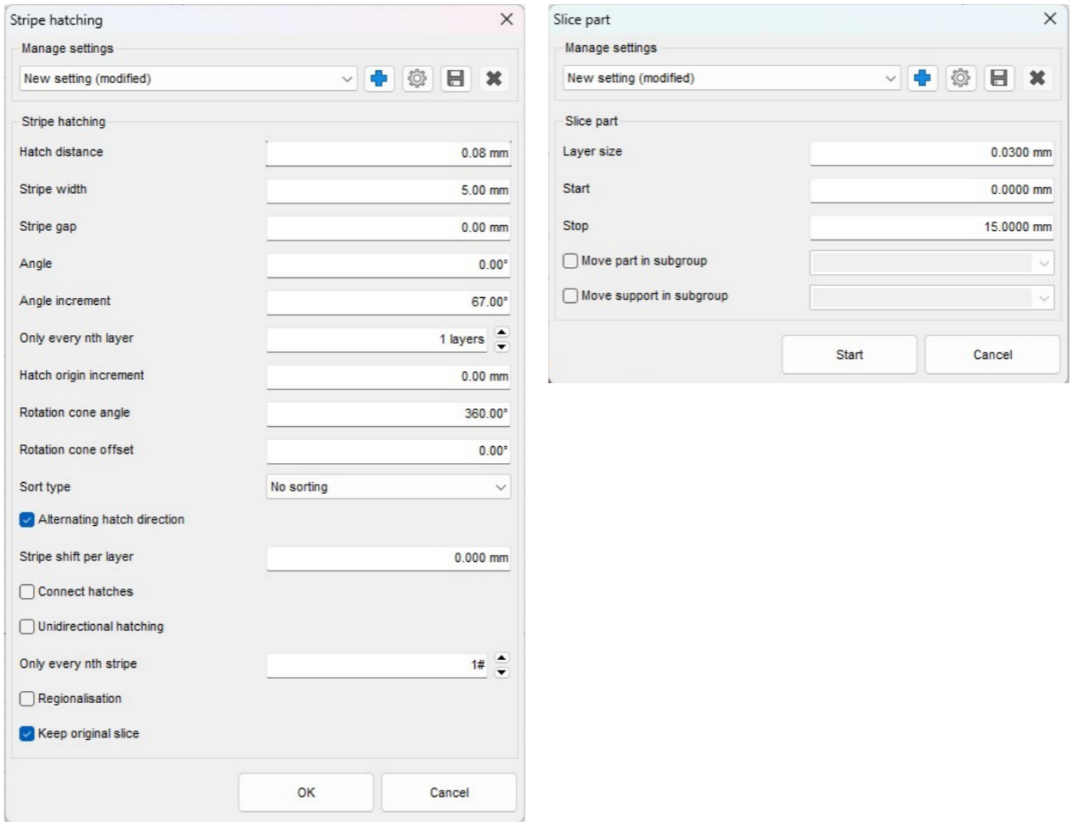

Figure 24: Parameters used for hatching and slicing the benchmark artifact in Autodesk Netfabb.

The stripe hatching settings window allows for the adjustment of parameters such as hatch distance (0.08 mm), stripe width (5.00 mm), and angle increment (67.00°). Additionally, some parameters were chosen for hatch direction. The slice part settings window includes parameters like layer size (Ø 0.03 mm), start (Ø 0.00 mm), and stop (Ø 15.00 mm) for slicing operations.

Figure 25 shows Sample 3, which was the initial design of the benchmark artifact, AMed at an angle about the initial position of the re-coater.

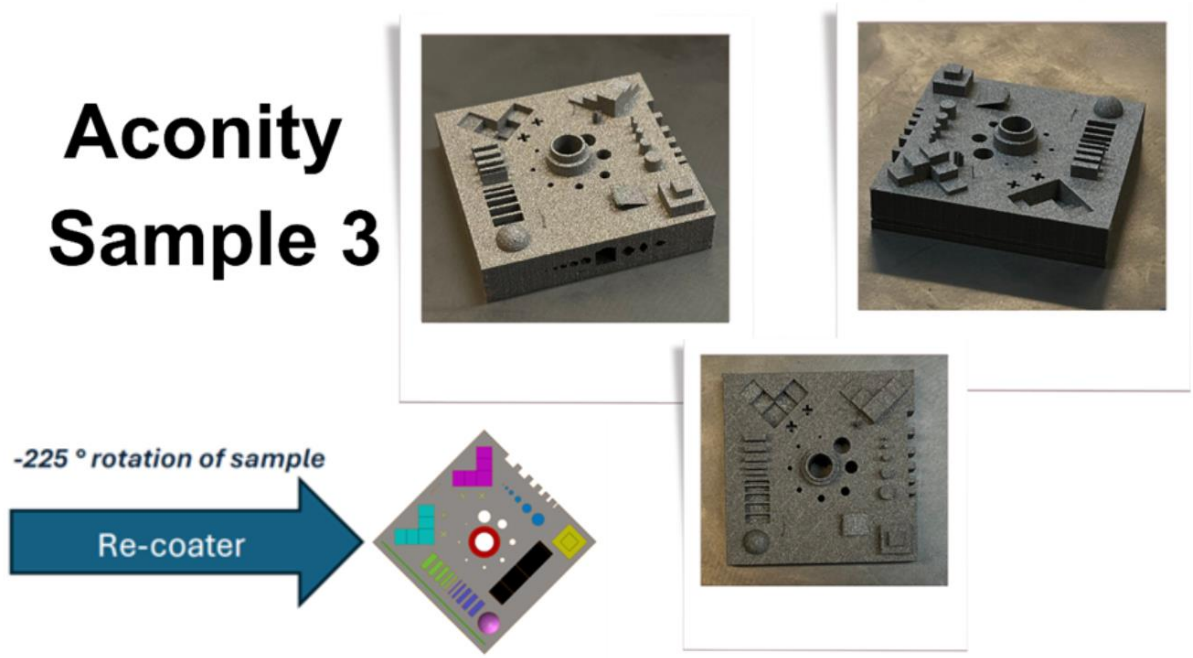

Figure 25: Single Benchmark artifact labeled sample 3 AMed on a build plate of Aconity3D MIDI+ with re-coater direction from left to right and rotated about -225°.

As illustrated in Figure 25, the AMed artifact displays missing features, including the thin features and the inclinations for overhangs, due to the reasons previously discussed.

In contrast, Figure 26 features Sample 2, which was AMed using the modified design of the benchmark artifact, incorporating manual adjustments to the contours in addition to the optimized parameters. This approach effectively addressed the deficiencies seen in the earlier sample.

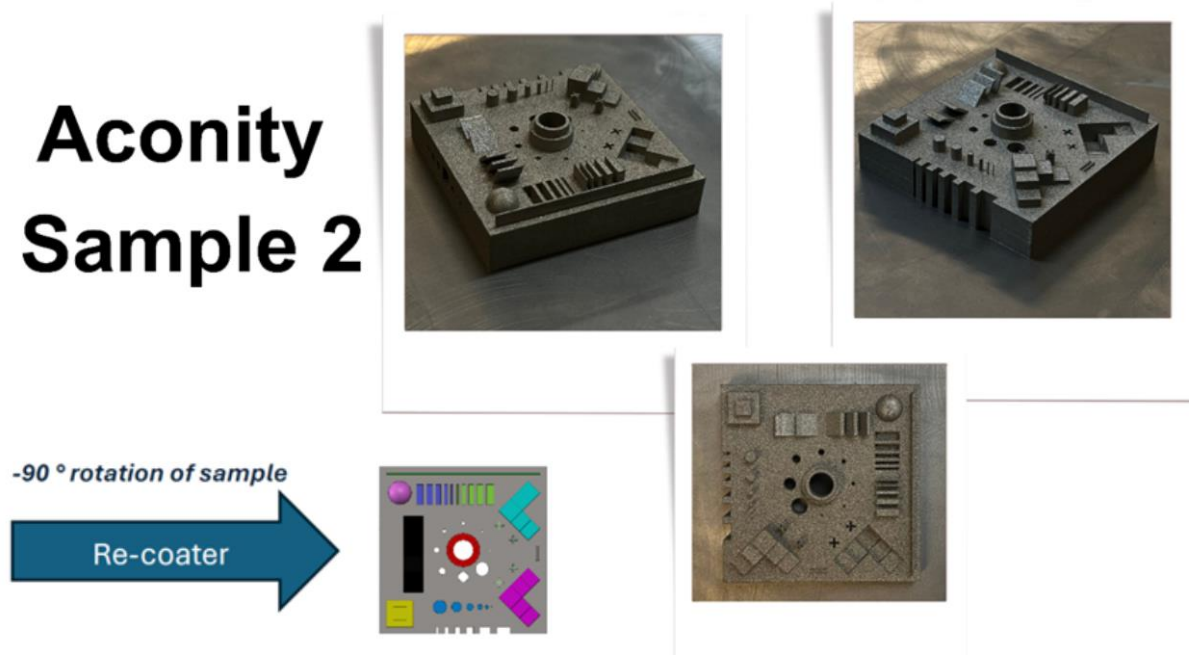

Figure 26: Single Benchmark artifact labeled sample 2 AMed on a build plate of Aconity3D MIDI+.

As seen from Figure 26, the AMed part successfully contains all the features with infill missing for the thin features. The angle of the artifact concerning the re-coater direction is also changed here compared to sample 3. While Figure 27 shows the Amed sample 1.

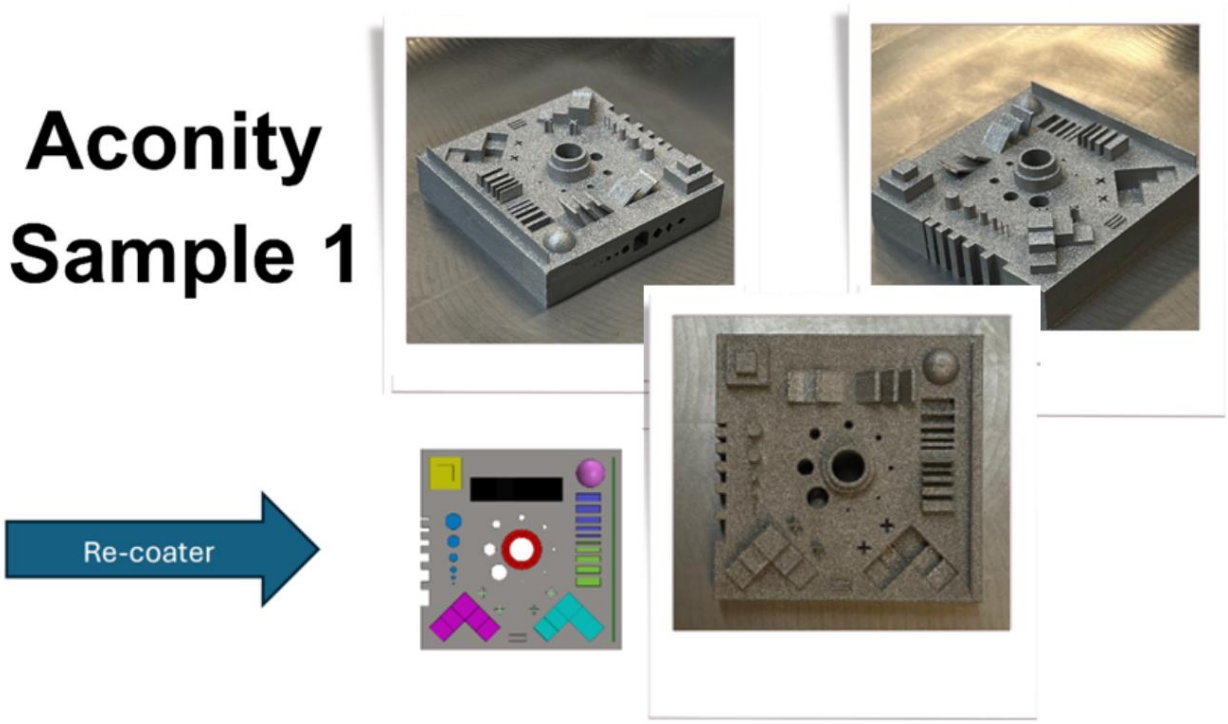

Figure 27: Single Benchmark artifact labeled sample 1 AMed on a build plate of Aconity3D MIDI+.

As shown in Figure 27, the Aconity3D MIDI+ successfully constructed Sample 1 with all features oriented in a different direction compared to Samples 2 and 3. However, the results for Sample 1 are like those of Sample 2 regarding the missing infill for thin features.

Figure 28 illustrates three AMed samples on the EOS M290, all on a single build plate. The direction of the re-coater movement for each sample is aligned with the powder reservoir. Moreover, as mentioned earlier, specific parameters used in the EOSPRINT software for slicing the benchmark artifacts were not disclosed.

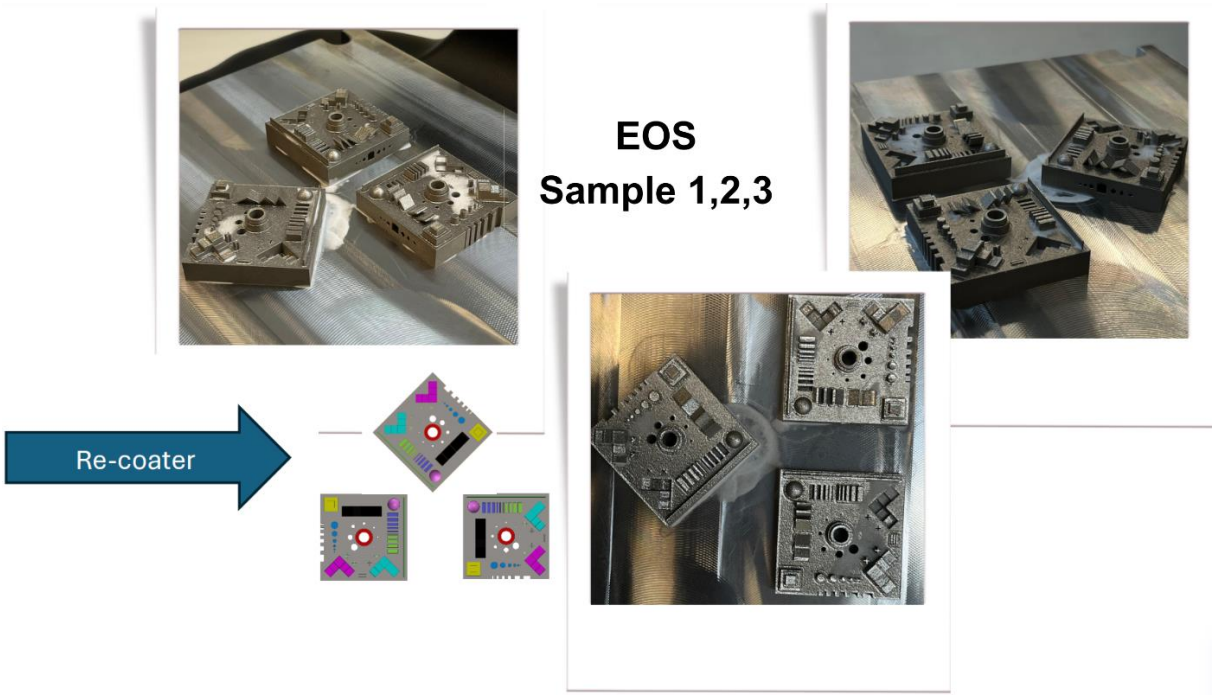

Figure 28: Three benchmark artifact samples AMed on a single build plate of the EOS M290 machine. The white color chemical shown on the benchmark is AESUB self-evaporating 3D scanning spray for improved measurements. Its application is discussed in the future work section later in this thesis.

As illustrated in Figure 28, the EOS M290 successfully AMed three samples, including all thin features. One of these samples was based on the initial design, which the Aconity3D MIDI+ had previously failed to construct effectively, while the other two were based on the modified design of the benchmark artifact. The EOS M290 produced the initial design of the benchmark sample with relative ease.

The direction of the re-coater for each benchmark sample on the EOS M290 was aligned similarly to that used in the Aconity3D MIDI+, as depicted in Figure 28. However, while the EOS M290 succeeded in generating the infill for the 0.40 mm features, this led to visible

distortion due to heat accumulation in these thin spaces. Additionally, the features on the lateral sides exhibited noticeable overhangs.

The impact of these issues on the parts' dimensional accuracy and geometrical integrity will be further analyzed in the geometrical evaluation section, which details the actual measurement differences observed.

5.9.2. Geometrical evaluation on Geomagic Control X

The geometrical evaluation of the benchmark artifact involves a series of steps to obtain the evaluation data. This section explains the evaluation of sample 2 AMed from Aconity3D MIDI+, and identical steps are followed for the rest of the samples. Figure 29 describes the initial crucial steps before the geometrical tolerance evaluations.

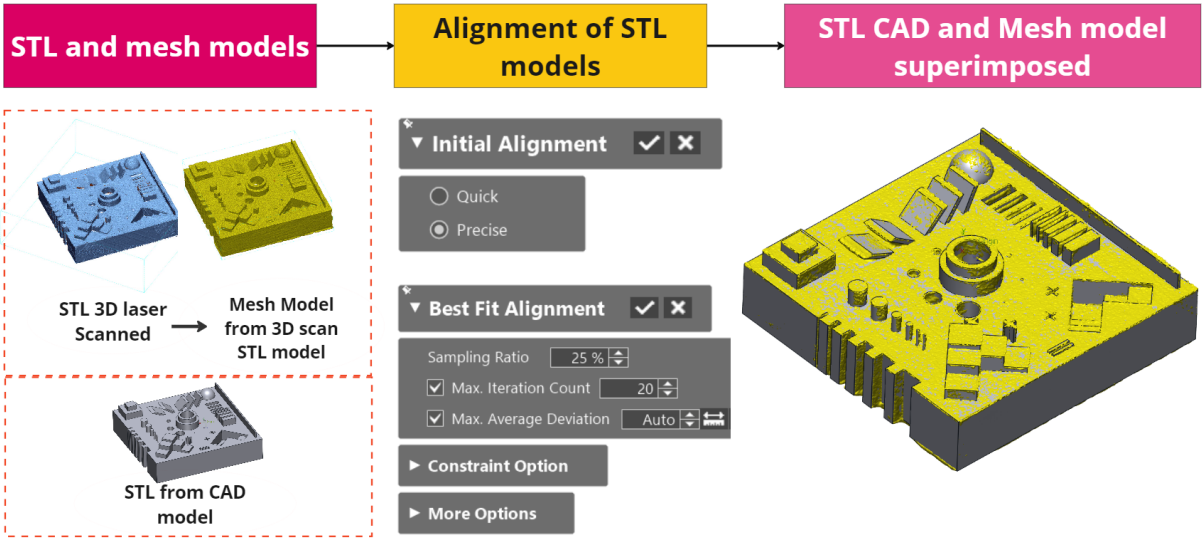

Figure 29: Steps for alignment of reference data (CAD model) to measured data (mesh model).

As depicted in Figure 29, the initial step involves using a 3D laser scanner to create an STL model of the AMed benchmark sample. This scanned model is then converted into a mesh model using Geomagic Control X. Conversely, the STL model of the original CAD design is generated using SolidWorks.

Geomagic Control X offers several options for aligning the reference data (the CAD model) with the measured data (the mesh model). In this case, the process involves precise initial alignment followed by best-fit alignment. This sequence is used to superimpose the reference data over the measured data, as shown in the final step of Figure 29. This alignment procedure is crucial for ensuring that the comparison between the CAD and the actual manufactured

sample is accurate and meaningful, facilitating detailed assessment and validation of the manufacturing process. Once the alignment is obtained, the next part is to 3D compare the two models to see the visual color mapping of geometrical evaluations, as seen in Figure 30.

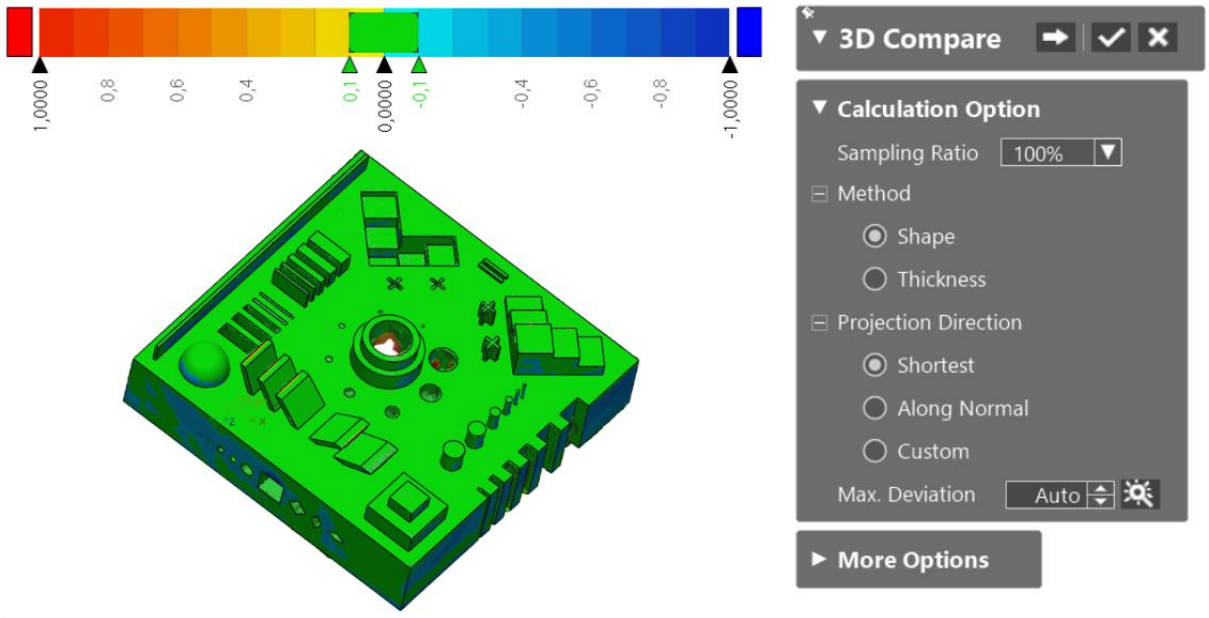

Name	Min.	Max.	Avg.	RMS	Std. Dev.	Var.	+Avg.	-Avg.
3D Compare1	-0,6531	0,6534	-0,0485	0,1168	0,1062	0,0113	0,064	-0,096

Figure 30: 3D comparison view of reference data (CAD model) to measured data (mesh model).

As seen in Figure 30, the 3D comparison view highlights the differences between the reference CAD model and the scanned mesh model once the models are correctly aligned. This visual representation is beneficial for identifying deviations. The values from the 3D comparison table indicate significant deviations between the scanned mesh model and the reference CAD model, with extremes of -0.65 mm and 0.65 mm, showing substantial undercuts and overcuts, respectively. The average deviation of -0.04 suggests a general trend where the scanned part is smaller than the CAD model. The RMS deviation of 0.11 highlights a significant average magnitude of deviation, while the standard deviation of 0.10 and variance of 0.01 indicate a moderate dispersion of these deviations around the average. These statistics collectively point to noticeable discrepancies between reference data (CAD model) and measured data (mesh model).

While the 3D comparison is a good starting point for the sake of MATLAB application to deduce results based on the deviation of individual geometries, a comparison of each feature needs to be recorded. The software can automatically detect shapes like circles, squares, and

planes to see the difference between measured and nominal values. Figure 31 shows an example of the software auto-detection of a diameter of various features.

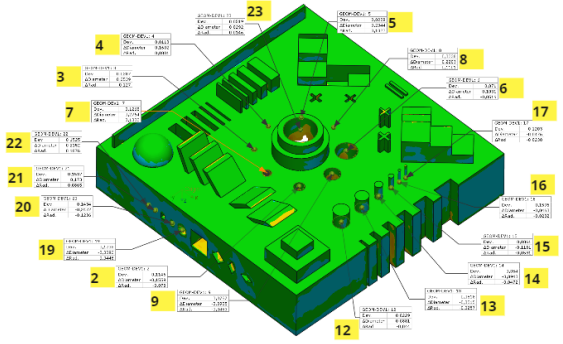

Label	Name	Radius	Pair Rad.	Deviation
2	GEOM-DEV:2	1	0,922	0,1146
3	GEOM-DEV:3	0,5	0,687	0,0287
4	GEOM-DEV:4	0,4	0,4801	0,0118
5	GEOM-DEV:5	0,25	0,3522	0,0229
6	GEOM-DEV:6	2	1,9484	0,071
7	GEOM-DEV:7	0,75	0,882	0,1268
8	GEOM-DEV:8	0,2	0,3101	0,0238
9	GEOM-DEV:9	1,5	1,4547	0,0757
12	GEOM-DEV:12	1,5	1,456	0,0229
13	GEOM-DEV:13	1,25	1,2243	0,0518
14	GEOM-DEV:14	0,75	0,7028	0,054
15	GEOM-DEV:15	0,5	0,4409	0,0861
16	GEOM-DEV:16	0,25	0,2268	0,1596
17	GEOM-DEV:17	0,2	0,1762	0,1203
19	GEOM-DEV:19	1	0,9554	0,1238
20	GEOM-DEV:20	0,5	0,3764	0,1434
21	GEOM-DEV:21	0,25	0,3365	0,1537
22	GEOM-DEV:22	0,2	0,3076	0,1525
23	GEOM-DEV:23	3	3,0146	0,0519

Figure 31: Automatic geometrical deviation of circular features on benchmark mesh model.

In Figure 31, software automated assessing geometrical deviations in various circular features is utilized. The process involves selecting predefined shapes within the software, such as planes, circles, slots, and cylinders. These predefined shapes help the software identify the geometry under evaluation. The software then generates comparison data between nominal and measured values, as shown in Figure 31. Specifically, the figure illustrates the radius of circular features and their corresponding deviation values.

While this approach is efficient and straightforward, it may require manual intervention to remove unwanted data and unrecognized geometrical features. Additionally, users can choose other predefined shapes, and the software will automatically evaluate deviation values for those shapes.

In some cases, automated software for assessing geometrical deviations may encounter challenges. It might struggle to identify features based on predefined shapes. To address this, the software provides a manual option where users can select specific points on the mesh body. However, manual selection can be time-consuming and may involve trial and error in pinpointing the correct points and measuring dimensions along the respective axes. Figure 32 illustrates this process with some of the dimensions shown.

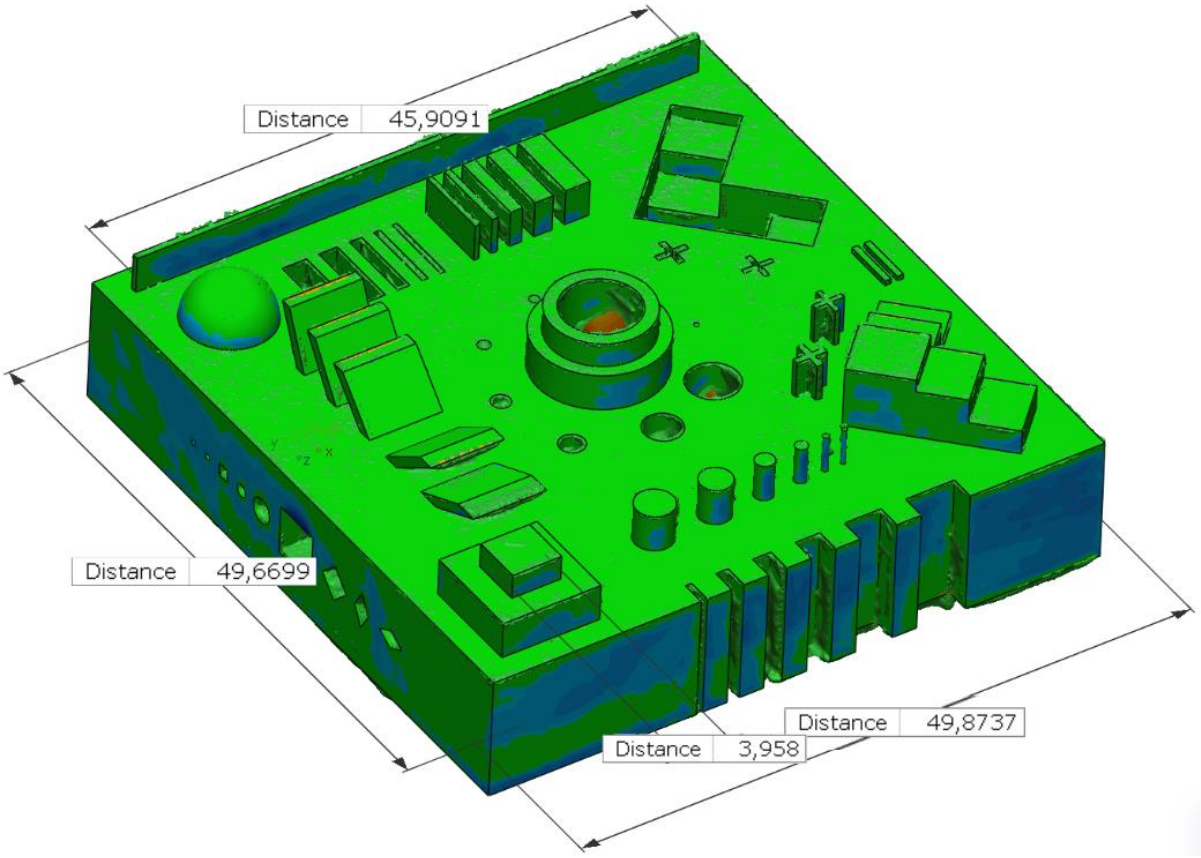

Figure 32: Manual selection for geometrical deviation of selected features on benchmark mesh model.

Figure 32 presents the geometric measurements between various selected points on the benchmark. These measurements allow for the calculation of deviations, particularly useful when assessing specific features. Another example of manual geometric measurements is shown in Figure 33.

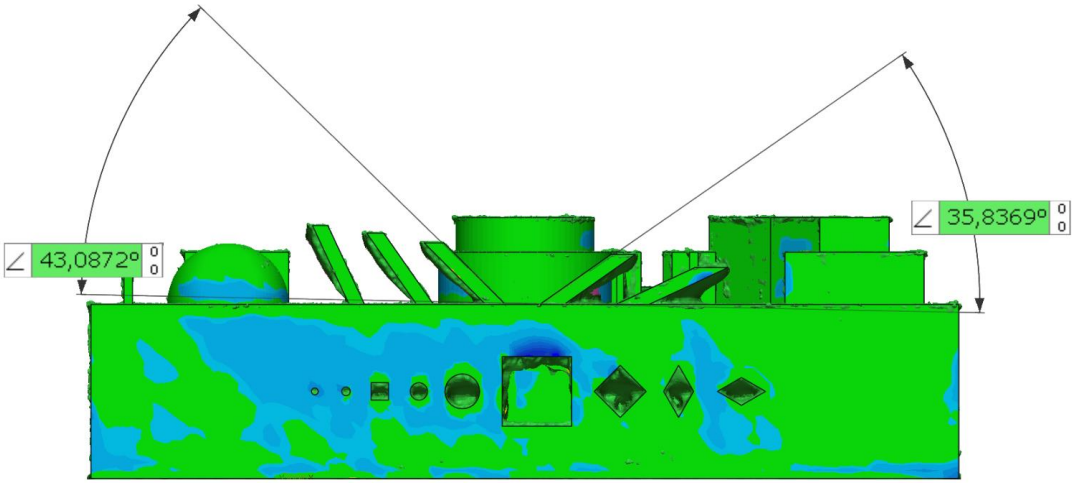

Figure 33: Measurements of inclinations features with different degrees of overhangs.

As shown in Figure 33, the angle of inclination between the horizontal surface and the inclined surface is displayed. It is essential to consider the measuring plane-specific dimensions to obtain accurate results. The planes in Figure 33, within which the angles are measured, may not be parallel to the horizontal, and this is because the final built artifact might have dispensaries. Only precise consideration of the measuring plane and specific features can lead to accurate deviation calculations in manual mode.

5.9.3. Surface quality evaluation on Alicona infinite focus G6

The surface quality of the designated single planar surface was evaluated using the Alicona Infinite Focus G6 across all benchmark samples employed in this study. The objective was to develop a methodology for this thesis research that could be expanded to encompass additional points of surface roughness evaluation. The procedure adopted in this thesis aligns with ISO 16610-71:2014 (ISO, 2022), which delineates the characteristics of the robust areal Gaussian regression filter.

This standard is significant for evaluating surfaces that may exhibit spike discontinuities and highs and lows (Alicona Imaging GmbH, 2024). It guides the distinction between large-scale and short-scale lateral components of the surfaces. This robust Gaussian filter facilitates a more dependable approach to assessing surfaces, particularly those presenting complex features. The areal roughness of the selected surface was measured using the standard method(Alicona Imaging GmbH, 2024). Moreover, Figure 34 shows the highlighted surface where the areal roughness was measured on each sample.

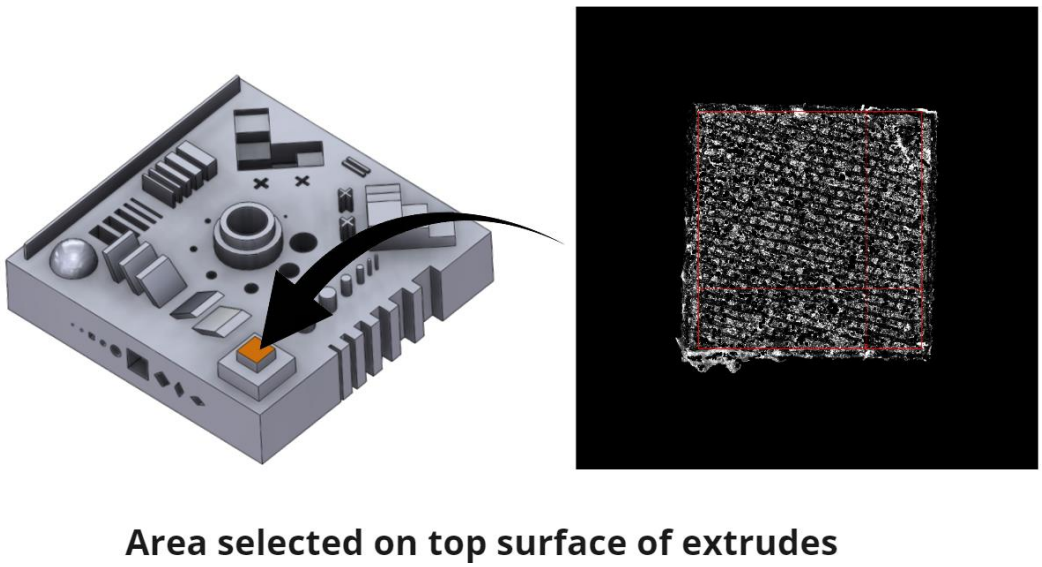

Figure 34: The surface area selected as designated red lines for areal roughness measurement.

As illustrated in Figure 34, the red lines delineate the designated area selected for measuring surface roughness, ensuring uniformity across all samples of the benchmark artifact. Once the area selection is completed, the surface model created by the Alicona Infinite Focus G6 scanner on principles of focus-variation microscopy, which combines the functions of a microscope with robust vertical scanning capabilities. The scanner software analyzes the collection of images to determine the best focus points across the field of view. A precise 3D image of the surface is reconstructed using these focus points, as seen in Figure 35.

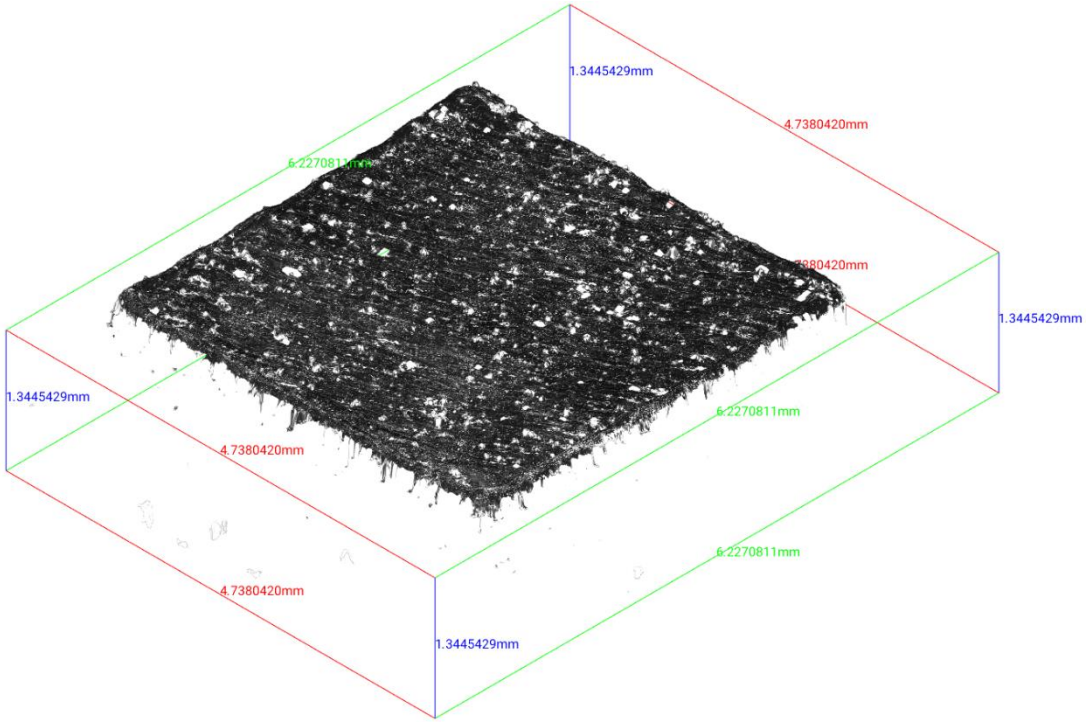

Figure 35: The visualization of a replicated planar form surface created by the Alicona Infinite Focus G6 scanner was created by optically scanning for EOS sample 2 of the benchmark artifact.

As shown in Figure 35, the scanner software analyzes the collection of images to determine the sharpest focus points across the field of view. It reconstructs a precise 3D topography of the surface using these focus points. Next, the calculation of the aerial roughness depends on the Gaussian filter aligning with ISO 16610-71:2014, as explained earlier, and the software calculates the following crucial parameters.

S_a**:** Arithmetic means the heights of the selected area.

S_q**:** Root means square of the heights of the selected area.

S_z**:** Maximum height of the selected surface.

The data distribution displayed with the high and lows over the selected surface is represented in terms of the S_a (mean arithmetic height), S_q (mean square height), and S_z (maximum height) (Alicona Imaging GmbH, 2024) as shown in Figure 36.

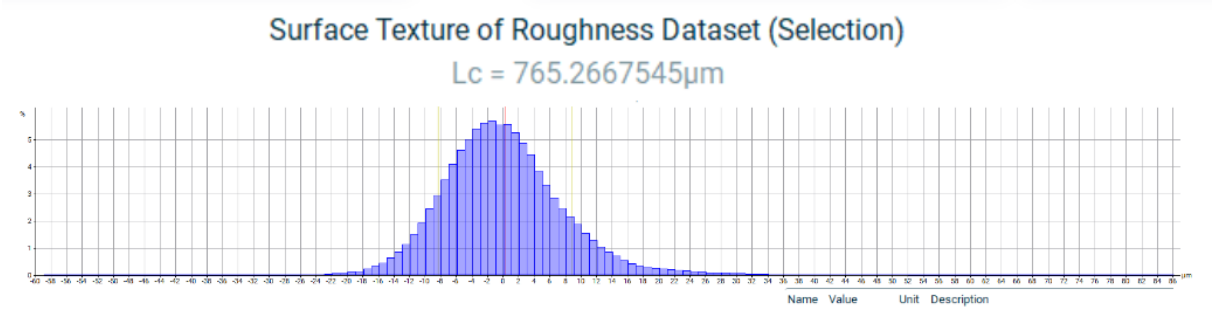

Name	Value	Unit	Description
Sa	6.2320741	µm	Average height of selected area
Sq	8.5705202	µm	Root-Mean-Square height of selected area
Sp	85.9202992	µm	Maximum peak height of selected area
Sv	58.9090596	µm	Maximum valley depth of selected area
Sz	144.8293588	µm	Maximum height of selected area
S10z	119.6798796	µm	Ten point height of selected area
Ssk	1.3515812		Skewness of selected area
Sku	8.1259884		Kurtosis of selected area
Sdq	0.5893464		Root mean square gradient
Sdr	14.8338730	%	Developed interfacial area ratio
FLTt	144.8293588	µm	Flatness using least squares reference plane
Lc	765.2667545	µm	LambdaC: cutoff wavelength

Figure 36: The parameters calculated by Alicona Infinite Focus G6 using the planar form surface generated by scanning for EOS sample 2 of the benchmark artifact.

Figure 36 shows numerous parameters, including S_a, the arithmetic means of the absolute values of the surface deviations measured from the mean plane. S_a value of 6.23 µm in the above instance is the focus of this thesis as it provides a general measure of average roughness, making it particularly useful in the decision-making process. S_a is advantageous when a general indicator of surface roughness is required, as it effectively focuses on the overall average texture of a surface rather than focusing on the extreme values or the distribution of high and low.

In other words, the distribution chart of areal surface roughness typically displays the statistical spread and characteristics of surface deviations across a measured area. Such charts are crucial for analyzing the texture and quality of a surface in a detailed and quantitative manner.

In the results obtained from all the observed AMed benchmark samples, the surface roughness of the EOS M290 was significantly better than that of the Aconity3D MIDI+. This difference can be attributed to the distinct manufacturing parameters used for each machine. If we focus solely on the surface energy deposition, as given by Eq. (25):

$$\left[\mathrm{E_A} = \frac{\text{Energy}}{\text{Spot Size X Scan Speed}}\right] \tag{25}$$

$$\left[E_A(\text{Aconity3D MIDI+}) = \frac{150}{0.08 \times 900}\right]$$
$$\approx 2.08\,\mathrm{J/mm^2}$$

$$\left[E_A(\text{EOS M 290}) = \frac{214.20}{0.08 \times 928.10}\right]$$
$$\approx 2.90\,\mathrm{J/mm^2}$$

where energy, spot size and scan speed from Table 12 used to calculate the energy deposition values for both machines with Eq. (25) show that the process parameters provide sufficient energy for material fusion during hatching, but the EOS M 290 has a slight advantage in terms of energy density. The higher energy deposition in the EOS M 290 ensures efficient material melting and bonding, contributing to its superior surface quality. Additionally, the significant difference in laser power in Table 12 during the hatch pattern between the two machines further impacts the observed surface quality. When evaluating surface quality, it is also essential to consider other factors, such as material properties, cooling, and layer height.

5.9.4. Build time

The approximate build times for constructing the benchmark artifact on different machines were recorded, providing valuable insights for decision-making in the MATLAB application. For example, the EOS M290 required approximately five hours to complete the task of three benchmark artifacts on a single plate. The Aconity3D MIDI+ required approximately eight hours to construct a single artifact on its build plate.

This disparity is attributed to the different sizes of the build envelopes of the two machines, wherein the EOS M290 has a considerably smaller build chamber. The reduced size of the chamber directly reflects the decrease in movement between the build plate and the re-coater

from the powder reservoir, which significantly enhances the efficiency of the EOS M290. Even while constructing three samples simultaneously on a single build plate, the EOS M290 demonstrated a significant speed advantage over the Aconity3D MIDI+. The chamber size of Aconity3D MIDI+ is considerable, and the movement of the re-coater from the powder reservoir to the construct plate takes considerable time.

It is important to note that the set-up times for the machines were not considered in this phase of the research. However, records indicate that the setup time for the Aconity3D MIDI+ was significantly longer due to its open, configurable technology, as opposed to the more streamlined industrial design of the EOS M290.

6. Experimental procedure (Part B: Implementation)

In this phase, the data acquired in the preceding stage is integrated into the backend of an intuitive user interface application. This application will efficiently harness the information gathered from the geometrical tolerances of benchmark artifacts. Users can interact with easy-to-use options through this interface by incorporating straightforward functionalities and MATLAB software visualization techniques.

Additionally, it will streamline the process of generating meaningful outputs tailored to customers' unique requirements and objectives. Ultimately, the interface will empower stakeholders to optimize their decision-making regarding additive manufacturing, enabling them to make well-informed choices based on the insights derived from the extensive dataset based on pre-defined rules in the framework obtained through fuzzy AHP and fuzzy TOPSIS.

6.1. Database integration with MATLAB application

The principal methodology for deriving actionable insights from the benchmark primarily centers around the linkage between the benchmark data and the fuzzy AHP and fuzzy TOPSIS algorithms. Figure 37 illustrates the comprehensive workflow employed in this thesis to generate the desired output of machine preference.

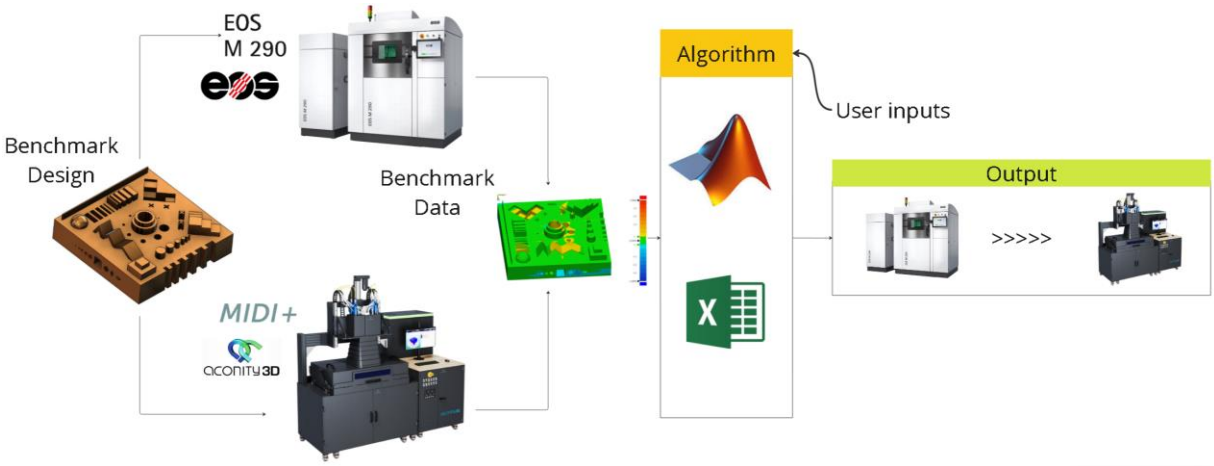

Figure 37: Flow chart of benchmark artifact deviation data linkage with MCDA.

As seen in Figure 37, the process begins with the manufacturing of multiple artifacts on PBF-LB/M machines M 290 from EOS GmbH and Aconity MIDI+ from Aconity3D GmbH, followed by geometrical analysis using a laser scanner to scan the artifact back to the 3D model. The geometrical measurements obtained from the scanner through software calculations are

typically recorded into an Excel sheet and then manually integrated into the backend of a MATLAB application, along with user inputs during the algorithm phase. The resulting output determines the machine efficiency based on the dataset and geometry that needs to be AMed, allowing users to select a preferred machine for their additive manufacturing job.

6.2. MATLAB application interface

The application interface was developed using MATLAB "App Designer," a graphical environment tailored for app creation. As elaborated in previous sections, this interface incorporates graphical scales for user reference to convert user inputs and RMSD crisp values into fuzzy scores. Multiple user interface objects (UIO) facilitate interaction within the app, including buttons, dropdown menus, and text boxes. These UIO elements are customized and designed to respond to user actions, enhancing the usability of the app.

For instance, dropdown menus offer three options: "High," "Medium," and "Low," enabling users to select preferences based on the geometry that needs to be additively manufactured. Meanwhile, preference buttons determine whether specific features and criteria influence the outcome. When a preference is set to "Off," the corresponding category and subcategory values are automatically assigned "Low" in pairwise comparison in fuzzy AHP.

In contrast, other criteria values adjust according to the user selection. Criteria such as build time, surface roughness, and residual stress offer options to include or exclude in the final preference calculation of the framework through "Yes" or "No" preference buttons.

Upon completing the selection of all criteria, users can confirm their choices by clicking the "Confirm" button, followed by the "Calculate" button. This action records user inputs in the backend framework and computer preferences for the machines best suited to the current AMed job. Users then click the "Click for Results" button to view the machine preferences relative to each other. This will show the result when images of machines M 290 from EOS GmbH and Aconity MIDI++ from Aconity3D GmbH are displayed in order of preference.

The MATLAB App Designer interface depicted in Figure 38 showcases various UIO elements corresponding to different criteria inputs.

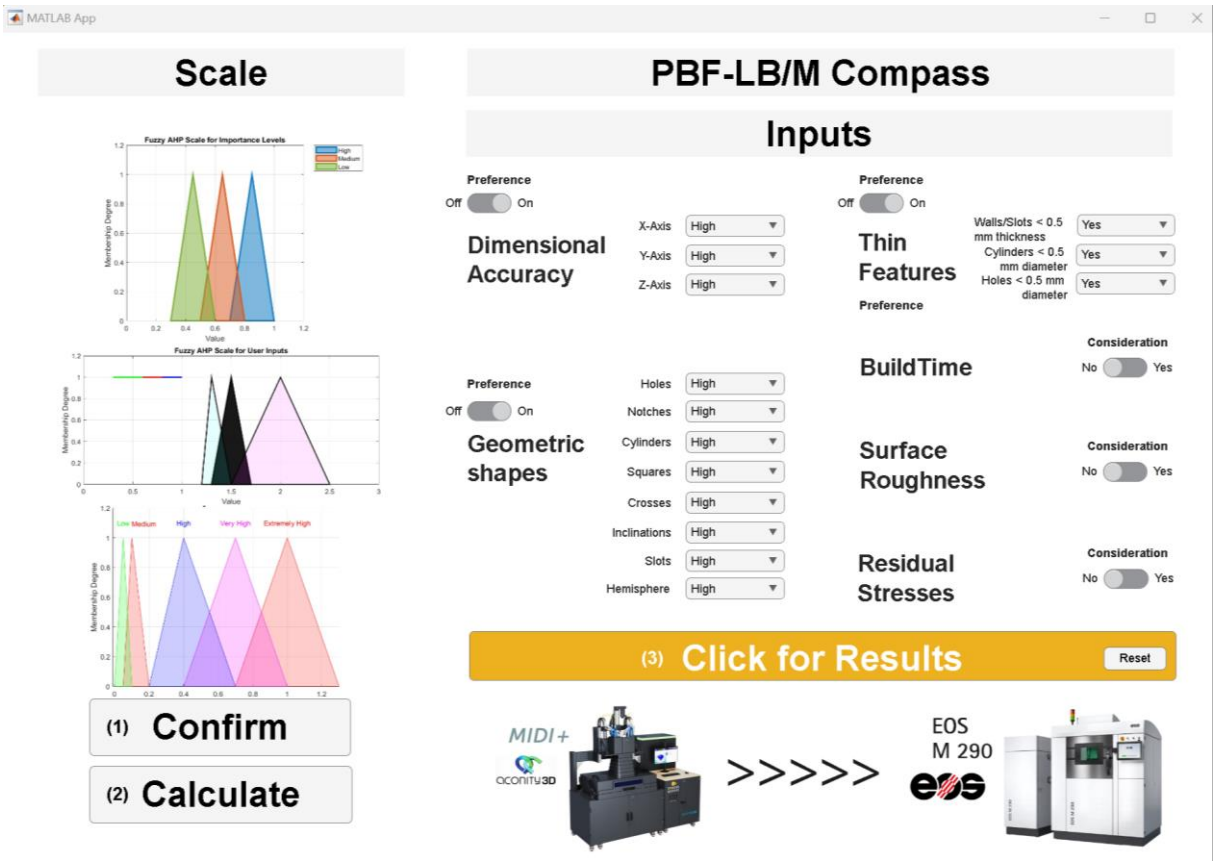

Figure 38: PBF-LB/M Compass as a MATLAB application interface for taking user input based on available options and generating the preference results of PBF-LB/M machines.

As seen in Figure 38, the inputs are recorded and used to calculate preferences on the backend, with the results displayed in the output section labeled "Click for Results." For instance, in the scenario depicted in Figure 38, the Aconity MIDI++ from Aconity3D GmbH is preferred over the M 290 from EOS GmbH. The results will be generated based on the chosen options, reflecting the geometry requirements specified by the users for additive manufacturing.

By making these adjustments and utilizing the MATLAB code in conjunction with the user-friendly interface provided by App Designer, users can efficiently analyze and compare preferences for different alternatives based on their specific manufacturing needs. The MATLAB code provided currently accommodates only two alternatives due to the limitations of this thesis. However, it can be easily modified by rearranging the decision matrix order in the fuzzy TOPSIS algorithm while keeping the rest of the script intact.

7. Results and discussion (Part A: Demonstration of the framework)

The data from the benchmark samples has been documented in Excel, as previously mentioned in Figure 14. The Table 13 provide a summary of the recorded values, as described in Appendix 1: Dimensional drawings of the benchmark artifact and Appendix 3: Data collected in Excel template for benchmark measurements for EOS M290 samples. Additionally, these values are situated within the membership functions of the RMSD scale in Table 13.

Table 13: RMSD values obtained by measurement of different features of geometric benchmark.

Criteria	Machine	RMSD value	Membership function value	Scale value
Accuracy				
Holes	Aconity3D MIDI+	0.21	(0.1, 0.2, 0.4)	High
	EOS M 290	0.20	(0.1, 0.2, 0.4)	High
Notches	Aconity3D MIDI+	0.09	(0.05, 0.1, 0.2)	Medium
	EOS M 290	0.19	(0.1, 0.2, 0.4)	High
Cylinders	Aconity3D MIDI+	0.08	(0.05, 0.1, 0.2)	Medium
	EOS M 290	0.22	(0.1, 0.2, 0.4)	High
Squares	Aconity3D MIDI+	0.18	(0.1, 0.2, 0.4)	High
	EOS M 290	0.40	(0.2, 0.4, 0.7)	Very High
Crosses	Aconity3D MIDI+	0.08	(0.05, 0.1, 0.2)	Medium
	EOS M 290	0.07	(0, 0.05, 0.1)	Low
Inclinations	Aconity3D MIDI+	1.08	(0.7, 1.0, 1.3)	Extremely High
	EOS M 290	0.23	(0.1, 0.2, 0.4)	High
Slots/walls	Aconity3D MIDI+	0.07	(0, 0.05, 0.1)	Low
	EOS M 290	0.71	(0.4, 0.7, 1.0)	Very High
Hemisphere	Aconity3D MIDI+	0.17	(0.1, 0.2, 0.4)	High
	EOS M 290	0.62	(0.4, 0.7, 1.0)	Very High
X-axis	Aconity3D MIDI+	0.78	(0.7, 1.0, 1.3)	Extremely High
	EOS M 290	0.10	(0.05, 0.1, 0.2)	Medium
Y-axis	Aconity3D MIDI+	0.18	(0.1, 0.2, 0.4)	High
	EOS M 290	0.20	(0.1, 0.2, 0.4)	High
Z-axis	Aconity3D MIDI+	0.06	(0, 0.05, 0.1)	Low
	EOS M 290	0.05	(0, 0.05, 0.1)	Low
Thin Features				
Walls/Slots < 0.5mm thickness	Aconity3D MIDI+	0.09	(0.05, 0.1, 0.2)	Medium
	EOS M 290	0.15	(0.1, 0.2, 0.4)	High

Cylinders < 0.5mm diameter	Aconity3D MIDI+	0.05	(0, 0.05, 0.1)	Low
	EOS M 290	0.26	(0.2, 0.4, 0.7)	Very High
Holes < 0.5mm diameter	Aconity3D MIDI+	0.20	(0.1, 0.2, 0.4)	High
	EOS M 290	0.19	(0.1, 0.2, 0.4)	High
Other Parameters				
Surface Roughness	Aconity3D MIDI+	2.00	(1.0, 1.3, 1.6)	Extremely High
	EOS M 290	0.05	(0, 0.05, 0.1)	Low
Build Speed	Aconity3D MIDI+	0.326	(0.2, 0.4, 0.7)	High
	EOS M 290	0.243	(0.2, 0.4, 0.7)	High
Residual Stresses Distortion	Aconity3D MIDI+	1.25	(1.0, 1.3, 1.6)	Extremely High
	EOS M 290	0.94	(0.7, 1.0, 1.3)	Extremely High

Table 13 compares the performance of two machines, the Aconity3D MIDI+ and the EOS M 290, across various criteria which paves the way for decision making in framework. Considering the value of RMSD for EOS M 290, it demonstrates superior performance, particularly in surface roughness, build speed, and handling inclinations, and earning Very Good (VG) and Good (G) ratings. The Aconity3D MIDI+ excels in precision for smaller features and certain geometric shapes like cylinders and squares, achieving Very Good (VG) ratings in these areas.

However, it lags in surface roughness and build speed, where it received Very Poor (VP) and Poor (P) ratings, respectively. Overall, considering only the RMSD values without taken in the consideration of the user inputs for their own respective geometry, the EOS M 290 seems to be better-performing machine for applications prioritizing surface quality and production speed, while the Aconity3D MIDI+ is more suited for high-precision tasks in smaller features and specific geometries.

7.1. Demonstration of the proposed framework

To demonstrate the complete usefulness of the framework and the results obtained in this thesis, a potential use case is explained here. The first step before using the decision-making framework is to identify the geometry of the object that needs to be AMed. After that, the constraints need to be identified in terms of the accuracy of individual geometric features, namely holes, overhangs, slots, and other features as outlined in Table 13. Additionally, the

user should consider whether for the AMed part, the residual distortion, build time, and surface roughness should be considered at this stage. Once the constraints have been identified, the requirements will be input in the form of a simple questionnaire selection from the MATLAB app interface, as illustrated previously in Figure 38.

If example of a geometry is taken as illustrated in Figure 39 that a user is considering for AM using two available PBF-LB/M technologies: Aconity3D MIDI+ and EOS M 290.

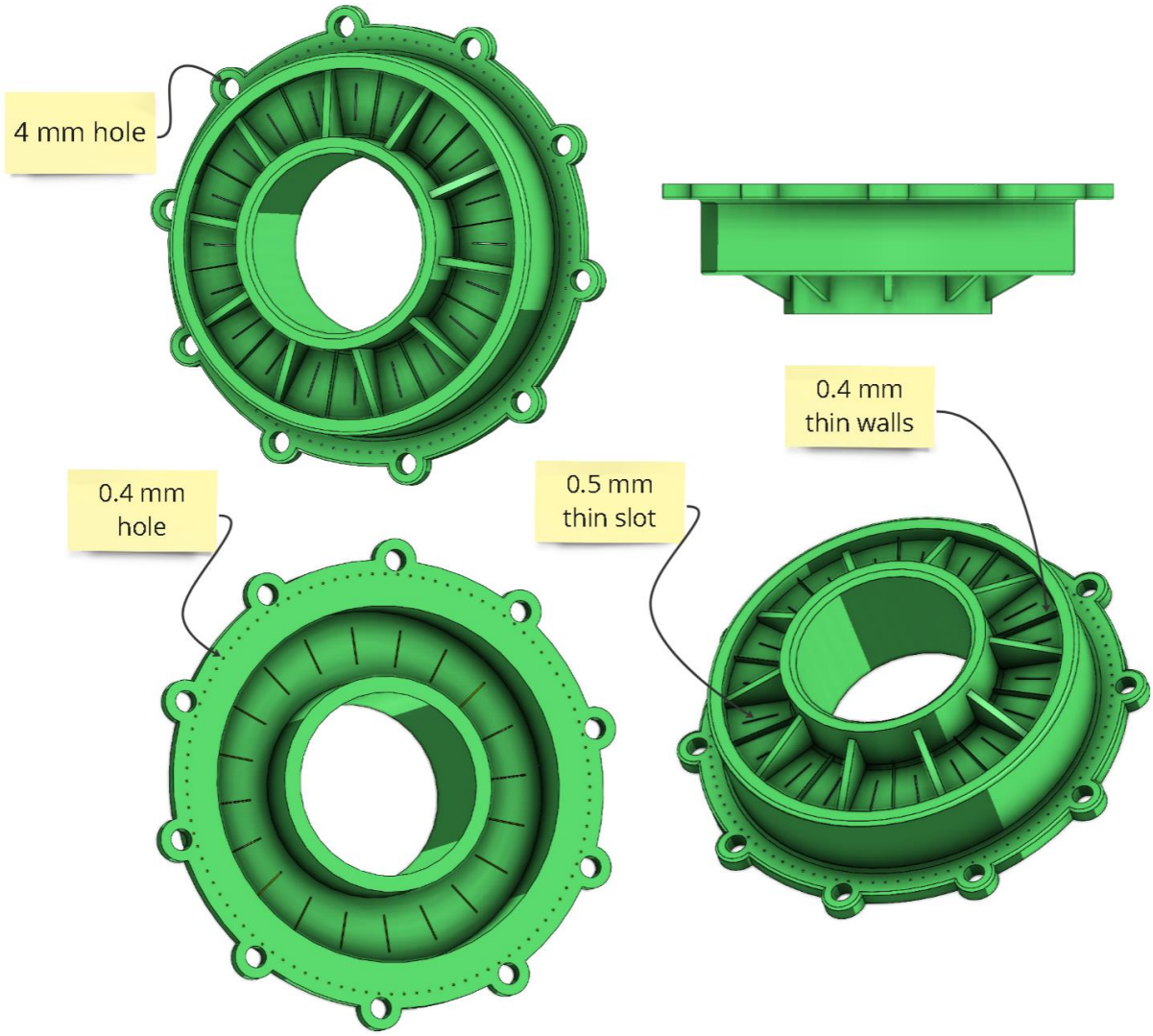

Figure 39: Design of the object needed to be AMed using the decision-making framework.

As seen in Figure 39, the object has distinctive features that needs to be AMed, but the question remains which machine to be used. This is where the geometry needs to be analyzed. The features of the object are shown where the holes are of different diameters ranging from 0.40 mm to 4 mm and even larger diameters holes. There are also small thin walls of 0.40 mm and 0.50 mm slots as well. To start using the framework now we have analysed the geometrical

features and now constrains also needs to be taken in considerations like if the user wants to see that 0.40 mm holes needs to be very precise along with thin walls of 0.40 mm and 0.50 slots as well and in this case the Figure 40 shows the selection of inputs in the MATLAB application interface.

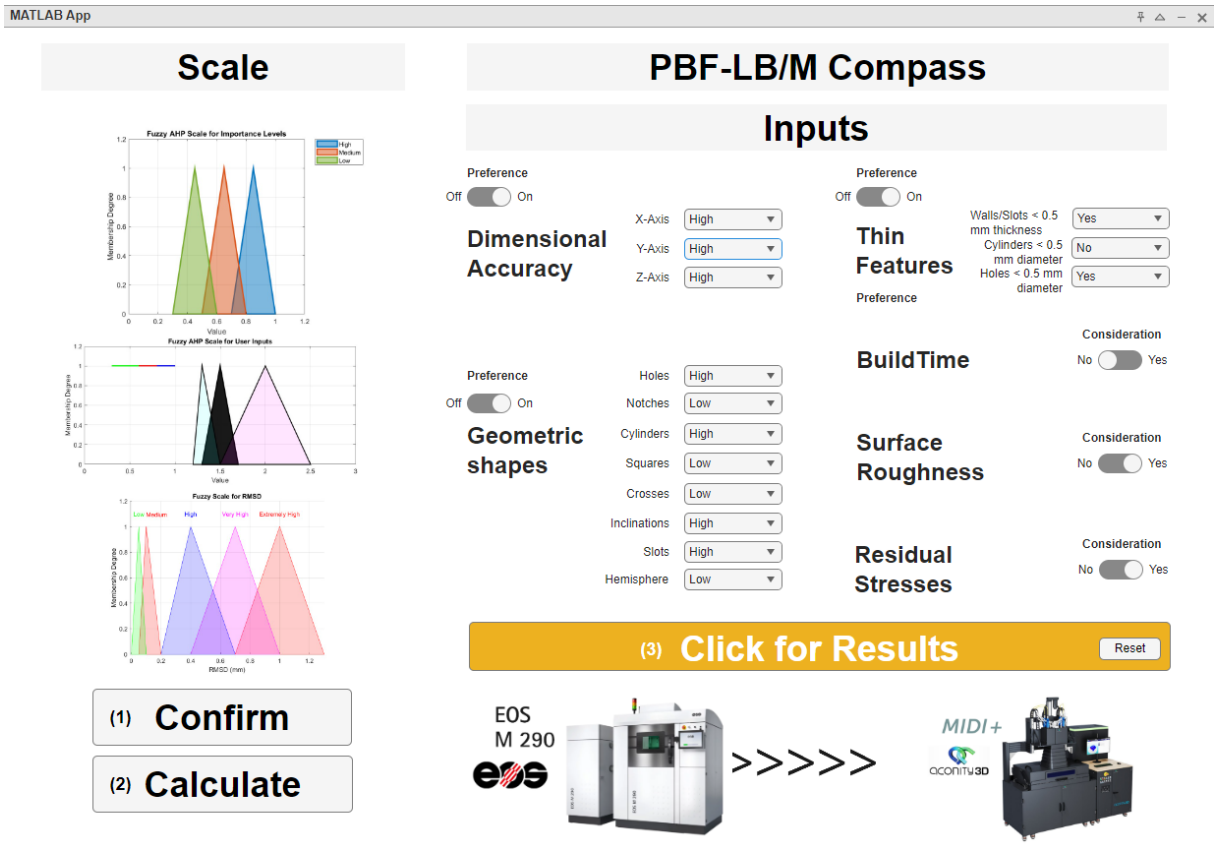

Figure 40: Selection of inputs in the MATLAB application interface for geometry that needs to be AMed.

As seen in Figure 40, based on the visual geometry analysis, there are 0.4 mm holes, 0.5 mm thin slots, and 0.5 mm thin walls. So, the selection options for thin features such as walls/slots with thicknesses less than 0.5 mm and holes with diameters less than 0.5 mm is set to "High." Additionally, the visual analysis of the geometry allows us to prioritize other geometrical shapes like slots, inclinations, cylinders, and holes as "High" preference.

If the user already knows that the part should not undergo extreme post-processing, they can set the options for surface roughness and residual stress to "Yes," while also setting dimensional accuracy to "High" for all axes. Based on these selections, the framework stores the user inputs in the backend and calculates the order of preferences. In Figure 40, the application shows that considering the user constraints and the machine database based on benchmark data, the EOS M290 is the preferred choice in this situation.

Now, if the user is not concerned about surface roughness and knows that the part will require post-processing, they can adjust the dimensional accuracy selections to "Yes." In this scenario, surface roughness can be set to "No" in the app interface, as seen in Figure 41.

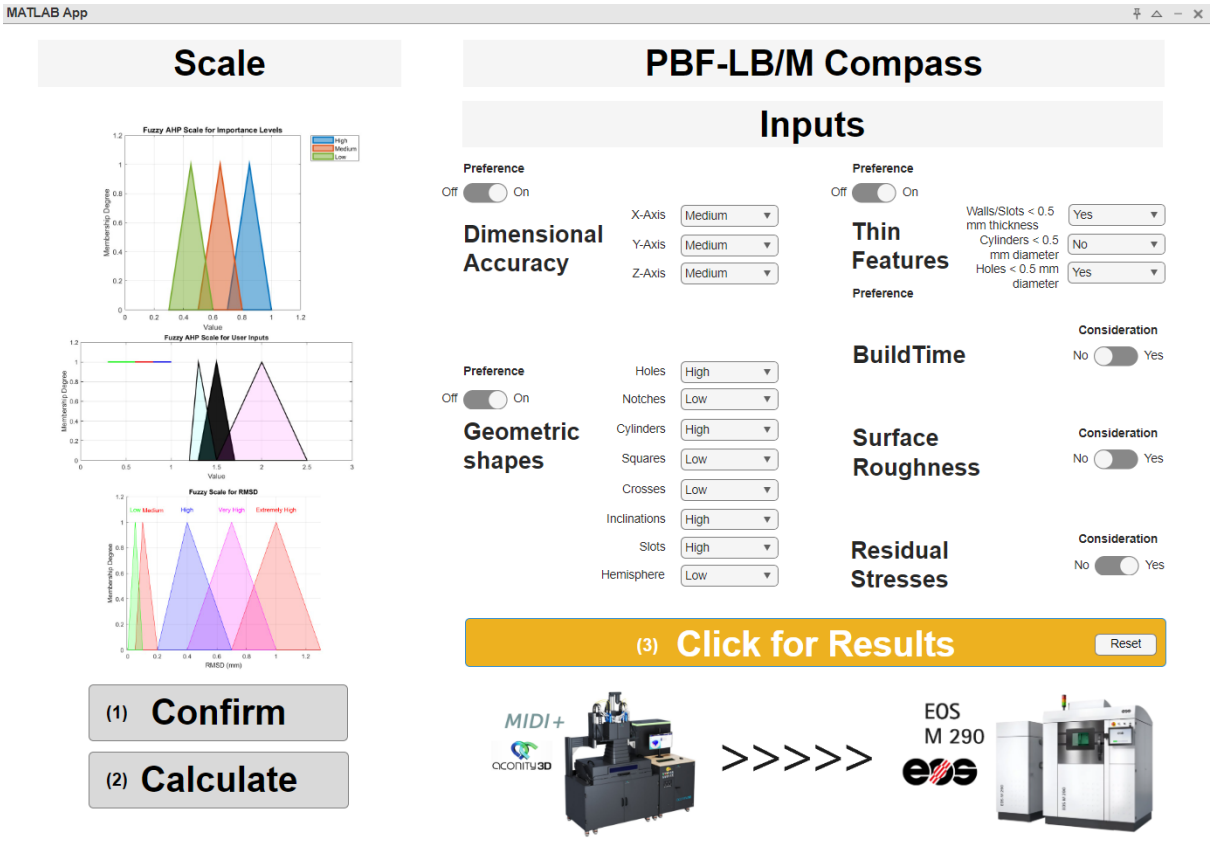

Figure 41: Re-selection of inputs in the MATLAB application interface for updated constraints from user.

As seen in Figure 41, based on the updated selection of surface roughness to "No" and dimensional accuracy to "Medium", the preference is now the Aconity3D MIDI+. Calculations on the backend suggest that the Aconity3D MIDI+ can also perform adequately when surface roughness is not a critical factor.

This simple case study suggests that by using the framework, in just minutes, users can move out of the thinking and guessing phase and decide which machine to choose for their additive manufacturing requirements.

8. Results and discussion (Part B: Framework constraints)

Several constraints have influenced the development of a decision-making framework, necessitating refinement and enhancement. Notably, within this framework, the formulation of the benchmark artifact is intricately linked with geometric data sourced from benchmarks specific to PBF-LB/M technology, primarily emphasizing EOS and Aconity3D systems.

The benchmarking procedure is custom-tailored to evaluate the efficacy of these systems utilizing a singular material, namely 316L stainless steel, within the PBF-L/M process domain. This deliberate selection facilitates a targeted assessment of pivotal performance indicators and ensures methodological consistency in benchmarking across various machines and materials within the horizon of the investigation. The current considerations are illustrated in Figure 42.

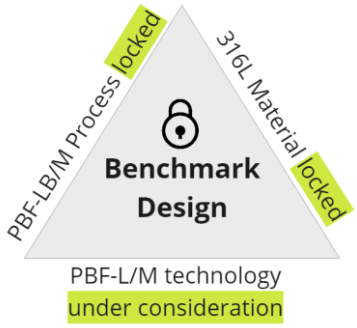

Figure 42: Framework considerations with benchmark design.

As illustrated in Figure 42, the benchmark design is predetermined for both the process and the material. However, it is essential to note that only the technology is under consideration here, aiming to streamline the complexity within the framework. The current state of the framework resembles an educated estimate for the best machines suited for the job, founded on pre-existing information concerning benchmark design and manufacturing, supplemented by data inputted through the MATLAB interface by the user. Enhanced refinement of results can be achieved with increased data input with more AMed samples. It is imperative to acknowledge that every alteration in material and process necessitates corresponding modifications within the framework.

Furthermore, the selection of various scales, such as user inputs depicted in Figure 18 and the RMSD scale discussed in Figure 19, was primarily based on initial estimations, and tailored to yield the desired outcomes for this thesis. However, these scales require refinement by

incorporating insights from experts in the AM field. This refinement process strengthens decision-making by ensuring greater accuracy, relevance, and expert experience.

Likewise, the current framework does not explicitly negate the influence of any criteria when preferences are switched "Off" from the interface. This is attributed to the mathematical computations required to calculate preferences, which could render the matrix unstable. Instead, the values are assigned as "Low" to minimize their impact as much as possible.

Currently, the logic for the framework coding is robust enough to accommodate any number of machines. However, it is designed to make decisions between two machines, aligning with the scope of this thesis research. Nevertheless, the code can be easily modified to a higher degree of decision matrix, albeit with a significant increase in computational overhead as more machines are included.

The interface is structured to have RMSD values preloaded on the application backend, preventing users from modifying them directly through the interface. The MATLAB script coding must manually access any adjustments to these RMSD values for both machines. Notably, for this thesis, only two samples from each machine contribute to the database, thereby influencing the RMSD values considered in the analysis.

Lastly, at this stage of the research for the thesis, even though the app works completely satisfactory and accurately based on the mathematical modelling of benchmark data and user inputs, it still requires experimentation to verify whether the suggestions of the application align with actual outcomes. This will require extensive research and is beyond the scope of this thesis, considering the time required for such a scale of research.

9. Further analysis

The decision-making framework developed is predicated upon the utilization of benchmark artifact samples manufactured utilizing two different PBF-LB/M technology machines. While this initial effort has laid the groundwork for establishing a database, there exists a clear imperative for further refinement to expand its effectiveness.

Although the results in previous section are based solely on the couple of samples AMed on these machines, for further fine tuning and making better use of the framework, a larger database is needed. This expanded dataset will not only enhance the reliability of the framework, but also provide more accurate and informed decision-making processes.

In addition to expanding the dataset collected from benchmark samples, there is a crucial need for refining the measurement strategy. Presently, measurements are conducted using a laser scanner, which, despite its utility, poses limitations in accurately capturing measurements based on geometry and surface reflective properties. Furthermore, measurement uncertainty arises from multiple sources, including device calibration, environmental factors, and inherent part characteristics.

A notable challenge lies in accurately measuring shiny surfaces, as the laser beam may not be adequately reflected or may be mispositioned, particularly around sharp corners and deep holes or slots. To mitigate this challenge, the use of 3D scanning spray, as illustrated in Figure 28, can enhance measurement accuracy. However, a new complication arises if scanning is performed after applying the 3D scanning spray, as the scanner no longer measures the original surface.

Addressing this issue necessitates research into developing compensation factors to adjust dimensions accurately. The compensation factor can be determined by numerous factors, such as the properties of the spray, the geometry of the object being scanned, and the specifications of the scanning equipment. This step is vital to ensure that measurements accurately reflect the true geometry of the benchmark artifact despite corrections introduced by the scanning spray.

10. Conclusion

This study aimed to develop and implement a framework using the geometric benchmark artifact AMed on PBF-LB/M technologies, specifically focusing on the EOS M290 and Aconity3D MIDI+ machines. MATLAB User interface was developed through comprehensive measurement and evaluation of the benchmark artifact, and a backend database was established for decision-making based on RMSD values and corresponding membership functions for user inputs.

The geometric benchmark analysis showed both machines demonstrated unique advantages depending on the criteria evaluated, emphasizing the importance of selecting the right machine for specific applications depending on what user needs to AMed.

Considering the comparison between Aconity3D MIDI+ and EOS M 290 machines using the RMSD scale reveals distinct capabilities for each machine. Aconity3D MIDI+ performs better in terms of notches, cylinders, and slots/walls, exhibiting lower RMSD values that fall within the 'Medium' to 'Low' ranges, indicating high precision in these features. EOS M 290 excels in cross and x-axis accuracy, showing 'Low' and 'Medium' scale values respectively, and achieves better results in surface roughness and build speed. Both machines have high performance in holes, Y-axis, and small hole features. However, EOS M 290 demonstrates significant superiority in maintaining lower residual stresses and surface roughness, while Aconity3D MIDI+ shows higher capabilities in certain geometric accuracies but higher surface roughness and residual stress distortions.

The case study presented in this thesis demonstrates the practical uses of the developed framework in AM. It effectively saves time reducing the trial-and-error phase in selecting the appropriate machine. Additionally, its statistical estimate that minimizes material wastage. Overall, the framework enables informed decision-making and optimized machine usage, leading to significant resource management improvements.

At this stage of research, the framework is at Technology readiness level 3 (TRL 3) which corresponds to " Experimental proof of concept". At this point, the decision-making framework was integrated and validated with the benchmark data through studies and laboratory measurements to evaluate analytical predictions. However, the framework has not yet been evaluated in a relevant operational environment to confirm its practical effectiveness and correctness in real-world scenarios. The framework still requires further experimentation to

verify whether the suggestions of the application correspond to the actual outcomes to take it to (TRL 4).

Future work should focus on expanding the dataset with additional benchmark samples and exploring compensation factors for improved accuracy in 3D laser measurements. Also, incorporating machine learning techniques into this framework holds potential for further enhancing decision-making processes, leading to more efficient, productive, and innovative outcomes in future work. The continued development and application of this framework can provide valuable insights for optimizing the use of PBF-LB/M technologies.

Overall, the scientific relevance of this research lies in its innovative approach to decision-making in AM by integrating a simplified geometric benchmark artifact with a MATLAB-based decision-making framework. From an industrial perspective, the relevance of this research is underscored by its potential to optimize the selection and usage of PBF-LB/M technologies.

11. Future work

In developing the future improved framework, it is crucial to acknowledge the complexity inherent in PBF-L/M technology, characterized by various parameters that influence the additive manufacturing process. While the framework presented in this thesis offers valuable insights into certain aspects of PBF-L/M, it is essential to note that not all parameters have been accounted for due to practical constraints. For instance, Aconity3D MIDI+ is known to have 150+ parameters to control the AM process, and as explained in Figure 6, abundant technological challenges correspond to various process parameters mentioned in Figure 2

However, these parameters were not explicitly addressed in this framework due to resource, time, and scope limitations. Nonetheless, the framework provides a structured approach to decision-making in PBF-L/M technology selection, offering a foundation for further research and refinement to encompass a broader range of parameters and considerations in future iterations. The limitations of the fuzzy principle to managing such large groups of parameters are unsuitable. This is where a larger framework consisting of machine learning (ML) focuses on creating algorithms and models that can learn from data and eliminate unnecessary parameters in decision-making, as illustrated in Figure 43.

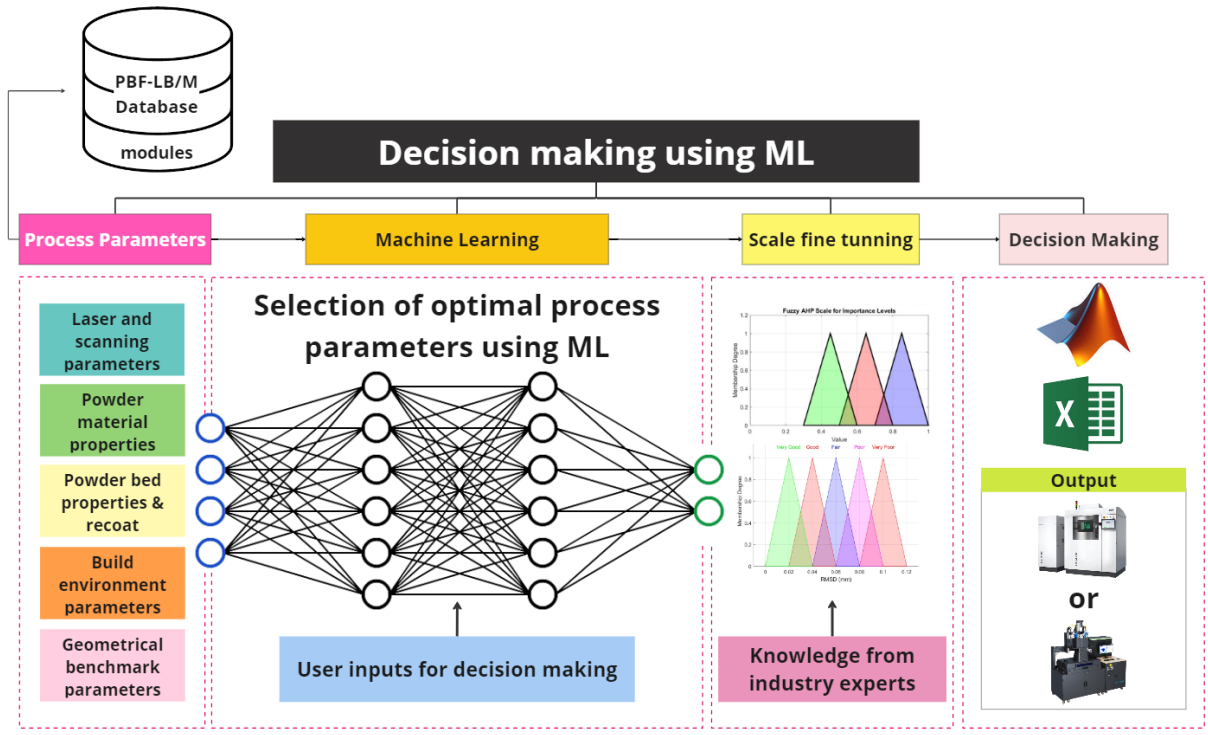

Figure 43: Future work framework considerations for improvement with the integration of ML.

The flowchart illustrated in Figure 43 summarises the possible intricate decision-making process by utilizing machine learning (ML) to select optimal process parameters in additive manufacturing, particularly within the PBF-LB/M domain.

The process begins with data from the PBF-LB/M database and user inputs, including various process optimization parameters. These inputs are processed through a machine learning model to optimize the selection of process parameters. The knowledge from industry experts is also used to scale fine-tuning before making a final decision and with the addition of a back-propagation algorithm to update the weights of criteria to minimize the errors. The final decision-making process is characterized by potential outcomes: technology selection for a specific job.

ML can potentially reform various aspects of AM, leading to improved efficiency, productivity, and innovation in decision-making. When integrated into the framework of decision-making, machine learning can contribute to more accurate results in future research in the context of this thesis.

12. References

Aconity3D. (2024a). *Aconity3D MIDI*.
https://configurator.aconity3d.com/EN/units/AconityTWO

Aconity3D. (2024b). *AconityMIDI+*. www.aconity3d.com

Aconity3D GmbH. (2024a). *Academy | Aconity3D*. https://aconity3d.com/academy/#

Aconity3D GmbH. (2024b). *Aconity3D GmbH - additive manufacturing*. Https://Aconity3d.Com/Machines/.

Alicona Imaging GmbH. (2024a). *Optical 3D Surface Roughness Measurement Instrument - Alicona*. https://www.alicona.com/en/products/infinitefocus

Alicona Imaging GmbH. (2024b). *The easy way to explain roughness - Alicona*. https://www.alicona.com/en/blog-posts/the-easy-way-to-explain-roughness

Anand, M. B., & Vinodh, S. (2018). Application of fuzzy AHP – TOPSIS for ranking additive manufacturing processes for microfabrication. *Rapid Prototyping Journal*, *24*(2), 424–435. https://doi.org/10.1108/RPJ-10-2016-0160

Attaran, M. (2017). The rise of 3-D printing: The advantages of additive manufacturing over traditional manufacturing. *Business Horizons*, *60*(5), 677–688. https://doi.org/10.1016/j.bushor.2017.05.011

Autodesk Inc. (2024). *Autodesk Fusion with Netfabb*. https://www.autodesk.fi/products/netfabb/overview?term=1-YEAR&tab=subscription&plc=F360NFP

Bai, Y., & Wang, D. (2006). Fundamentals of fuzzy logic control — fuzzy sets, fuzzy rules and defuzzifications. *Advances in Industrial Control*, *9781846284687*, 17–36. https://doi.org/10.1007/978-1-84628-469-4_2

Bartlett, J. L., & Li, X. (2019). An overview of residual stresses in metal powder bed fusion. *Additive Manufacturing*, *27*, 131–149. https://doi.org/10.1016/j.addma.2019.02.020

Beau Jackson. (2017). *How EOS, Concept Laser and SLM Solutions are transforming additive automation*. Https://3dprintingindustry.Com/News/Eos-Concept-Laser-Slm-Solutions-Transforming-Additive-Automation-124616/.

Bernsmann, J. S. L., Hillebrandt, S., Rommerskirchen, M., Bold, S., & Schleifenbaum, J. H. (2023). On the Use of Metal Sinter Powder in Laser Powder Bed Fusion Processing (PBF-LB/M). *Materials 2023, Vol. 16, Page 5697*, *16*(16), 5697. https://doi.org/10.3390/MA16165697

Brian Lord. (2018). *3D Printing News Sliced, $11M project call, SLM Solutions, Aconity3D, Onshape*. Https://3dprintingindustry.Com/News/3d-Printing-News-Sliced-11m-Project-Call-Slm-Solutions-Aconity3d-Onshape-137970/.

Byun, H. S., & Lee, K. H. (2003). Design of a new test part for benchmarking the accuracy and surface finish of rapid prototyping processes. *Lecture Notes in Computer Science (Including Subseries Lecture Notes in Artificial Intelligence and Lecture Notes in Bioinformatics)*, *2669*, 731–740. https://doi.org/10.1007/3-540-44842-X_74/COVER

Byun, H. S., & Lee, K. H. (2005). A decision support system for the selection of a rapid prototyping process using the modified TOPSIS method. *International Journal of Advanced Manufacturing Technology*, *26*(11–12), 1338–1347. https://doi.org/10.1007/S00170-004-2099-2/METRICS

Carl Zeiss AG. (2024). *ZEISS T-Scan 20*. https://www.zeiss.co.uk/metrology/campaigns/zeiss-t-scan-20.html

Chua, C. K., Wong, C. H., & Yeong, W. Y. (2017). Benchmarking for Additive Manufacturing. *Standards, Quality Control, and Measurement Sciences in 3D Printing and Additive Manufacturing*, 181–212. https://doi.org/10.1016/B978-0-12-813489-4.00008-8

Cruz Sanchez, F. A., Boudaoud, H., Muller, L., & Camargo, M. (2014). Towards a standard experimental protocol for open-source additive manufacturing: This paper proposes a benchmarking model for evaluating accuracy performance of 3D printers. *Virtual and Physical Prototyping*, *9*(3), 151–167. https://doi.org/10.1080/17452759.2014.919553

Dassault Systèmes. (2024). *SOLIDWORKS PREMIUM THE POWER YOU NEED TO DRIVE INNOVATION*. www.solidworks.com/simulation.

de Pastre, M.-A., Toguem Tagne, S.-C., & Anwer, N. (2020). Test artefacts for additive manufacturing: A design methodology review. *CIRP Journal of Manufacturing Science and Technology*, *31*, 14–24. https://doi.org/10.1016/j.cirpj.2020.09.008

Debasis Samanta. (2024). *Chapter 3 Fuzzy Membership Function Formulation and Parameterization*. Retrieved March 25, 2024, from https://cse.iitkgp.ac.in/~dsamanta/courses/archive/sca/Archives/Chapter%203%20Fuzzy%20Membership%20Functions.pdf

Delgado, J., Ciurana, J., Reguant, C., & Cavallini, B. (2010). Studying the repeatability in DMLS technology using a complete geometry test part. *Innovative Developments in Design and Manufacturing - Advanced Research in Virtual and Rapid Prototyping*, 349–353. https://doi.org/10.1201/9780203859476-63/STUDYING-REPEATABILITY-DMLS-TECHNOLOGY-USING-COMPLETE-GEOMETRY-TEST-PART-DELGADO-CIURANA-REGUANT-CAVALLINI

Douligeris, C. (2001). Computer networks design using hybrid fuzzy expert systems. *Soft Computing 2001 5:4*, *5*(4), 272–286. https://doi.org/10.1007/S005000100101

Dr. Seema Mishra. (2023). *A BRIEF INTRODUCTION OF FUZZY SETS AND FUZZY LOGIC – Patna Women's College | Best College in Patna | Best MCA College in Patna for Women's*. https://patnawomenscollege.in/a-brief-introduction-of-fuzzy-sets-and-fuzzy-logic/

Emrouznejad, A., & St, C. (2022). *Fuzzy Analytic Hierarchy Process*. https://www.researchgate.net/publication/362269475

EOS GmbH. (2024a). *Benefit from Our New Generation of Job and Process Management Software*. https://www.eos.info/systems_solutions/software

EOS GmbH. (2024b). *EOS M 290*. https://www.eos.info/en-us/metal-solutions/metal-printers/data-sheets/sds-eos-m-290?topdf

EOS GmbH. (2024c). *SDS EOS M 290*. Https://Www.Eos.Info/En-Us/Metal-Solutions/Metal-Printers/Data-Sheets/Sds-Eos-m-290.

EOS GmbH. (2024d). *StainlessSteel 316L*.

Ertürk, E., Musil, B., Diez, G., Felber, C., & Höfer, P. (2023). Surface morphology influences of PBF-LB manufactured Ti6Al4V parts on adhesive bond strength—investigation of as-built and surface-treated conditions. *Progress in Additive Manufacturing*, *8*(4), 719–731. https://doi.org/10.1007/S40964-023-00450-7/FIGURES/14

Gogus, O., & Boucher, T. O. (1998). Strong transitivity, rationality and weak monotonicity in fuzzy pairwise comparisons. *Fuzzy Sets and Systems*, *94*(1), 133–144. https://doi.org/10.1016/S0165-0114(96)00184-4

Hanine, M., Boutkhoum, O., Tikniouine, A., & Agouti, T. (2016). Application of an integrated multi-criteria decision making AHP-TOPSIS methodology for ETL software selection. *SpringerPlus*, *5*(1). https://doi.org/10.1186/s40064-016-1888-z

Herzog, D., Seyda, V., Wycisk, E., & Emmelmann, C. (2016). Additive manufacturing of metals. *Acta Materialia*, *117*, 371–392. https://doi.org/10.1016/j.actamat.2016.07.019

Huber, F., Papke, T., Scheitler, C., Hanrieder, L., Merklein, M., & Schmidt, M. (2018). In Situ Formation of a Metastable β-Ti Alloy by Laser Powder Bed Fusion (L-PBF) of Vanadium and Iron Modified Ti-6Al-4V. *Metals*, *8*(12), 1067. https://doi.org/10.3390/met8121067

Ishak, A., & Wanli. (2020). Analysis of Fuzzy AHP-TOPSIS Methods in Multi Criteria Decision Making: Literature Review. *IOP Conference Series: Materials Science and Engineering*, *1003*(1), 012147. https://doi.org/10.1088/1757-899X/1003/1/012147

ISO. (2022). *ISO 16610-71:2014 - Geometrical product specifications (GPS) — Filtration — Part 71: Robust areal filters: Gaussian regression filters*. https://www.iso.org/standard/60159.html

ISO. (2023). *Additive manufacturing of metals*. https://www.iso.org/standard/78529.html

Jensch, F., Buhl, J., Laue, R., & Härtel, S. (2023). Application of the plane-strain-compression-test to determine the local mechanical properties of LPBF-manufactured 316l components. *Materials Research Proceedings*, *28*, 149–158. https://doi.org/10.21741/9781644902479-17

KDM Fabrication. (2023, August 8). *Laser Powder Bed Fusion: Revolutionizing 3D Manufacturing for Metal Parts*. Https://Kdmfab.Com/Laser-Powder-Bed-Fusion/#Understanding_Laser_Powder_Bed_Fusion_LPBF_Technology.

Kniepkamp, M., Fischer, J., & Abele, E. (2016). *Dimensional Accuracy of Small Parts Manufactured by Micro Selective Laser Melting*. https://hdl.handle.net/2152/89691

Kranz, J., Herzog, D., & Emmelmann, C. (2015). Design guidelines for laser additive manufacturing of lightweight structures in TiAl6V4. *Journal of Laser Applications*, *27*(S1), 48. https://doi.org/10.2351/1.4885235/221702

Kruth, J. P. (1991). Material Incress Manufacturing by Rapid Prototyping Techniques. *CIRP Annals*, *40*(2), 603–614. https://doi.org/10.1016/S0007-8506(07)61136-6

Kruth, J., Vandenbroucke, B., Vaerenbergh, J., & Mercelis, P. (2005). *Benchmarking of different SLS/SLM processes as Rapid Manufacturing techniques*.

Kusumawardani, R. P., & Agintiara, M. (2015). Application of Fuzzy AHP-TOPSIS Method for Decision Making in Human Resource Manager Selection Process. *Procedia Computer Science*, *72*, 638–646. https://doi.org/10.1016/J.PROCS.2015.12.173

Lan, H., Ding, Y., & Hong, J. (2005). Decision support system for rapid prototyping process selection through integration of fuzzy synthetic evaluation and an expert system. *International Journal of Production Research*, *43*(1), 169–194. https://doi.org/10.1080/00207540410001733922

Laura Castillo. (2005). *Study about the rapid manufacturing of complex parts of stainless steel and titanium*. https://publications.tno.nl/publication/34639026/gfJMtd/castillo-2005-study.pdf

Luisa, S., Contuzzi, N., Angelastro, A., & Domenico, A. (2010). Capabilities and Performances of the Selective Laser Melting Process. In *New Trends in Technologies: Devices, Computer, Communication and Industrial Systems* (pp. 233–250). Sciyo. https://doi.org/10.5772/10432

Mahapatra, S. S., & Panda, B. N. (2013). Benchmarking of rapid prototyping systems using grey relational analysis. *International Journal of Services and Operations Management*, *16*(4), 460. https://doi.org/10.1504/IJSOM.2013.057509

Mahesh, M., Fuh, J. Y. H., Wong, Y. S., & Loh, H. T. (2005). *Benchmarking for Decision Making in Rapid Prototyping Systems*.

MANI MAHESH. (2004). *Rapid prototyping and manufacturing benchmarking. ScholarBank@NUS Repository.* https://scholarbank.nus.edu.sg/handle/10635/14697

Martucci, A., Aversa, A., Bondioli, F., Fino, P., & Lombardi, M. (2022). Synergic strategies to improve the PBF-LB\M processability of a cracking-sensitive alloy. *Materials & Design*, *224*, 111396. https://doi.org/10.1016/J.MATDES.2022.111396

Melia, M. A., Duran, J. G., Koepke, J. R., Saiz, D. J., Jared, B. H., & Schindelholz, E. J. (2020). How build angle and post-processing impact roughness and corrosion of additively manufactured 316L stainless steel. *Npj Materials Degradation 2020 4:1*, *4*(1), 1–11. https://doi.org/10.1038/s41529-020-00126-5

Metal AM magazine. (2023, August 23). *Tailored materials for additive manufacturing: Expanding diversity with "powder kits" in PBF-lb*. Https://Www.Metal-Am.Com/Articles/Tailored-Materials-for-Additive-Manufacturing-Expanding-Diversity-Powder-Kits-Pbf-Lb/.

Moshiri, M., Candeo, S., Carmignato, S., Mohanty, S., & Tosello, G. (2019). Benchmarking of laser powder bed fusion machines. *Journal of Manufacturing and Materials Processing*, *3*(4). https://doi.org/10.3390/jmmp3040085

Moylan, S., Slotwinski, J., Cooke, A., Jurrens, K., & Alkan Donmez, M. (2012). *PROPOSAL FOR A STANDARDIZED TEST ARTIFACT FOR ADDITIVE MANUFACTURING MACHINES AND PROCESSES*. http://www.nist.gov/el/isd/sbm/matstandaddmanu.cfm.

Nădăban, S., Dzitac, S., & Dzitac, I. (2016). Fuzzy TOPSIS: A General View. *Procedia Computer Science*, *91*, 823–831. https://doi.org/10.1016/j.procs.2016.07.088

Nayakappa, P. A., Gaurish, W., & Mahesh, G. (2019). *Grey Relation Analysis Methodology and its Application*. www.rrjournals.com

NIST. (2023). *Additive Manufacturing Benchmark Test Series (AM-Bench) | NIST*. AM Bench 2022. https://www.nist.gov/ambench

Oqton. (2024). *Geomagic Control X Software | Metrology Software | Oqton*. https://oqton.com/geomagic-controlx/

Piili, H. (2023). *A conceptual, holistic framework to overcome limitations and constraints of design in laser-based powder bed fusion of metals: Case novel separation and purification units*. https://lutpub.lut.fi/handle/10024/166570

Pouti, N. (2022). Design and Development of the Rapid Prototyping Techniques Ontology with the Appropriate Technique Selection Approach. *2022 8th International Conference on Web Research, ICWR 2022*, 94–106. https://doi.org/10.1109/ICWR54782.2022.9786249

Protolabs. (2024). *Metal 3D printing: The manufacturing & design guide | Protolabs Network*. Retrieved March 9, 2024, from https://www.hubs.com/guides/metal-3d-printing/#rules

Ransikarbum, K., & Khamhong, P. (2021). Integrated Fuzzy Analytic Hierarchy Process and Technique for Order of Preference by Similarity to Ideal Solution for Additive Manufacturing Printer Selection. *Journal of Materials Engineering and Performance*, *30*(9), 6481–6492. https://doi.org/10.1007/s11665-021-05816-y

Rebaioli, L., & Fassi, I. (2017). A review on benchmark artifacts for evaluating the geometrical performance of additive manufacturing processes. *International Journal of Advanced*

Manufacturing Technology, *93*(5–8), 2571–2598. https://doi.org/10.1007/s00170-017-0570-0

Renishaw plc. (2014). *Design for metal AM - a beginner's guide*. https://www.renishaw.com/en/design-for-metal-am-a-beginners-guide--43333

Richter, L. G. (1991). *Das Problem der Bedingung*. Brill. https://brill.com/display/book/9789004455665/B9789004455665_s008.xml

S. Hussain Ather. (2020). *How to calculate RMSD*. Https://Sciencing.Com/Calculate-Rmsd-5146965.Html. https://sciencing.com/calculate-rmsd-5146965.html

Sercombe, T. B., & Hopkinson, N. (2006). Process Shrinkage and Accuracy during Indirect Laser Sintering of Aluminium. *Advanced Engineering Materials*, *8*(4), 260–264. https://doi.org/10.1002/ADEM.200500265

SLM Solutions. (2024). *SLM 280HL*. https://www.3dprintekzo.be/wp-content/uploads/2016/08/151028_slm280_en_0.pdf

Spears, T. G., & Gold, S. A. (2016). In-process sensing in selective laser melting (SLM) additive manufacturing. In *Integrating Materials and Manufacturing Innovation* (Vol. 5, Issue 1, pp. 16–40). Springer Science and Business Media Deutschland GmbH. https://doi.org/10.1186/s40192-016-0045-4

Spurek, M. A., Spierings, A. B., Lany, M., Revaz, B., Santi, G., Wicht, J., & Wegener, K. (2022). In-situ monitoring of powder bed fusion of metals using eddy current testing. *Additive Manufacturing*, *60*, 103259. https://doi.org/10.1016/J.ADDMA.2022.103259

Sun, C. C. (2010). A performance evaluation model by integrating fuzzy AHP and fuzzy TOPSIS methods. *Expert Systems with Applications*, *37*(12), 7745–7754. https://doi.org/10.1016/j.eswa.2010.04.066

Taylor, H. C., Garibay, E. A., & Wicker, R. B. (2021). Toward a common laser powder bed fusion qualification test artifact. *Additive Manufacturing*, *39*. https://doi.org/10.1016/j.addma.2020.101803

Tofail, S. A. M., Koumoulos, E. P., Bandyopadhyay, A., Bose, S., O'Donoghue, L., & Charitidis, C. (2018). Additive manufacturing: scientific and technological challenges, market uptake and opportunities. In *Materials Today* (Vol. 21, Issue 1, pp. 22–37). Elsevier B.V. https://doi.org/10.1016/j.mattod.2017.07.001

Vantage Market Research, https://www. vantagemarketresearch. com/. (2023, December 6). *Additive Manufacturing Market - Global Industry Assessment & Forecast*.

Vock, S., Klöden, B., Kirchner, A., Weißgärber, T., & Kieback, B. (2019). Powders for powder bed fusion: a review. *Progress in Additive Manufacturing*, *4*(4), 383–397. https://doi.org/10.1007/S40964-019-00078-6/TABLES/3

Xu, F., Wong, Y. S., & Loh, H. T. (2001). Toward generic models for comparative evaluation and process selection in rapid prototyping and manufacturing. *Journal of Manufacturing Systems*, *19*(5), 283–296. https://doi.org/10.1016/S0278-6125(01)89001-4

Yap, Y. L., Sing, S. L., & Yeong, W. Y. (2020). A review of 3D printing processes and materials for soft robotics. In *Rapid Prototyping Journal* (Vol. 26, Issue 8, pp. 1345–1361). Emerald Group Holdings Ltd. https://doi.org/10.1108/RPJ-11-2019-0302

Yi, H., Cao, H., Liu, M., & Jia, L. (2023). *Additive Manufacturing (AM) for Advanced Materials and Structures Green and Intelligent Development Trend*. https://doi.org/https://doi.org/10.3390/books978-3-0365-6334-3

Zhang, W., Hou, W., Deike, L., & Arnold, C. B. (2020). Using a dual-laser system to create periodic coalescence in laser powder bed fusion. *Acta Materialia*, *201*, 14–22. https://doi.org/10.1016/J.ACTAMAT.2020.09.071

Zhang, Y., Xu, Y., & Bernard, A. (2014). A new decision support method for the selection of RP process: Knowledge value measuring. *International Journal of Computer Integrated Manufacturing*, *27*(8), 747–758. https://doi.org/10.1080/0951192X.2013.834474

Zheng, P., Wang, Y., Xu, X., & Xie, S. Q. (2017). A weighted rough set based fuzzy axiomatic design approach for the selection of AM processes. *International Journal of Advanced Manufacturing Technology*, *91*(5–8), 1977–1990. https://doi.org/10.1007/S00170-016-9890-8/METRICS

13. Appendix 1: Dimensional drawings of the benchmark artifact

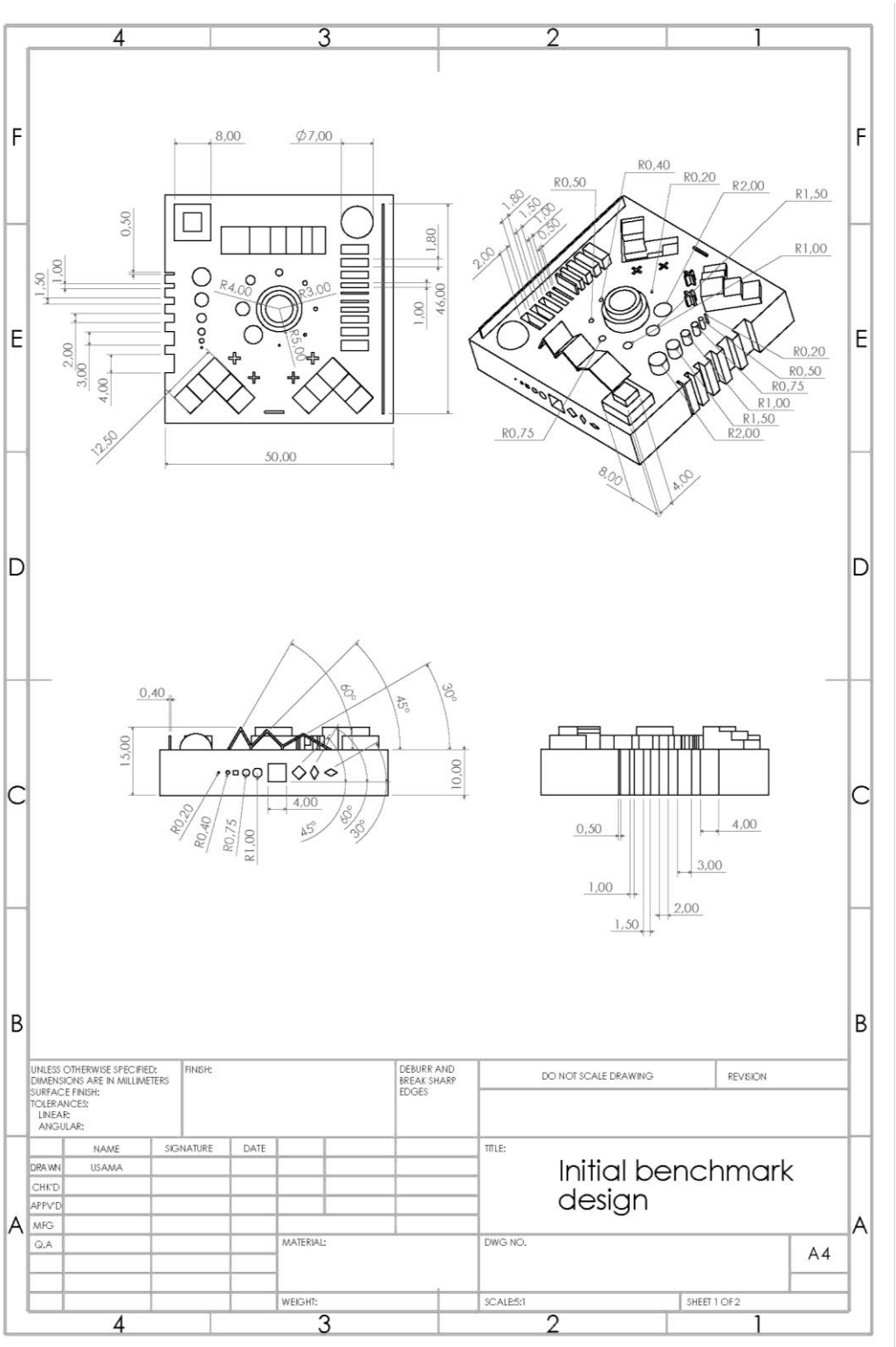

Figure 44: Dimensional drawing of benchmark artifact used for the decision-making process.

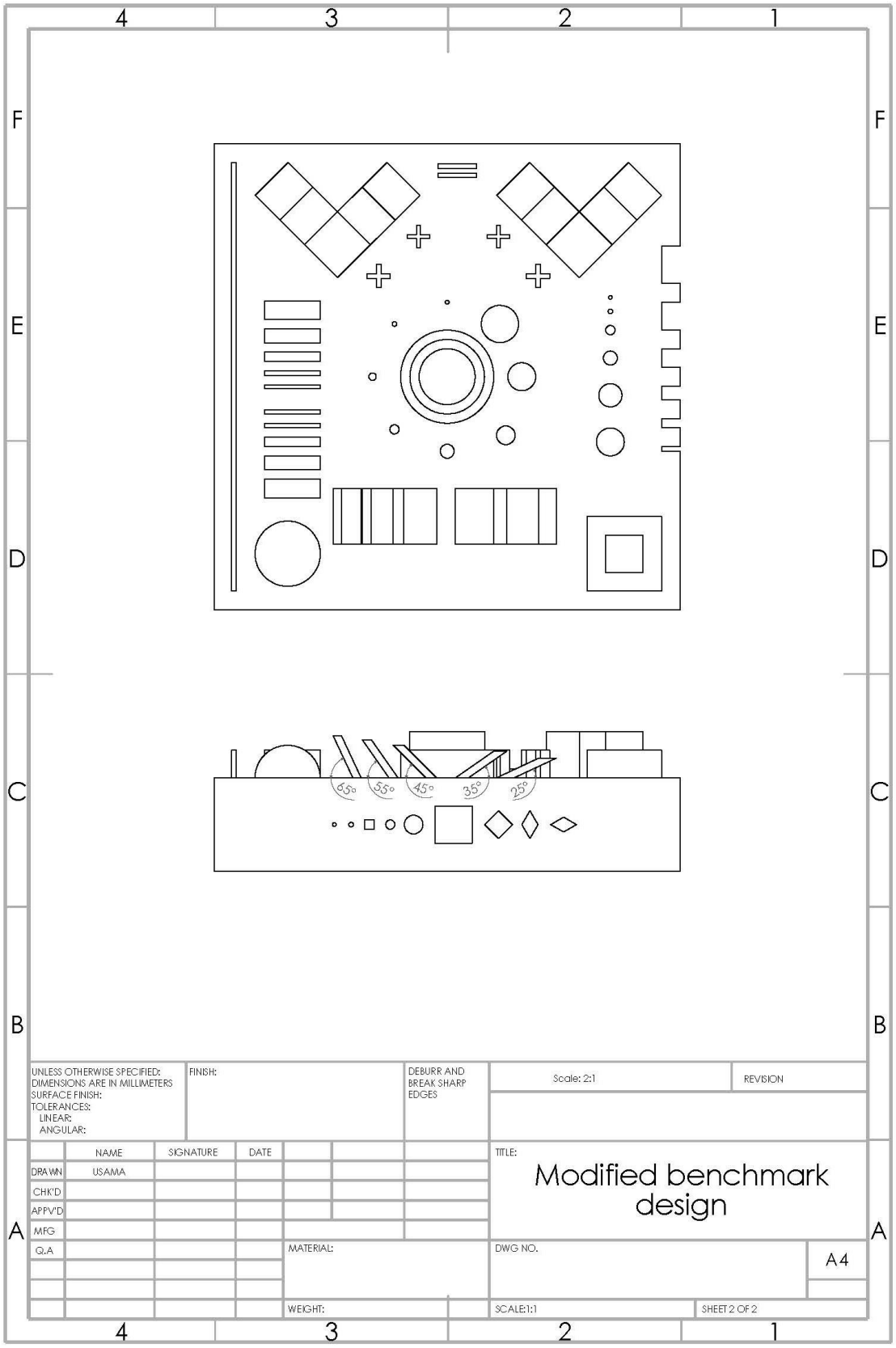

Figure 45: Dimensional drawing of benchmark artifact used for the decision-making process.

14. Appendix 2: Data collected in Excel template for benchmark measurements for Aconity3D MIDI+ samples.

Below are measurements recorded for the two samples AMed on Aconity3D MIDI+. These tables collect all the data to be used calculate the RMSD values on the backend of MATLAB application for decision making. The highlighted yellow values are the only measurements recorded now for scope of this thesis for two samples AMed with the modified design of benchmark artifact.

Table 13 to 24 shows the recorded measurements for measuring the accuracy aspects of AMed benchmark samples on Aconity3D MIDI+.

Table 14: Measurements for overhanging inclination structures.

Inclinations										
#	feature ID	Axis	Nominal Value	Measured Values			Mean	SD	Mean Deviation	RMSD
				Sample 1	Sample 2	Sample 3				
1	Inclination	ZY	0.00	0.00	0.00	0.00	0.00	0.00	0.00	0.00
2			0.00	0.00	0.00	0.00	0.00	0.00	0.00	0.00
			45.00	45.22	43.09	0.00	44.16	1.19	0.84	1.36
			35.00	35.90	35.84	0.00	35.87	0.05	0.87	0.87
3			25.00	25.29	26.41	0.00	25.85	0.79	0.85	1.02
Recommend minimum of 2 measurement points									**Mean RMSD**	1.08

Table 15: Measurements for cicular hole features diameters.

Holes										
#	feature ID	Axis	Nominal Value	Measured Values			Mean	SD	Mean Deviation	RMSD
				Sample 1	Sample 2	Sample 3				
1	B1	Z	6.00	5.94	6.03	0.00	5.98	0.02	0.02	0.05
2	B2	Z	0.00	0.00	0.00	0.00	0.00	0.00	0.00	0.00
3	B3	Z	0.00	0.00	0.00	0.00	0.00	0.00	0.00	0.00
4	B4	Z	2.00	1.80	1.84	0.00	1.82	0.03	0.18	0.18
5	B5	Z	0.00	0.00	0.00	0.00	0.00	0.00	0.00	0.00
6	B6	Z	1.00	1.41	1.25	0.00	1.33	0.11	0.33	0.34
7	B7	Z	0.00	0.00	0.00	0.00	0.00	0.00	0.00	0.00
8	D1	Z	0.00	0.00	0.00	0.00	0.00	0.00	0.00	0.00

Holes										
9	D2	Z	0.00	0.00	0.00	0.00	0.00	0.00	0.00	0.00
10	I3	X	1.00	1.45	0.75	0.00	1.10	0.14	0.10	0.36
11	I4	X	2.00	1.85	1.91	0.00	1.88	0.04	0.12	0.12
									Mean RMSD	0.21

Recommend minimum of 4 measurement points

Table 16: Measurements for circular extruded feature diameters.

Cylinders										
#	Feature ID	Axis	Nominal Value	Measured Values			Mean	SD	Mean Deviation	RMSD
				Sample 1	Sample 2	Sample 3				
1	N1	Z	3.00	3.05	2.91	0.00	2.98	0.02	0.02	0.07
2	N2	Z	2.50	2.59	2.45	0.00	2.52	0.03	0.02	0.08
3	N3	Z	1.50	1.55	1.41	0.00	1.48	0.03	0.02	0.08
4	N4	Z	1.00	1.02	0.88	0.00	0.95	0.07	0.05	0.09
									Mean RMSD	0.08

Recommend minimum of 3 measurement points

Table 17: Measurements for notch feature width in X direction as illustrated in Figure 12.

Notches										
#	Feature ID	Axis	Nominal Value	Measured Values			Mean	SD	Mean Deviation	RMSD
				Sample 1	Sample 2	Sample 3				
1	C6	X	4.00	3.98	4.10	0.00	4.04	0.06	0.04	0.07
		Y	0.00	0.00	0.00	0.00	0.00	0.00	0.00	0.00
2	C5	X	3.00	3.23	3.06	0.00	3.15	0.12	0.15	0.17
		Y	0.00	0.00	0.00	0.00	0.00	0.00	0.00	0.00
3	C4	X	2.00	2.03	2.05	0.00	2.04	0.01	0.04	0.04
		Y	0.00	0.00	0.00	0.00	0.00	0.00	0.00	0.00
4	C3	X	1.50	1.43	1.34	0.00	1.39	0.07	0.11	0.12
		Y	0.00	0.00	0.00	0.00	0.00	0.00	0.00	0.00
5	C2	X	1.00	1.01	1.00	0.00	1.00	0.01	0.00	0.01
		Y	0.00	0.00	0.00	0.00	0.00	0.00	0.00	0.00
6	C1	X	0.50	0.41	0.37	0.00	0.39	0.03	0.11	0.11
		Y	0.00	0.00	0.00	0.00	0.00	0.00	0.00	0.00

Notches		
Recommend minimum of 3 measurement points in X or Y	**Mean RMSD**	0.09

Table 18: Measurements for slots feature width in X direction as illustrated in Figure 12.

Slots / Walls										
#	Feature ID	Axis	Nominal Value	Measured Values			Mean	SD	Mean Deviation	RMSD
				Sample 1	Sample 2	Sample 3				
1	J1	X	2.00	1.98	1.98	0.00	1.98	0.00	0.02	0.02
		Y	0.00	0.00	0.00	0.00	0.00	0.00	0.00	0.00
2	J2	X	1.50	1.39	1.48	0.00	1.43	0.06	0.07	0.08
		Y	0.00	0.00	0.00	0.00	0.00	0.00	0.00	0.00
3	J3	X	0.00	0.00	0.00	0.00	0.00	0.00	0.00	0.00
		Y	0.00	0.00	0.00	0.00	0.00	0.00	0.00	0.00
4	K1	X	2.00	1.91	2.02	0.00	1.97	0.05	0.03	0.07
		Y	0.00	0.00	0.00	0.00	0.00	0.00	0.00	0.00
5	K2	X	1.50	1.47	1.62	0.00	1.55	0.07	0.05	0.09
		Y	0.00	0.00	0.00	0.00	0.00	0.00	0.00	0.00
6	K3	X	1.00	1.16	0.95	0.00	1.05	0.08	0.05	0.12
		Y	0.00	0.00	0.00	0.00	0.00	0.00	0.00	0.00
recommend minimum of 2 measurements									**Mean RMSD**	0.07

Table 19: Measurements for crosses feature width in X direction as illustrated in Figure 12.

Crosses										
#	feature ID	Axis	Nominal Value	Measured Values			Mean	SD	Mean Deviation	RMSD
				Sample 1	Sample 2	Sample 3				
6	L1	X	0.40	0.47	0.39	0.00	0.43	0.05	0.03	0.05
7	L2	X	0.50	0.63	0.62	0.00	0.63	0.01	0.13	0.13
8	L3	X	0.40	0.31	0.36	0.00	0.34	0.03	0.06	0.07
9	L4	X	0.50	0.55	0.44	0.00	0.49	0.01	0.01	0.06
Recommend minimum of 2 measurements									**Mean RMSD**	0.08

Table 20: Measurements for squares feature width in X direction as illustrated in Figure 12.

Squares										
#	Feature ID	Axis	Nominal Value	Measured Values			Mean	SD	Mean Deviation	RMSD
				Sample 1	Sample 2	Sample 3				
1	E1	X	8.00	8.07	7.93	0.00	8.00	0.00	0.00	0.07
		Y	0.00	0.00	0.00	0.00	0.00	0.00	0.00	0.00
2	E2	X	4.00	3.98	3.60	0.00	3.79	0.27	0.21	0.29
		Y	0.00	0.00	0.00	0.00	0.00	0.00	0.00	0.00
									Mean RMSD	0.18

recommend minimum of 2 measurements

Table 21: Measurements for Hemisphere radius in X direction as illustrated in Figure 12.

Sphere / Hemisphere										
#	Feature ID	Axis	Nominal Value	Measured Values			Mean	SD	Mean Deviation	RMSD
				Sample 1	Sample 2	Sample 3				
1	H1	X	3.00	3.53	3.50	0.00	3.52	0.02	0.52	0.52
		Y	0.00	0.00	0.00	0.00	0.00	0.00	0.00	0.00
		Z	0.00	0.00	0.00	0.00	0.00	0.00	0.00	0.00
									Mean RMSD	0.17

Recommend minimum of 1 measurement

Table 22: Measurements for surface roughness.

Surface Roughness								
#	Axis	Sa (Average height of selected area)			Mean	SD	Mean Deviation	RMSD
		Sample 1	Sample 2	Sample 3				
1	Top surface of extrudes E1	22.60	20.60	0.00	21.60	1.41	1.00	2.00
2	Side Surface	0.00	0.00	0.00				
3	Ramp	0.00	0.00	0.00				
							Mean RMSD	2.00

Recommend minimum of 1 measurement

Table 23: Measurements for X directional accuracy.

X- Accuracy										
#	Axis	Feature ID	Nominal Value	Measured Values			Mean	SD	Mean Deviation	RMSD
				Sample 1	Sample 2	Sample 3				
1	X	A1	46.00	45.89	45.88	0.00	45.88	0.01	0.12	0.12
2	X	E1	0.00	0.00	0.00	0.00	0.00	0.00	0.00	0.00
3	X	E2	0.00	0.00	0.00	0.00	0.00	0.00	0.00	0.00
4	X	F1	0.00	0.00	0.00	0.00	0.00	0.00	0.00	0.00
5	X	F2	0.00	0.00	0.00	0.00	0.00	0.00	0.00	0.00
6	X	F3	0.00	0.00	0.00	0.00	0.00	0.00	0.00	0.00
7	X	F4	0.00	0.00	0.00	0.00	0.00	0.00	0.00	0.00
8	X	F5	0.00	0.00	0.00	0.00	0.00	0.00	0.00	0.00
9	X	G1	5.00	5.10	4.88	0.00	4.99	0.02	0.01	0.11
10	X	G2	3.75	3.57	8.70	0.00	6.13	3.37	2.38	3.50
11	X	G3	0.00	0.00	0.00	0.00	0.00	0.00	0.00	0.00
12	X	G4	3.75	3.76	3.74	0.00	3.75	0.01	0.00	0.01
13	X	G5	0.00	0.00	0.00	0.00	0.00	0.00	0.00	0.00
14	X	K1	0.00	0.00	0.00	0.00	0.00	0.00	0.00	0.00
15	X	K2	0.00	0.00	0.00	0.00	0.00	0.00	0.00	0.00
16	X	K3	0.00	0.00	0.00	0.00	0.00	0.00	0.00	0.00
17	X	K4	0.00	0.00	0.00	0.00	0.00	0.00	0.00	0.00
18	X	K5	0.00	0.00	0.00	0.00	0.00	0.00	0.00	0.00
19	X	O	50.00	49.87	49.78	0.00	49.82	0.06	0.18	0.19
									Mean RMSD	0.78

Recommend minimum of 5 measurement points

Table 24: Measurements for Y directional accuracy.

Y- Accuracy										
#	Axis	Feature ID	Nominal Value	Measured Values			Mean	SD	Mean Deviation	RMSD
				Sample 1	Sample 2	Sample 3				
1	Y	A1	0.50	0.40	0.41	0.00	0.40	0.00	0.10	0.10
2	Y	E1	8.00	7.73	7.73	0.00	7.73	0.00	0.27	0.27
3	Y	E2	0.00	0.00	0.00	0.00	0.00	0.00	0.00	0.00
4	Y	F1	5.00	5.17	5.08	0.00	5.12	0.06	0.12	0.13
5	Y	F2	0.00	0.00	0.00	0.00	0.00	0.00	0.00	0.00

Y- Accuracy										
6	Y	F3	0.00	0.00	0.00	0.00	0.00	0.00	0.00	0.00
7	Y	F4	0.00	0.00	0.00	0.00	0.00	0.00	0.00	0.00
8	Y	F5	0.00	0.00	0.00	0.00	0.00	0.00	0.00	0.00
9	Y	G1	5.00	4.89	4.87	0.00	4.88	0.01	0.12	0.12
10	Y	G2	0.00	0.00	0.00	0.00	0.00	0.00	0.00	0.00
11	Y	G3	0.00	0.00	0.00	0.00	0.00	0.00	0.00	0.00
12	Y	G4	0.00	0.00	0.00	0.00	0.00	0.00	0.00	0.00
13	Y	G5	0.00	0.00	0.00	0.00	0.00	0.00	0.00	0.00
14	Y	K1	0.00	0.00	0.00	0.00	0.00	0.00	0.00	0.00
15	Y	K2	0.00	0.00	0.00	0.00	0.00	0.00	0.00	0.00
16	Y	K3	0.00	0.00	0.00	0.00	0.00	0.00	0.00	0.00
17	Y	K4	0.00	0.00	0.00	0.00	0.00	0.00	0.00	0.00
18	Y	K5	0.00	0.00	0.00	0.00	0.00	0.00	0.00	0.00
19	Y	O	50.00	49.80	49.66	0.00	49.73	0.09	0.27	0.28
									Mean RMSD	0.18

recommend minimum of 5 measurement points

Table 25: Measurements for Z directional accuracy.

Z- Accuracy										
#	Axis	Feature ID	Nominal Value	Measured Values			Mean	SD	Mean Deviation	RMSD
				Sample 1	Sample 2	Sample 3				
1	Z	D1	0.00	0.00	0.00	0.00	0.00	0.00	0.00	0.00
2	Z	D2	0.00	0.00	0.00	0.00	0.00	0.00	0.00	0.00
3	Z	E1	0.00	0.00	0.00	0.00	0.00	0.00	0.00	0.00
4	Z	E2	0.00	0.00	0.00	0.00	0.00	0.00	0.00	0.00
5	Z	F1	5.00	4.96	5.01	0.00	4.99	0.02	0.01	0.03
6	Z	F2	0.00	0.00	0.00	0.00	0.00	0.00	0.00	0.00
7	Z	F3	0.00	0.00	0.00	0.00	0.00	0.00	0.00	0.00
8	Z	F4	0.00	0.00	0.00	0.00	0.00	0.00	0.00	0.00
9	Z	F5	0.00	0.00	0.00	0.00	0.00	0.00	0.00	0.00
10	Z	G1	5.00	5.04	4.97	0.00	5.01	0.01	0.01	0.03
11	Z	G2	4.00	3.99	4.02	0.00	4.01	0.01	0.01	0.01
12	Z	G3	0.00	0.00	0.00	0.00	0.00	0.00	0.00	0.00

Z- Accuracy										
13	Z	G4	0.00	0.00	0.00	0.00	0.00	0.00	0.00	0.00
14	Z	G5	1.00	1.06	0.97	0.00	1.01	0.02	0.01	0.05
15	Z	H1	0.00	0.00	0.00	0.00	0.00	0.00	0.00	0.00
16	Z	I5	0.00	0.00	0.00	0.00	0.00	0.00	0.00	0.00
17	Z	I6	0.00	0.00	0.00	0.00	0.00	0.00	0.00	0.00
18	Z	I7	0.00	0.00	0.00	0.00	0.00	0.00	0.00	0.00
19	Z	I8	0.00	0.00	0.00	0.00	0.00	0.00	0.00	0.00
20	Z	I9	0.00	0.00	0.00	0.00	0.00	0.00	0.00	0.00
21	Z	K1	0.00	0.00	0.00	0.00	0.00	0.00	0.00	0.00
22	Z	K2	0.00	0.00	0.00	0.00	0.00	0.00	0.00	0.00
23	Z	K3	0.00	0.00	0.00	0.00	0.00	0.00	0.00	0.00
24	Z	K4	0.00	0.00	0.00	0.00	0.00	0.00	0.00	0.00
25	Z	K5	0.00	0.00	0.00	0.00	0.00	0.00	0.00	0.00
26	Z	M1	0.00	0.00	0.00	0.00	0.00	0.00	0.00	0.00
27	Z	M2	0.00	0.00	0.00	0.00	0.00	0.00	0.00	0.00
28	Z	M3	0.00	0.00	0.00	0.00	0.00	0.00	0.00	0.00
29	Z	O	10.00	10.01	10.23	0.00	10.12	0.16	0.12	0.17
									Mean RMSD	0.06

Recommend minimum of 5 measurement points

Table 25 to 27 shows the recorded measurements for measuring the accuracy of thin features.

Table 26: Measurements for thin wall and slots for ≤ 0.5mm features

Thin walls and slots										
#	feature ID	Axis	Nominal Value	Measured Values			Mean	SD	Mean Deviation	RMSD
				Sample 1	Sample 2	Sample 3				
1	K4	X	0.50	0.60	0.64	0.00	0.62	0.03	0.12	0.12
		Y	0.00	0.00	0.00	0.00	0.00	0.00	0.00	0.00
2	K5	X	0.40	0.42	0.38	0.00	0.40	0.0014	0.001	0.02
		Y	0.00	0.00	0.00	0.00	0.00	0.00	0.00	0.00
3	J4	X	0.50	0.36	0.44	0.00	0.40	0.06	0.10	0.11
		Y	0.00	0.00	0.00	0.00	0.00	0.00	0.00	0.00
4	J5	X	0.40	0.24	0.37	0.00	0.30	0.09	0.10	0.11
		Y	0.00	0.00	0.00	0.00	0.00	0.00	0.00	0.00
									Mean RMSD	0.09

Recommended all

Table 27: Measurements for thin cylinders for ≤ 0.5mm features

Thin cylinders										
#	Feature ID	Normal axis	Nominal Value	Measured Values			Mean	SD	Mean Deviation	RMSD
				Sample 1	Sample 2	Sample 3				
1	N5	Z	0.50	0.53	0.45	0.00	0.49	0.01	0.01	0.04
2	N6	Z	0.40	0.48	0.35	0.00	0.41	0.02	0.01	0.06
									Mean RMSD	0.05

Recommended all

Table 28: Measurements for holes for ≤ 0.5mm features

Small holes										
#	Feature ID	Normal axis	Nominal Value	Measured Values			Mean	SD	Mean Deviation	RMSD
				Sample 1	Sample 2	Sample 3				
1	I1	X	0.40	0.57	0.62	0.00	0.59	0.03	0.19	0.19
2	I2	X	0.50	0.65	0.67	0.00	0.66	0.02	0.16	0.16
3	B8	Z	0.50	0.76	0.70	0.00	0.73	0.04	0.23	0.23
4	B9	Z	0.40	0.56	0.62	0.00	0.59	0.04	0.19	0.19
									Mean RMSD	0.20

Recommended all

Table 28 shows the recorded measurements for time for each sample which got approximated same value for all three samples.

Table 29: Measurements for time required to complete job.

Build Speed						
#	Accuracy	feature ID	Measured Values			Excel Time Conversion as a replacement of RMSD
			Hour	Minutes	Seconds	
1	Speed	Benchmark	7	50	0	0.326389

Table 29 shows the distortion angle due to residual stresses with respect to horizontal plane.

Table 30: Measurements of distortion angle due to residual stresses

Angle of X to horizontal plane										
#	Parallel to	feature ID	Nominal Value	Measured Values			Mean	SD	Mean Deviation	RMSD
				Sample 1	Sample 2	Sample 3				
1	Parallelism to X surface of feature O	A1	90.00	89.20	88.43	0.00	88.81	0.54	1.19	1.25
									Mean RMSD	1.25

15. Appendix 3: Data collected in Excel template for benchmark measurements for EOS M290 samples.

Below are measurements recorded for the two samples AMed on EOS M290. These tables collect all the data to be used calculate the RMSD values on the backend of MATLAB application for decision making. The highlighted yellow values are the only measurements recorded now for scope of this thesis for two samples AMed with the modified design of benchmark artifact.

Table 30 to 41 shows the recorded measurements for measuring the accuracy aspects of AMed benchmark samples on EOS M290.

Table 31: Measurements for overhanging inclination structures.

Inclinations										
#	Feature ID	Axis	Nominal Value	Measured Values			Mean	SD	Mean Deviation	RMSD
				Sample 1	Sample 2	Sample 3				
1	Inclination	ZY	0.00	0.00	0.00	0.00	0.00	0.00	0.00	0.00
2			0.00	0.00	0.00	0.00	0.00	0.00	0.00	0.00
3			45.00	44.73	44.91	0.00	44.82	0.13	0.18	0.20
4			35.00	34.88	35.24	0.00	35.06	0.08	0.06	0.19
5			25.00	25.39	24.80	0.00	25.09	0.13	0.09	0.31
									Mean RMSD	0.23

Recommend minimum of 2 measurement points

Table 32: Measurements for circular hole features diameters.

Holes										
#	Feature ID	Axis	Nominal Value	Measured Values			Mean	SD	Mean Deviation	RMSD
				Sample 1	Sample 2	Sample 3				
1	B1	Z	6.00	5.83	5.80	0.00	5.81	0.02	0.19	0.19
2	B2	Z	0.00	0.00	0.00	0.00	0.00	0.00	0.00	0.00
3	B3	Z	0.00	0.00	0.00	0.00	0.00	0.00	0.00	0.00
4	B4	Z	2.00	2.09	1.59	0.00	1.84	0.23	0.16	0.30
5	B5	Z	0.00	0.00	0.00	0.00	0.00	0.00	0.00	0.00
6	B6	Z	1.00	1.11	1.13	0.00	1.12	0.02	0.12	0.12
7	B7	Z	0.00	0.00	0.00	0.00	0.00	0.00	0.00	0.00
8	D1	Z	0.00	0.00	0.00	0.00	0.00	0.00	0.00	0.00

Holes										
9	D2	Z	0.00	0.00	0.00	0.00	0.00	0.00	0.00	0.00
10	I3	X	1.00	1.24	1.25	0.00	1.24	0.01	0.24	0.24
11	I4	X	2.00	2.21	1.95	0.00	2.08	0.12	0.08	0.15
									Mean RMSD	0.20

Recommend minimum of 4 measurement points

Table 33: Measurements for circular extruded feature diameters.

Cylinders										
#	feature ID	Axis	Nominal Value	Measured Values			Mean	SD	Mean Deviation	RMSD
				Sample 1	Sample 2	Sample 3				
1	N1	Z	3.00	3.19	3.27	0.00	3.23	0.06	0.23	0.23
2	N2	Z	2.50	2.70	2.67	0.00	2.68	0.03	0.18	0.19
3	N3	Z	1.50	1.75	1.72	0.00	1.73	0.02	0.23	0.23
4	N4	Z	1.00	1.25	1.24	0.00	1.25	0.00	0.25	0.25
									Mean RMSD	0.22

Recommend minimum of 3 measurement points

Table 34. Measurements for notch feature width in X direction as illustrated in Figure 12.

Notches										
#	feature ID	Axis	Nominal Value	Measured Values			Mean	SD	Mean Deviation	RMSD
				Sample 1	Sample 2	Sample 3				
1	C6	X	4.00	4.04	3.90	0.00	3.97	0.04	0.03	0.08
		Y	0.00	0.00	0.00	0.00	0.00	0.00	0.00	0.00
2	C5	X	3.00	2.76	2.66	0.00	2.71	0.07	0.29	0.29
		Y	0.00	0.00	0.00	0.00	0.00	0.00	0.00	0.00
3	C4	X	2.00	1.80	2.13	0.00	1.96	0.05	0.04	0.17
		Y	0.00	0.00	0.00	0.00	0.00	0.00	0.00	0.00
4	C3	X	1.50	1.31	1.77	0.00	1.54	0.06	0.04	0.23
		Y	0.00	0.00	0.00	0.00	0.00	0.00	0.00	0.00
5	C2	X	1.00	0.72	0.76	0.00	0.74	0.03	0.26	0.26
		Y	0.00	0.00	0.00	0.00	0.00	0.00	0.00	0.00
6	C1	X	0.50	0.47	0.38	0.00	0.42	0.06	0.08	0.09
		Y	0.00	0.00	0.00	0.00	0.00	0.00	0.00	0.00

Notches		
Recommend minimum of 3 measurement points in X or Y	**Mean RMSD**	0.19

Table 35: Measurements for slots feature width in X direction as illustrated in Figure 12.

Slots / Walls										
#	feature ID	Axis	Nominal Value	Measured Values			Mean	SD	Mean Deviation	RMSD
				Sample 1	Sample 2	Sample 3				
1	J1	X	2.00	1.96	2.27	0.00	2.11	0.16	0.11	0.19
		Y	0.00	0.00	0.00	0.00	0.00	0.00	0.00	0.00
2	J2	X	1.50	1.32	1.57	0.00	1.44	0.08	0.06	0.14
		Y	0.00	0.00	0.00	0.00	0.00	0.00	0.00	0.00
3	J3	X	0.00	0.00	0.00	0.00	0.00	0.00	0.00	0.00
		Y	0.00	0.00	0.00	0.00	0.00	0.00	0.00	0.00
4	K1	X	2.00	2.17		0.00	2.17	1.29	0.17	1.42
		Y	0.00	0.00	0.00	0.00	0.00	0.00	0.00	0.00
5	K2	X	1.50	1.71		0.00	1.71	0.91	0.21	1.07
		Y	0.00	0.00	0.00	0.00	0.00	0.00	0.00	0.00
6	K3	X	1.00	1.19		0.00	1.19	0.58	0.19	0.72
		Y	0.00	0.00	0.00	0.00	0.00	0.00	0.00	0.00
Recommend minimum of 2 measurements									**Mean RMSD**	0.71

Table 36: Measurements for crosses feature width in X direction as illustrated in Figure 12.

Crosses										
#	feature ID	Axis	Nominal Value	Measured Values			Mean	SD	Mean Deviation	RMSD
				Sample 1	Sample 2	Sample 3				
6	L1	X	0.40	0.48	0.52	0.00	0.50	0.03	0.10	0.10
7	L2	X	0.50	0.62	0.54	0.00	0.60	0.09	0.10	0.19
8	L3	X	0.40	0.34	0.37	0.00	0.36	0.02	0.04	0.05
9	L4	X	0.50	0.44	0.48	0.00	0.46	0.03	0.04	0.05
Recommend minimum of 2 measurements									**Mean RMSD**	0.07

Table 37: Measurements for squares feature width in X direction as illustrated in Figure 12.

Squares										
#	feature ID	Axis	Nominal Value	Measured Values			Mean	SD	Mean Deviation	RMSD
				Sample 1	Sample 2	Sample 3				
1	E1	X	8.00	8.12	8.56	0.00	8.34	0.31	0.34	0.41
		Y	0.00	0.00	0.00	0.00	0.00	0.00	0.00	0.00
3	E2	X	4.00	4.17	4.54	0.00	4.36	0.26	0.36	0.40
		Y	0.00	0.00	0.00	0.00	0.00	0.00	0.00	0.00
									Mean RMSD	0.40

Recommend minimum of 1 measurement

Table 38: Measurements for Hemisphere radius in X direction as illustrated in Figure 12.

Sphere / Hemisphere										
#	Feature ID	Axis	Nominal Value	Measured Values			Mean	SD	Mean Deviation	RMSD
				Sample 1	Sample 2	Sample 3				
1	H1	X	3.00	3.57	3.67	0.00	3.62	0.07	0.62	0.62
		Y	0.00	0.00	0.00	0.00	0.00	0.00	0.00	0.00
		Z	0.00	0.00	0.00	0.00	0.00	0.00	0.00	0.00
									Mean RMSD	0.62

Recommend minimum of 1 measurement

Table 39: Measurements for surface roughness.

Surface Roughness								
#	Axis	Sa (Average height of selected area)			Mean	SD	Mean Deviation	RMSD
		Sample 1	Sample 2	Sample 3				
1	Top surface of extrudes E1	6.18	6.23	0.00	6.21	0.04	0.03	0.05
2	Side Surface	0.00	0.00	0.00				
3	Ramp	0.00	0.00	0.00				
							Mean RMSD	0.05

Recommend minimum of 1 measurement

Table 40: Measurements for X directional accuracy.

X- Accuracy										
#	Axis	feature ID	Nominal Value	Measured Values			Mean	SD	Mean Deviation	RMSD
				Sample 1	Sample 2	Sample 3				
1	X	A1	46.00	46.12	46.13	0.00	46.13	0.01	0.13	0.13
2	X	E1	0.00	0.00	0.00	0.00	0.00	0.00	0.00	0.00
3	X	E2	0.00	0.00	0.00	0.00	0.00	0.00	0.00	0.00
4	X	F1	0.00	0.00	0.00	0.00	0.00	0.00	0.00	0.00
5	X	F2	0.00	0.00	0.00	0.00	0.00	0.00	0.00	0.00
6	X	F3	0.00	0.00	0.00	0.00	0.00	0.00	0.00	0.00
7	X	F4	0.00	0.00	0.00	0.00	0.00	0.00	0.00	0.00
8	X	F5	0.00	0.00	0.00	0.00	0.00	0.00	0.00	0.00
9	X	G1	5.00	5.04	5.01	0.00	5.02	0.02	0.02	0.03
10	X	G2	3.75	3.72	3.77	0.00	3.75	0.01	0.00	0.03
11	X	G3	0.00	0.00	0.00	0.00	0.00	0.00	0.00	0.00
12	X	G4	3.75	3.71	3.65	0.00	3.68	0.04	0.07	0.07
13	X	G5	0.00	0.00	0.00	0.00	0.00	0.00	0.00	0.00
14	X	K1	0.00	0.00	0.00	0.00	0.00	0.00	0.00	0.00
15	X	K2	0.00	0.00	0.00	0.00	0.00	0.00	0.00	0.00
16	X	K3	0.00	0.00	0.00	0.00	0.00	0.00	0.00	0.00
17	X	K4	0.00	0.00	0.00	0.00	0.00	0.00	0.00	0.00
18	X	K5	0.00	0.00	0.00	0.00	0.00	0.00	0.00	0.00
19	X	O	50.00	50.06	50.33	0.00	50.20	0.19	0.20	0.24
									Mean RMSD	0.10

Recommend minimum of 5 measurement points

Table 41: Measurements for Y directional accuracy.

Y- Accuracy										
#	Axis	feature ID	Nominal Value	Measured Values			Mean	SD	Mean Deviation	RMSD
				Sample 1	Sample 2	Sample 3				
1	Y	A1	0.50	0.67	0.57	0.00	0.62	0.08	0.12	0.13
2	Y	E1	8.00	8.24	8.21	0.00	8.22	0.02	0.22	0.22
3	Y	E2	0.00	0.00	0.00	0.00	0.00	0.00	0.00	0.00
4	Y	F1	5.00	4.61	4.53	0.00	4.57	0.06	0.43	0.43
5	Y	F2	0.00	0.00	0.00	0.00	0.00	0.00	0.00	0.00
6	Y	F3	0.00	0.00	0.00	0.00	0.00	0.00	0.00	0.00

Y- Accuracy										
7	Y	F4	0.00	0.00	0.00	0.00	0.00	0.00	0.00	0.00
8	Y	F5	0.00	0.00	0.00	0.00	0.00	0.00	0.00	0.00
9	Y	G1	5.00	5.14	5.17	0.00	5.16	0.02	0.16	0.16
10	Y	G2	0.00	0.00	0.00	0.00	0.00	0.00	0.00	0.00
11	Y	G3	0.00	0.00	0.00	0.00	0.00	0.00	0.00	0.00
12	Y	G4	0.00	0.00	0.00	0.00	0.00	0.00	0.00	0.00
13	Y	G5	0.00	0.00	0.00	0.00	0.00	0.00	0.00	0.00
14	Y	K1	0.00	0.00	0.00	0.00	0.00	0.00	0.00	0.00
15	Y	K2	0.00	0.00	0.00	0.00	0.00	0.00	0.00	0.00
16	Y	K3	0.00	0.00	0.00	0.00	0.00	0.00	0.00	0.00
17	Y	K4	0.00	0.00	0.00	0.00	0.00	0.00	0.00	0.00
18	Y	K5	0.00	0.00	0.00	0.00	0.00	0.00	0.00	0.00
19	Y	O	50.00	50.10	49.96	0.00	50.03	0.04	0.03	0.07
									Mean RMSD	0.20

Recommend minimum of 5 measurement points

Table 42: Measurements for Z directional accuracy.

Z- Accuracy										
#	Axis	feature ID	Nominal Value	Measured Values			Mean	SD	Mean Deviation	RMSD
				Sample 1	Sample 2	Sample 3				
1	Z	D1	0.00	0.00	0.00	0.00	0.00	0.00	0.00	0.00
2	Z	D2	0.00	0.00	0.00	0.00	0.00	0.00	0.00	0.00
3	Z	E1	0.00	0.00	0.00	0.00	0.00	0.00	0.00	0.00
4	Z	E2	0.00	0.00	0.00	0.00	0.00	0.00	0.00	0.00
5	Z	F1	5.00	5.10	5.05	0.00	5.08	0.03	0.08	0.08
6	Z	F2	0.00	0.00	0.00	0.00	0.00	0.00	0.00	0.00
7	Z	F3	0.00	0.00	0.00	0.00	0.00	0.00	0.00	0.00
8	Z	F4	0.00	0.00	0.00	0.00	0.00	0.00	0.00	0.00
9	Z	F5	0.00	0.00	0.00	0.00	0.00	0.00	0.00	0.00
10	Z	G1	5.00	5.00	5.00	0.00	5.00	0.00	0.00	0.00
11	Z	G2	4.00	4.03	3.97	0.00	4.00	0.00	0.00	0.03
12	Z	G3	0.00	0.00	0.00	0.00	0.00	0.00	0.00	0.00
13	Z	G4	0.00	0.00	0.00	0.00	0.00	0.00	0.00	0.00
14	Z	G5	1.00	0.98	0.96	0.00	0.97	0.01	0.03	0.03
15	Z	H1	0.00	0.00	0.00	0.00	0.00	0.00	0.00	0.00

Z- Accuracy										
16	Z	I5	0.00	0.00	0.00	0.00	0.00	0.00	0.00	0.00
17	Z	I6	0.00	0.00	0.00	0.00	0.00	0.00	0.00	0.00
18	Z	I7	0.00	0.00	0.00	0.00	0.00	0.00	0.00	0.00
19	Z	I8	0.00	0.00	0.00	0.00	0.00	0.00	0.00	0.00
20	Z	I9	0.00	0.00	0.00	0.00	0.00	0.00	0.00	0.00
21	Z	K1	0.00	0.00	0.00	0.00	0.00	0.00	0.00	0.00
22	Z	K2	0.00	0.00	0.00	0.00	0.00	0.00	0.00	0.00
23	Z	K3	0.00	0.00	0.00	0.00	0.00	0.00	0.00	0.00
24	Z	K4	0.00	0.00	0.00	0.00	0.00	0.00	0.00	0.00
25	Z	K5	0.00	0.00	0.00	0.00	0.00	0.00	0.00	0.00
26	Z	M1	0.00	0.00	0.00	0.00	0.00	0.00	0.00	0.00
27	Z	M2	0.00	0.00	0.00	0.00	0.00	0.00	0.00	0.00
28	Z	M3	0.00	0.00	0.00	0.00	0.00	0.00	0.00	0.00
29	Z	O	10.00	9.92	9.86	0.00	9.89	0.04	0.11	0.12
									Mean RMSD	0.05

Recommend minimum of 5 measurement points

Table 43: Measurements for thin wall and slots for ≤ 0.5mm features

Thin walls and slots										
#	Feature ID	Axis	Nominal Value	Measured Values			Mean	SD	Mean Deviation	RMSD
				Sample 1	Sample 2	Sample 3				
1	K4	X	0.50	0.68	0.76	0.00	0.72	0.06	0.22	0.22
		Y	0.00	0.00	0.00	0.00	0.00	0.00	0.00	0.00
2	K5	X	0.40	0.52	0.66	0.00	0.59	0.10	0.19	0.20
		Y	0.00	0.00	0.00	0.00	0.00	0.00	0.00	0.00
3	J4	X	0.50	0.44	0.55	0.00	0.49	0.01	0.01	0.05
		Y	0.00	0.00	0.00	0.00	0.00	0.00	0.00	0.00
4	J5	X	0.40	0.38	0.56	0.00	0.47	0.10	0.07	0.11
		Y	0.00	0.00	0.00	0.00	0.00	0.00	0.00	0.00
									Mean RMSD	0.15

Recommended all

Table 44: Measurements for thin cylinders for ≤ 0.5mm features

Thin cylinders										
#	feature ID	Normal axis	Nominal Value	Measured Values			Mean	SD	Mean Deviation	RMSD
				Sample 1	Sample 2	Sample 3				
1	N5	Z	0.50	0.71	0.80	0.00	0.75	0.07	0.25	0.26
2	N6	Z	0.40	0.53	0.75	0.00	0.64	0.16	0.24	0.26
									Mean RMSD	0.26

Recommended all

Table 45: Measurements for holes for ≤ 0.5mm features

Small holes										
#	feature ID	Normal axis	Nominal Value	Measured Values			Mean	SD	Mean Deviation	RMSD
				Sample 1	Sample 2	Sample 3				
1	I1	X	0.40	0.59	0.65	0.00	0.62	0.04	0.22	0.22
2	I2	X	0.50	0.63	0.63	0.00	0.63	0.00	0.13	0.13
3	B8	Z	0.50	0.70	0.69	0.00	0.70	0.00	0.20	0.20
4	B9	Z	0.40	0.62	0.63	0.00	0.62	0.01	0.22	0.22
									Mean RMSD	0.19

Recommended all

Table 46: Measurements for time required to complete job.

Build Speed						
#	Accuracy	Feature ID	Measured Values			Excel Time Conversion as a replacement of RMSD
			Hour	Minutes	Seconds	
1	Speed	Benchmark	5	50	0	0.243056

Table 47: Measurements of distortion angle due to residual stresses

Angle of X to horizontal plane										
#	Parallel to	feature ID	Nominal Value	Measured Values			Mean	SD	Mean Deviation	RMSD
				Sample 1	Sample 2	Sample 3				
1	Parallelism to X surface of feature O	A1	90.00	91.13	89.31	0.00	90.22	0.31	0.22	0.94
									Mean RMSD	0.94